OBSERVATIONS AND MODELS OF
INERTIAL WAVES
IN THE DEEP OCEAN

by

LEE-LUENG FU

B.S., National Taiwan University
(1972)

SUBMITTED IN PARTIAL FULFILLMENT
OF THE REQUIREMENTS FOR THE
DEGREE OF DOCTOR OF
PHILOSOPHY

at the

MASSACHUSETTS INSTITUTE OF TECHNOLOGY

and the

WOODS HOLE OCEANOGRAPHIC INSTITUTION

February, 1980

© Massachusetts Institute of Technology 1980

Signature of Author_____

Joint Program in Oceanography, Massachusetts Institute
of Technology-Woods Hole Oceanographic Institution, and
Department of Meteorology, Massachusetts Institute of
Technology, February, 1980.

Certified by_____

Thesis supervisor

Accepted by_____

Chairman, Joint Oceanography Committee in Earth
Sciences, Massachusetts Institute of Technology-
Woods Hole Oceanographic Institution.

OBSERVATIONS AND MODELS OF INERTIAL WAVES
IN THE DEEP OCEAN

by

Lee-Lueng Fu

Submitted to the Massachusetts Institute of Technology-
Woods Hole Oceanographic Institution Joint Program in
Oceanography on December 7, 1979 in partial fulfillment
of the requirements for the degree of Doctor of Philosophy

Abstract

The structure of the inertial peak in deep ocean kinetic energy
spectra is studied here. Records were obtained from Polymode arrays
deployed in the Western North Atlantic Ocean (40°W to 70°W, 15°N
to 42°N). The results are interpreted both in terms of local sources
and of turning point effects on internal waves generated at lower
latitudes.

In most of the data, there is a prominent inertial peak slightly
above f; however, the peak height above the background continuum varies
with depth and geographical environment. Three classes of environment
and their corresponding spectra emerge from peak height variations:
class 1 is the 1500 m level near the Mid-Atlantic Ridge, with the
greatest peak height of 18 db; class 2 includes (a) the upper ocean
(depth less than 2000 m), (b) the deep ocean (depth greater than 2000 m)
over rough topography, and (c) the deep ocean underneath the Gulf
Stream, with intermediate peak height of 11.5 db; class 3 is the deep
ocean over smooth topography, with the lowest peak height of 7.5 db.
Near f, the horizontal coherence scale is 0(60 km) at depths from 200 m
to 600 m, and the vertical coherence scale is 0(200 m) just below the
main thermocline.

A one turning point model is developed to describe inertial waves at
mid-latitudes, based on the assumption that inertial waves are randomly
generated at lower latitudes (global generation) where their frequency-
wavenumber spectrum is given by the model of Garrett and Munk (1972 a,
1975). Using the globally valid wave functions obtained by Munk and
Phillips (1968), various frequency spectra near f are calculated
numerically. The model yields a prominent inertial peak of 7 db in the
horizontal velocity spectrum but no peaks in the temperature spectrum.
The model is latitudinally dependent: the frequency shift and bandwidth
of the inertial peak decrease with latitude; energy level near f is
minimum at about 30° and higher at low and high latitudes. The
observations of class 3 can be well-described by the model; a low zonal
wavenumber cutoff is required to produce the observed frequency shift of
the inertial peak.

\

3

The differences between the global generation model and the observations of class 1 and class 2 are interpreted as the effects of local sources. A locally forced model is developed based on the latitudinal modal decomposition of a localized source function. Asymptotic eigensolutions of the Laplace's tidal equation are therefore derived and used as a set of expansion functions. The forcing is through a vertical velocity field specified at the top or bottom boundaries of the ocean. For white noise forcing, the horizontal velocity spectrum of the response has an inertial peak which diminishes in the far-field. With the forcing located at either the surface or the bottom, several properties of the class 2 observations can be described qualitatively by a combination of the global and local models.

The reflection of inertial waves from a turbulent benthic boundary layer is studied by a slab model of given depth. Frictional effects are confined to the boundary layer and modelled by a quadratic drag law. For given incident waves, reflection coefficients are found to be greater than 0.9 for the long waves which contain most of the energy. This result suggests that energy-containing inertial waves can propagate over great distance as is required by the validity of the model of global generation.

Thesis Supervisor :   Carl Wunsch
Title :   Cecil and Ida Green Professor of
          Physical Oceanography
          Chairman, Department of Earth and
          Planetary Sciences

Ackowledgements

I wish to thank Professor Carl Wunsch of M.I.T., my thesis supervisor, for his introducing me to this research field and for his constant guidance and encouragement through this work. Without his illuminating comments on the presentation of this work, this thesis would be much less readable.

I thank Dr. Nicholas Fofonoff of W.H.O.I. for his careful review of this manuscript and constant encouragement through my graduate study. I am grateful to Professor Glenn Flierl of M.I.T. and Dr. Nelson Hogg of W.H.O.I. for several valuable discussions and critical reviews of this manuscript. I thank Dr. Melbourne Briscoe of W.H.O.I. for discussions and comments on this manuscript. I thank Professor Charles Eriksen of M.I.T. for discussions.

I thank Professor Walter Munk of Scripps Institution of Oceanography for his comments on this manuscript.

I am grateful to Dr. William Schmitz and the Buoy Group of W.H.O.I. for providing unpublished data for the use in this study.

I thank Dr. Thomas Sanford of the University of Washington for his generosity to share some unpublished results with me. I am also grateful to Professor Peter Niiler of Oregon State University for allowing me to use his unpublished data (PMIII C).

I thank Charmaine King and Barbara Grant of M.I.T. for their programming assistance for most of the computation in this study.

Above all others, I wish to express my special thanks to my dear wife, Cecilia, for her endless encouragement and self-sacrifice as being a graduate student's wife. To her I owe so much.

To Cecilia

Table of Contents

Table of Contents (contd.)

8

Table of Contents (contd.)

List of Figures

List of Figures (contd.)

List of Figures (contd.)

List of Figures (contd.)

Chapter 1 <u>Introduction</u>

Inertial waves (sometimes called inertial oscillations, or inertial motions, etc.) have been observed in the ocean for almost half a century (for a historical review see Webster, 1968). They are characterized as a transient rotation (clockwise in the Northern Hemisphere) of horizontal current with frequency near the local inertial frequency f, defined as $2\Omega\sin\phi$, where Ω is the rotational frequency of the earth and ϕ is latitude. Webster (1968) documented their world-wide existence at all depths and described their general properties. In his words, inertial waves are "essentially transient phenomena of thin vertical extent". Their coherence scale is at least several kilometers in the horizontal (Webster, 1968 ; Schott, 1971) but only a few tens of meters in the vertical (Webster, 1968 ; Fomin and Savin, 1973). In frequency space, inertial waves are represented by a rather broad spectral peak located slightly above f; they are the most energetic components of the internal wave field. One of the important recent observations of inertial waves was their vertical phase propagation reported by Sanford (1975) and Leaman and Sanford (1975). They showed evidence of a dominant upward phase propagation with near-inertial periods in their profiler measurements in the open ocean. The same feature has also been observed in near-shore regions (Johnson et al, 1976; Kundu, 1976) and shallow seas (Fomin and Yampol'skiy, 1975). These findings constitute direct evidence for the interpretation of inertial waves as propagating internal waves. In the atmosphere, inertial waves have not been observed in the troposphere; however, evidence of their existence and downward

phase propagation in the stratosphere has been recently reported by
Thompson (1977). Thus the observed helical vertical structures of
ionospheric winds at heights from 90 km to 150 km (Rosenberg, 1968) may
be indeed manifestations of inertial waves generated in the lower
atmosphere as proposed by Moses (1971).

The importance of inertial waves as transient response of the ocean
to impulsive external forcing has been recognized for a long time (e.g.,
Rossby, 1938; Pollard, 1970). Hence knowledge of inertial waves is
crucial to the understanding of the energetics of ocean circulation as
the result of atmospheric forcing. On the other hand, recent work on
resonant interactions of internal waves (e.g., Olbers, 1976; McComas and
Bretherton, 1977) suggests that inertial waves are important in internal
wave dynamics at mid-latitudes: low vertical wavenumber inertial waves
serve as an energy source for high frequency waves with relatively high
wavenumbers through a diffusive mechanism in wavenumber space; high
vertical wavenumber inertial waves serve as an energy sink for waves
with twice the frequency and relatively low wavenumbers as the result of
subharmonic instability, and the energy then is dissipated through the
mechanism of shear instability. Garrett and Munk (1972 b) have shown
that the shear instability in the latter case could be an important
dissipation mechanism for oceanic internal waves and hence provide the
turbulent mixing energy in the thermocline. Disturbances caused by the
internal wave field in which inertial waves are most energetic are the
major sources of noise in undersea accoustic communications; hence the
study of inertial waves also has its important military and commercial
applications.

In the last decade, research in oceanic internal waves was greatly

enhanced by the advent of the frequency-wavenumber spectrum (f-w

spectrum hereafter) developed by Garrett and Munk (1972 a, 1975). With

the synthesis of a great number of observations, they deduced a

universal model spectrum for internal waves in the deep ocean using

linear dynamics under the hypothesis of horizontal isotropy and vertical

symmetry of the wave field. This attempt to estimate the complete energy

spectrum of internal waves from existing observations led to the design

of critical experiments such as the Internal Wave Experiment (IWEX;

Briscoe, 1975) to directly measure the wave field in frequency and

wavenumber space. The results reported by Müller et at (1978) have

confirmed the general validity of the Garrett-Munk model (GM model

hereafter) in the frequency regime away from f, $N(z)$, and the tidal

frequencies ($N(z)$ is the buoyancy frequency at depth z). The problem at

f is two-fold : theoretically, the WKBJ approximation of wave functions

underlying the GM model fails near f, which is a latitudinal turning

point; observationally, the IWEX record is too short (40 days) to draw

statistically significant conclusions with sufficient resolution near f.

The latter limitation also explains the general lack of a detailed

spectral description of inertial waves after so many years'

proliferation of moored measurements. For example, a frequency

resolution of the order of two percent of f at mid-latitudes requires

six months' data to obtain five degrees of freedom for spectral

estimates. Most pre-Polymode (for a description of Polymode see US

POLYMODE Organizing Committee, 1976) observations simply do not meet

this requirement. Because the Polymode arrays were originally designed

to study the variability of meso-scale eddy field in the North Atlantic, there was at least nine months' continuous record at each mooring site. Thus, the Polymode arrays have provided an excellent data base for us to attempt an up-to-date spectral description of inertial waves in a wide-range of latitude and geographical environment in a typical open ocean. Such a description is presented in Chapter 2 with emphases on the answers to the following questions:

(a) Is there a universal frequency spectrum near f in the deep ocean? If not, how does the spectrum vary with the physical environment (instrument depth, topography, etc.) ?

(b) What are the coherence scales of inertial waves in the deep ocean ? Are they consistent with existing theories and observations ?

Because this study is confined to inertial waves in the ocean interior (we will call it the "deep ocean"), i.e., away from both the horizontal and vertical boundaries, those data within 100 m from either the surface or the bottom were excluded from the discussion. Due to the fact that in the inertial frequency band moored temperature measurements are subject to possible contamination from both the mooring motion and horizontal advection (discussed in Appendix A), the descriptions in Chapter 2 are restricted to velocity data only.

The failure of the WKBJ approximation also accounts for the inaccuracy of the GM model near $N(z)$, which is a vertical turning point. Using an exponential $N(z)$, Desaubies (1975) derived uniformly valid vertical wave functions with a single turning point to remove this

apparent singularity and to successfully describe observed spectra near
N(z). Eriksen (1978) used a two turning point model to describe high
frequency waves trapped in the main thermocline. Thus by using
appropriate latitudinal wave functions, we can proceed in the same way
to describe the observed spectra near f in terms of the GM model.
Latitudinal wave functions with global validity were obtained by Munk
and Phillips (1968; MP hereafter). They used the spheroidal wave
equation to approximate the Laplace's tidal equation and obtained
approximate one turning point solutions which are valid globally with
error terms no greater than $O(\epsilon^{-1/3})$, where ϵ is a large parameter
($\gtrsim 10^5$). For the description of mid-latitude inertial waves which are
our major concerns, the one turning point solutions are appropriate
because the waves are unlikely to form latitudinal modes by phase
locking between the two turning latitudes. However, at low latitudes
where there is strong evidence for the existence of latitudinal modes
(Wunsch and Gill, 1976), two turning point solutions must be used. Using
equatorial modes on a beta plane, Eriksen (1979) developed a spectral
model for equatorially trapped waves.

The latitudinal wave functions of horizontal velocity obtained by MP
are proportional to the Airy function which is evanescent poleward
(oscillatory equatorward) of the turning latitude. The Airy function
reaches its maximum when the argument is slightly above zero. Thus, by
using these wave functions in the construction of various frequency
spectra, one would expect to obtain a spectral peak slightly above f in
the horizontal velocity spectrum simply due to the kinematic turning
point effects on internal waves, without the need of a specific forcing

mechanism. The possible use of such a model to account for the observed

inertial peak was independently noticed in a recent review paper by

Garrett and Munk (1979), and has been investigated using a beta plane

model by Munk (1979).

With the appropriate wave functions available, an adequate f-w

spectrum is needed to calculate various spectral quantities. Munk and

Phillips (1968) attempted to calculate the velocity spectrum using a

crude model of the f-w spectrum, with a relatively weak inertial peak in

the resulting spectrum. Today a decade later, detailed knowledge of the

f-w spectrum near f is still lacking. The GM model is not applicable

near f; nevertheless, it is a good description of high frequency waves

far from f, i.e., far from their turning latitudes. Hence the part of

the inertial wave energy which results from random sources sufficiently

equatorward of the observation site can be readily calculated using the

GM model. Under the assumption of linear propagation, all the low

frequency internal waves can be traced to the equator where the ω^{-2} GM

frequency spectrum is valid over an extensive frequency range. Thus,

once the f-w spectrum at the equator is known, we can, in principle ,

calculate the spectrum at all latitudes and obtain a unified

interpretation of measurements at different latitudes. It is quite

reasonable to define this part of the inertial wave field as the "global

wave field". However, with a beta plane model whose validity is

restricted to low latitudes, such calculations would be very inaccurate.

Apart from the random global generation mechanism, it is well known

that the local wind could be an effective source for inertial waves in

the upper ocean. Ekman (1905) in his classical paper showed that

inertial waves could be generated by changes in the wind field. Rossby

(1938) pointed out that inertial waves could be generated as transients

during the flow adjustment toward geostrophic equilibrium. Using a

two-layer model with a body force acting on the upper layer, Veronis

(1956) showed that inertial waves were most efficiently generated by an

impulsive wind field. Pollard (1970) refined Veronis' model to include

continuous stratification and showed that the amplitudes of

wind-generated inertial waves were realistic at the surface but too

small to account for the maximum amplitude observed in the deep ocean.

Furthermore, Pollard and Millard (1970) demonstrated that observed

inertial currents in the surface layer could indeed be simulated by

their model using local wind data. Using a different approach, Kroll

(1975) considered the forcing imposed by a vertical velocity field which

resulted from the divergence of a viscous Ekman layer generated by

surface winds. For sudden onset of the wind field, inertial oscillations

were generated in the Ekman layer with frequencies slightly above f;

these disturbances radiated downward along their ray paths which Kroll

derived from a beta plane model. Because the wave amplitudes generally

increase with decreasing forcing scale which enhances the divergence of

the Ekman layer, small scale severe storms (scale $\sim$ 100 km, stress $\sim$

10 cm^2/sec^2) could, in Kroll's model, give wave amplitudes of

10 cm/sec at great depths. But the forcing used in Pollard's model is

the wind stress itself, not its curl, and hence is insensitive to

forcing scales; even for a wind stress of 10 cm^2/sec^2, the maximum

speed at great depths is only order 1 cm/sec.

In the context of wave-current interaction, Stern (1977) showed that
deep inertial waves could be reinforced by surface wind through an
over-reflection mechanism at the base of the mixed layer. Ageostrophic
instability of the mean flow as a local source for inertial waves is
currently being investigated by Tai (ongoing PhD thesis, Harvard
University).

The observed dominance of downward energy (upward phase) propagation
with near-inertial frequencies is a direct evidence of significant local
generation (Leaman and Sanford, 1975). It seems relevant to define a
"local wave field" to represent these inertial waves which are forced by
some specific local sources. The distinction between the global and
local wave field is that, the latter is generated locally as <u>inertial
waves</u>, whereas the former is generated at lower latitudes as
<u>super-inertial internal waves</u>, which are well described by the GM model
and only appear as inertial waves when they reach their turning
latitudes. As pointed out in MP, the observed inertial wave energy is
most likely a mixture of these two sources. To distinguish these two
contributions from each other in moored measurements is the main task of
this study. The first step is to calculate a model spectrum for the
global wave field using globally valid wave functions and the GM model.

In Chapter 3, the general theory of low frequency internal waves on
a rotating sphere is reviewed. In Chapter 4, the construction of a model
spectrum for the global wave field is presented; its limitations and
sensitivities to model parameters are discussed; comparisons between the
model and observations are made with the differences interpreted as the

contribution from local sources.

In order to explain the observed spectra in terms of forced waves, we need the oceanic response spectrum for a specified forcing spectrum. The ratio of these two is usually called the transfer function. Because most of the existing models of this kind are based on the f-plane approximation, a spurious infinite response at the inertial frequency usually occurs. For instance, using a balance between wind generation and dissipation by vertical friction, Käse and Tang (1976) derived a response spectrum which had an infinite cusp at f. However, this apparent singularity can be removed by including the variation of f with latitude (i.e., the beta effect) in the equations of motion. In Chapter 5, the spectral response of the ocean to a highly idealized forcing is derived, using asymptotic eigenfunctions of the Laplace's tidal equation. The purpose is to explain the qualitative difference between some of the observed spectra and the global wave model.

The existence of the global wave field requires that the dissipation of low frequency waves, especially those energetic long waves, be small enough. Presumably most of the dissipation of these waves with large vertical wavelengths is taking place near the bottom. Because most of the existing models (e.g. Phillips, 1963; Leaman, 1975) of the reflection of near-inertial waves off rigid boundaries are of laminar Ekman layer type, they become singular (boundary layer depth is of order one) when $\omega \approx$ f. However, the benthic boundary layer is turbulent and of small depth -- of order 20 m (c.f. Wimbush and Munk, 1970; Armi and D'Asaro, 1979); its dynamics are different from the ocean interior and this should be taken into account. A simple model is presented in

Chapter 6 to describe the possible effects of the benthic boundary layer
on the reflection of inertial waves propagating from a laminar, inviscid
interior. A slab model is used to describe the boundary layer and the
frictional effects are modelled by a conventional quadratic drag law.
The major purpose is to calculate the resulting reflection coefficient
and to assess the possibility of the existence of the global wave field.

Conclusion and discussion appear in Chapter 7.

Chapter 2 Spectral Description of Inertial Waves in the

Western North Atlantic

2.1 Introduction

The major purpose of this chapter is to describe the internal wave

spectrum based on long term (usually $\gtrsim$ 9 months) moored current

velocity data. These data are primarily from various Polymode arrays

located in the Western North Atlantic. The emphasis is in the inertial

frequency band; with sufficient frequency resolution, characteristics of

the inertial peak -- energy level, frequency, and bandwidth -- were

analyzed to study their variability; spatial coherences were calculated

wherever there were closely spaced instruments, and coherence scales

(both horizontal and vertical) were estimated. Theoretical

interpretation of these observational results is the main task of later

chapters.

2.2 Data base and analysis procedure

Listed in Tables 2.1 and 2.2 are the moored current velocity data

used in this study. All of them are from the Polymode Array I, II, and

III (PMI, PMII, PMIII hereafter) except mooring 520, which is part of

the Muir Seamount Experiment (c.f. Wunsch, 1976). There are altogether

thirty-five stations and ninty-nine instrument levels. The mooring

positions and topography (from Uchupi, 1971) are displayed in Fig. 2.1.

The area covers approximately twenty-seven degrees of latitude (from

15°N to 42°N) and a variety of topographic features : abyssal

plains, seamounts, mid-ocean ridge and its associated fracture zones.

At each instrument level of the Polymode arrays, there is at least

one segment of continuous data of approximately eight months duration.
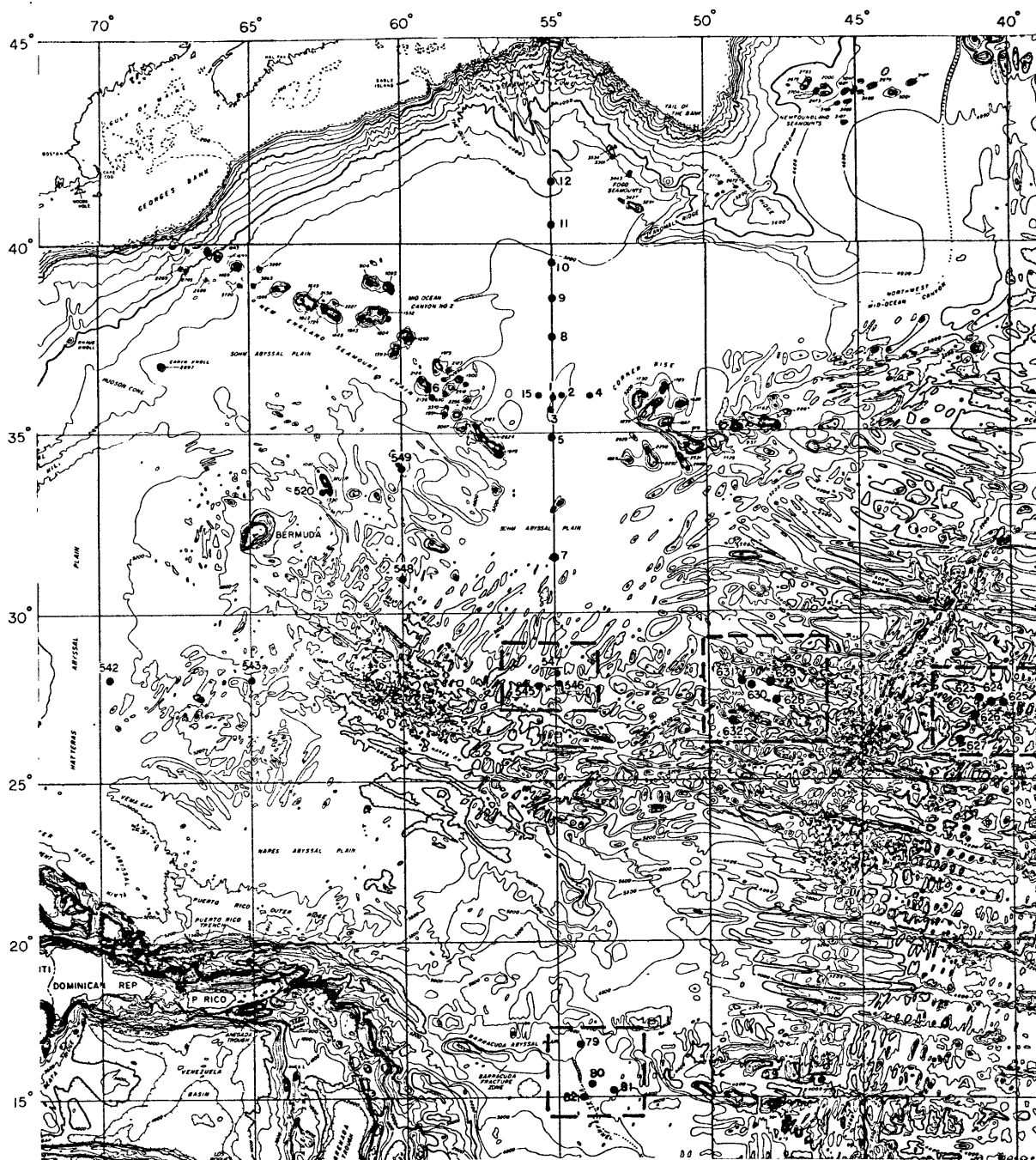
Figure 2.1   Mooring positions and topography. Stations in rough
areas are enclosed with square boxes for identification.

Table 2.1

Tabulation of Records From the Polymode Array II. Latitudes are North, Longitudes West (in deg). Depths Are in Meters, Data Lengths in Hours. Record ID are WHOI Designation Numbers.

Station # (latitude, longitude) water depth	Record ID			Instrument Depth	Data Length	$\Delta\omega/f$	PH(db)	ω_p/f	Class
1	5571		6081	600	5460 x 2	.05	14	1.05	2a
(35.9, 55)	5573	5833	6083	1000	4320 x 3	.13	10.5	.99	2a
5054	5575	5835	6085	1500	5460 x 3	.18	9.5	.99	2a
	55710	58310		4000	5460 x 2	.05	7.5	1.02	3
2		5791	6001	600	5664 x 2	.1	11	1.03	2a
(36, 54.7)		5793	6003	1000	"	.15	11	.96	2a
5318		5794	6004	1500	"	.05	11	1.00	2a
	5589	5796	6006	4000	5312 x 3	.15	6.5	1.08	3
3	5651	5821	6091	600	5336 x 3	.1	11.5	1.05	2a
(35.6, 55.1)	5653		6093	1000	5336 x 2	.04	15	1.00	2a
5115	5654	5824	6094	1500	"	.03	12.5	1.00	2a
	5656	5826	6096	4000	"	.13	7.5	1.03	3
4	5591	5781	6011	600	5280 x 3	.1	9	1.01	2a
(36, 53.8)		5783	6013	1000	5640 x 2	.07	12.5	1.01	2a
5467	5594	5784	6014	1500	5280 x 3	.05	9.5	1.02	2a
	5595	5785	6015	4000	4300 x 3	.14	8	1.13	3
5	5661	5811	6111	600	5320 x 3	.05	13.5	.99	2a
(34.9, 55)	5663	5813	6113	1000	"	.1	12	.99	2a
5506	5664	5814	6114	1500	5312 x 3	.11	10	.99	2a
	5665	5815		4000	5312 x 2	.1	6.5	1.08	3

Table 2.1 (cont'd.)

Station # (latitude, longitude) water depth	Record ID			Instrument Depth	Data Length	Δω/f	PH(db)	ω_p/f	Class
6	5681			600	5220 x 1	.1	10	.98	2a
(35.9, 59)	5683	5843	5983	1000	4770 x 3	.04	14	1.02	2a
5206	5684	5844	5984	1500	5220 x 3	.14	10	1.04	2a
		5845	5985	4000	5664 x 2		4.5	1.04	3
7	5671	5801		600	4032 x 2	.09	10	.99	2a
(31.6, 55.1)	5673	5803	6125	1000	5152 x 3	.09	13	1.02	2a
5595		5804	6126	1500	5856 x 3	.1	11	1.07	2a
	5675	5805	6129	4000	5152 x 3	.1	9.5	1.06	3
8	5641	5771		600	5170 x 2	.08	12.5	.99	2a
(37.5, 55)	5643	5773	6063	1000	5152 x 3	.19	9	1.04	2a
5334	5644	5774	6064	1500	"	.13	10	.96	2a
	5645	5775	6065	4000	"	.15	7.5	1.04	3
9		5761	6051	4000	6384 x 2	.05	9.5	1.05	2c
(38.5, 54.9) 5340									
10		5751	6041	4000	6432 x 2	.08	9	1.04	2c
(39.5, 55) 5266									
11	5611	5741	6031	4000	5152 x 3	.05	11	1.00	2c
(40.5, 55.1) 5173									
12			6021	4000	6552 x 1	.08	15	1.01	2c
(41.5, 55) 4772									

Table 2.2

As Table 2.1 Except For Records Other Than the Polymode Array II.

Station # (latitude, longitude) water depth	Experiment	Record ID	Instrument Depth	Data Length	$\Delta\omega/f$	PH(db)	ω_p/f	Class
542 (28, 69.7) 5462	PMI	5421	500	6500	.1	14	1.01	2a
		5424	1500	5000	.1	11.5	1.04	2a
		5427	4000	"	.09	9.5	1.07	3
543 (28, 65) 5363	"	5431	500	6496	.06	15	.96	2a
		5435	4000	5700	.05	12	.97	2b
545 (27.8, 55.6) 6015	"	5451	500	6720	.11	12.5	1.07	2a
		5453	1000	"	.1	11	.99	2a
		5454	2000	"	.06	12.5	1.02	2a
		5456	4000	5616	.09	11	1.03	2b
546 (27.9, 54.9) 5773	"	5461	500	6720	.1	12.5	.99	2a
		5463	1000	"	.09	12.5	1.02	2a
		5465	2000	"	.1	13.5	1.04	2a
		5467	4000	5616	.13	12	.96	2b
547 (28.2, 54.9) 5785	"	5471	500	6720	.06	14	1.03	2a
		5473	1000	"	.09	12.5	1.00	2a
		5475	4000	5616	.05	12	.98	2b
548 (31, 60) 5550	PMI	5481	500	6664	.09	11	.98	2a
		5485	2000	6600	.07	15	.98	2a
		5486	4000	5160	.1	12	1.01	2b
549 (34, 60) 4687	"	5491	500	6400	.07	11.5	1.03	2a
		5494	2000	5670	.08	12	1.08	2a
		5495	4000	6400	.07	11	1.08	2b

Table 2.2 (cont'd.)

Station # (latitude, longitude) water depth	Experiment	Record ID	Instrument Depth	Data Length	Δω/f	PH(db)	ω_p/f	Class
520 (33.5, 62.6) 4400	Muir Smt.	5202	3023	3182	.21	7.5	1.01	3
623 (27.4, 41.1) 4307	PMIII B	6231	128	8160	.2	10	1.03	2a
		6234	1426	"	.06	18.5	1.00	1
		6237	3927	"	.11	11	1.06	2b
624 (27.3, 40.8) 4372	"	6242	529	"	.09	15	1.00	2a
		6243	1528	"	.06	19	1.00	1
		6245	4028	4150	.2	9.5	1.12	2b
625 (27.2, 40.4) 4723	PMIII B	6251	189	8160	.21	9	1.12	2a
		6253	1488	"	.09	17.5	1.02	1
		6255	3990	"	.11	13	1.02	2b
626 (26.9, 41.2)	"	6263	1514	"	.1	18	1.03	1
		6265	4014	"	.08	10	1.1	2b
627 (26.2, 41.7) 3857	"	6271	206	"	.12	8.5	1.03	2a
		6273	1505	"	.2	15	1.03	1
628 (27.4, 47.8) 4961	PMIII A	6283	1489	7920	.1	17	1.05	1
629 (28, 48.1) 4954	"	6291	203	"	.18	10	1.04	2a
		6293	1500	"	.08	20	1.01	1
		6295	4006	"	.05	16	1.04	2b

Table 2.2 (cont'd.)

Station # (latitude, longitude) water depth	Experiment	Record ID	Instrument Depth	Data Length	$\Delta\omega/f$	PH(db)	ω_p/f	Class
630 (27.9, 48.7) 4908	PMIII A	6301	200	7920	.09	13	.99	2a
		6304	1498	"	.1	17.5	.99	1
631 (27.9, 48.9) 5106	"	6311	212	"	.05	14.5	1.02	2a
		6315	4016	"	.14	14	.99	2b
632 (26.9, 49.2) 4881	"	6321	190	"	.15	11.5	1.03	2a
		6323	1488	3936	.1	18.5	1.00	1
		6325	3993	7920	.05	15.5	.99	2b
79 (16.7, 54.3) 5523	PMIII C	7901	194	8400	.1	10.5	1.03	2a
		7903	338	"	.16	10.5	1.01	2a
		7904	538	"	.21	7.5	1.06	2a
		7908	4038	"	.27	7.0	1.15	2b
80 (15.4, 53.9) 5294	"	8003	319	"	.16	9.5	1.04	2a
		8004	520	"	.11	9.5	1.06	2a
		8008	4020	"	.19	9.5	1.13	2b
81 (15.2, 53.2) 5281	PMIII C	8101	160	8400	.11	9.5	1.01	2a
		8104	510	"	.13	9.5	1.09	2a
		8107	2508	"	.19	9.5	1.00	2b
		8108	4008	"	.15	10.0	1.04	2b
82 (15, 54.2) 5248	"	8201	172	"	.1	10.0	1.00	2a
		8203	322	"	.15	9.5	1.02	2a
		8204	522	"	.26	6.5	1.03	2a
		8207	2446	"	.19	9.0	1.08	2b
		8208	3946	"	.24	10.0	1.13	2b

Up to three consecutive segments of data have been collected (~ 27

months) at some sites of the PMII. In order to avoid contamination from

low frequency motions, each segment of data was first tapered to zero at

both ends and then Fourier transformed. The tapering data window is

$$w_t = 0.5 - 0.5 \cos(10 \pi \ t/T) \quad \text{for } 0 \leq t \leq 0.1 \ T$$
$$\text{and } 0.9 \ T \leq t \leq T , \quad (2.1)$$

$$w_t = 1 \quad \text{for } 0.1 \ T \leq t \leq 0.9 \ T,$$

where T is the data length. The leakage of power to adjacent bands is

less than 10 % (see Hendry, 1975, Appendix A). Compromising between

resolution and stability, the spectral estimates were obtained by

averaging the resulting periodogram over several adjacent frequency

bands. Near the inertial frequency f, the resulting resolution is about

0.0012 cph, which is, for instance, 2.4 % of f at 36°. For those

stations with more than one segment of data, the spectrum of each

segment was then ensemble averaged to obtain more degrees of freedom.

The least degrees of freedom is 14.

2.3 The observed spectra

For a typical record in the main thermocline (600 m at Station 5),

the two cartesian components of horizontal kinetic energy spectrum are

displayed in Fig. 2.2. Because these two spectra generally cannot be

distinguished in the whole internal wave band, either one can be used to

represent the horizontal kinetic energy spectrum $F_H(\omega)$. For

frequencies remote from the inertial, tidal, and buoyancy frequencies,

$F_H(\omega)$ can be well described by a power law of the following form :
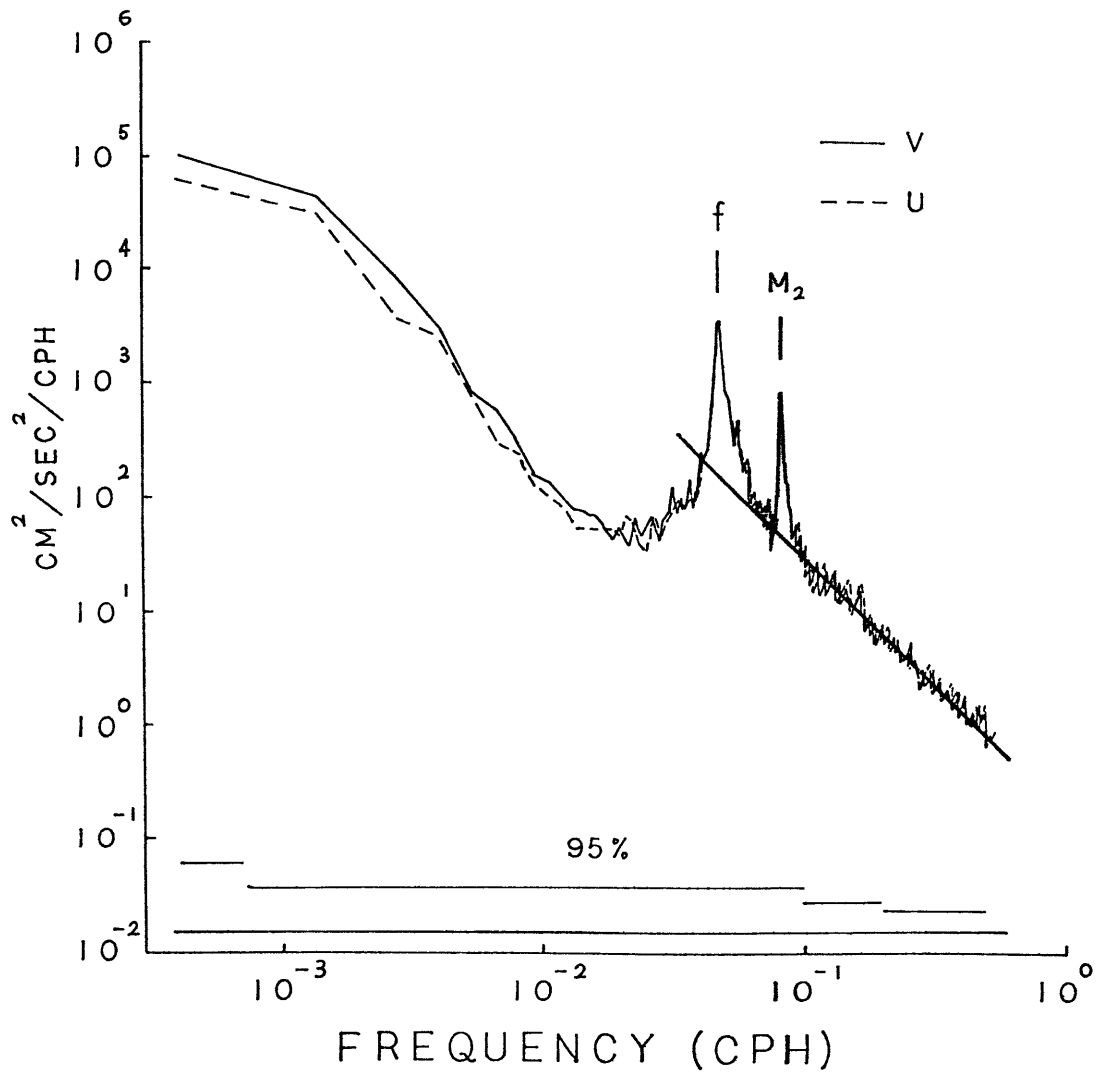
Figure 2.2   Spectra of u and v components at 600 m at Station 5 of the PMII. CPH represents cycle per hour. The straight line represents the power law $E_oN \omega^{-p}$ with N = 2.27 cph, E_o=0.096 $cm^2/sec^2/cph^2$, and p = 2.23. Shown on the bottom are the 95 % confidence intervals.

$$F_H(\omega) = N(z)\, E_o\, (\omega/\omega_o)^{-P}, \qquad\qquad (2.2)$$

where N(z) is the buoyancy frequency in cph at depth z, E_o a constant
in $cm^2/sec^2/cph^2$, ω a frequency in cph, $\omega_o = 1$ cph, and p a
dimensionless constant. Presumably the constants E_o and p are
independent of z, because in this frequency regime $F_H(\omega)$ should be
proportional to N(z) as consistent with the WKBJ scaling. As ω
approaches f, the spectral level begins to rise above that given by
(2.2) and forms a prominent peak near f -- the so-called inertial peak.
Because the essential characteristics of a spectral peak are its energy
level, frequency ω_p, and bandwidth $\Delta\omega$, we have tabulated these three
parameters for each record in Tables 2.1 and 2.2. The bandwidth is
defined as the difference between the frequencies where the power falls
to one half of its peak value. The tabulated values of both ω_p and $\Delta\omega$
are in units of f. The energy level of the peak is expressed in terms of
its ratio to the value given by (2.2) with ω equal to the peak
frequency, and the logarithm of this ratio is defined as the "peak
height", denoted by PH in decibels (db hereafter, defined as $10 \times \log_{10}$).
For the spectrum shown in Fig. 2.2, $\Delta\omega = .05$ f, $\omega_p = $ f, and PH= 13.5 db
(with $E_o = .096$, p= 2.23).

In order to determine the peak height in a precise way, we first
need a standard procedure to determine the constants E_o and p in
(2.2). For the universal spectrum proposed by Garrett and Munk (1972),
$E_o \approx 0.13$, and $p \approx 2$. Because significant deviations from the
universal spectrum have been documented by Wunsch (1976) and Wunsch and
Webb (1979), we will not use the universal values but apply a

least-squares to fit the observed spectra to (2.2) between 0.1 cph and

0.8 $N(z)$ for each record, with E_o and p as parameters to be found. All

the tabulated values of PH were estimated based on E_o and p obtained

through this procedure. As expected, the values of E_o and p do not

vary much over most of the records, but we have found some anomalous

records. For selected stations which are representative of nearby ones,

if any, within 200 km, the values of E_o and p are listed in Table 2.3

together with those of E_{H5}', which is the value of $F_H(\omega)/N(z)$

calculated at the frequency corresponding to a 5-hour period (for GM

spectrum, $E_{H5}' \approx 3.3$). Note that E_{H5}' is different from E_5'

tabulated by Wunsch (1976); this latter is the normalized total energy

at 5-hour period.

The anomalous records are those of the PMIII clusters A and B,

where the values of E_o and p at nominal depths 1500 m and 4000 m are

significantly different from the others -- E_o is higher and p is

lower. The values of E_{H5}' are also higher here, but by less than an

order of magnitude; together with the small values of p, the higher

values of E_{H5}' imply that internal wave energy at periods shorter than

5 hours is significantly higher in these records than the others, up to

an order of magnitude. The WKBJ scaling does not work here at all (see

Fig. 2.3c), but it works so well at other stations that the values at

one depth are representative of the whole water column (away from the

upper and lower boundaries though). The reason for the breakdown of WKBJ

scaling here is unclear; however, it is very likely associated with the

proximity to the Mid-Atlantic Ridge (about 300 km from either cluster)

and the very rough underlying topography.

Table 2.3

Tabulation of Estimated Buoyancy Frequency N, Parameters Eo and p in Eq. (2.2)
(parenthetical values are standard errors of fit), and the normalized
horizontal kinetic energy at 5 h period (E_{H5}') for selected records.

Station #	Experiment	Latitude (N), Longitude (W) (deg)	Instrument Depth (m)	N (cph)	E_0	p	E_{H5}'
1	PMII	35.9, 55	600	2.16	.14 (.17, .12)	2.13 ± .11	4.3
4	"	36, 53.8	600	2.23	.087 (.11, .071)	2.28 ± .13	3.4
5	"	34.9, 55	"	2.27	.096 (.12, .078)	2.23 ± .14	3.5
6	"	35.9, 59	"	2.34	.084 (.1, .071)	2.13 ± .11	2.6
7	"	31.6, 55.1	"	2.3	.061 (.073, .051)	1.97 ± .12	1.5
8	"	37.5, 55	"	2.35	.097 (.12, .079)	2.25 ± .13	3.6
10	"	39.5, 55	4000	.4	.078 (.11, .057)	2.41 ± .18	3.8
12	"	41.5, 55	"	.36	.041 (.064, .027)	2.56 ± .25	2.6
542	PMI	28, 69.7	500	2.18	.042 (.05, .035)	2.03 ± .11	1.1
543	"	28, 65	500	2.32	.046 (.055, .039)	2.04 ± .11	1.2
546	"	27.9, 54.9	"	2.32	.066 (.084, .051)	1.96 ± .16	1.6
548	"	31, 60	"	2.1	.047 (.057, .039)	2.2 ± .13	1.6
549	"	34, 60	"	2.12	.053 (.066, .043)	2.3 ± .14	2.2
6231	PMIII B	27.4, 41.1	128	2.92	.16 (.2, .12)	1.65 ± .15	2.2
6234	"	"	1426	.97	1.2 (1.6, .96)	.86 ± .16	4.9
6237	"	"	3927	.22	1.7 (4.2, .66)	1.05 ± .5	9.0
6291	PMIII A	28, 48.1	203	2.32	.14 (.18, .11)	1.71 ± .16	2.2
6293	"	"	1500	.96	.96 (1.2, .75)	.97 ± .16	4.6
6295	"	"	4006	.32	.59 (1.25, .28)	1.27 ± .41	4.6
82	PMIII C	15, 54.2	522	2.03	.061 (.071, .053)	1.91 ± .1	1.3

2.3a Variability and classification

The three parameters discussed above can be used as three different indices for the description of the spectral shape near f, while the corresponding energy level can be inferred with the aid of Table 2.3. A variety of spectral shapes have been reflected in the great variability of these parameters : from 4 db to 20 db for PH; from .03 f to .27 f for $\Delta \omega$; from 0.96 f to 1.15 f for ω_p . Hence a universal frequency spectrum near f is impossible. One of the major tasks of this chapter is to find if there is any correlation between this variability and the physical environment (instrument depth, topography, etc.) in which the measurements were taken. Because the spectral shape is grossly determined by its peak height, we first consider the variability of the peak height.

Normalized spectra of horizontal kinetic energy at three stations which are typical of three different topographic features –– abyssal plain, rough relief, and very rough relief close to the Mid-Atlantic Ridge–– are displayed in Figs. 2.3a, b, and c respectively. In Fig 2.3a the peak height at 4000 m ($\sim$ 7 db) is significantly less than that at upper levels ($\gtrsim$ 10 db), but the high frequency portion of the spectra scale in the WKBJ sense. In Fig. 2.3b spectra at different levels are almost indistinguishable from one another through the whole internal wave band, with peak height about the same as that at upper levels in Fig. 2.3a. Displayed in Fig. 2.3c are the anomalous spectra noted before; the peak height at 1426 m is outstanding as compared to the other two levels where the peak height is about the same as in Fig. 2.3b. The separation of spectral levels at high frequencies is striking here; at
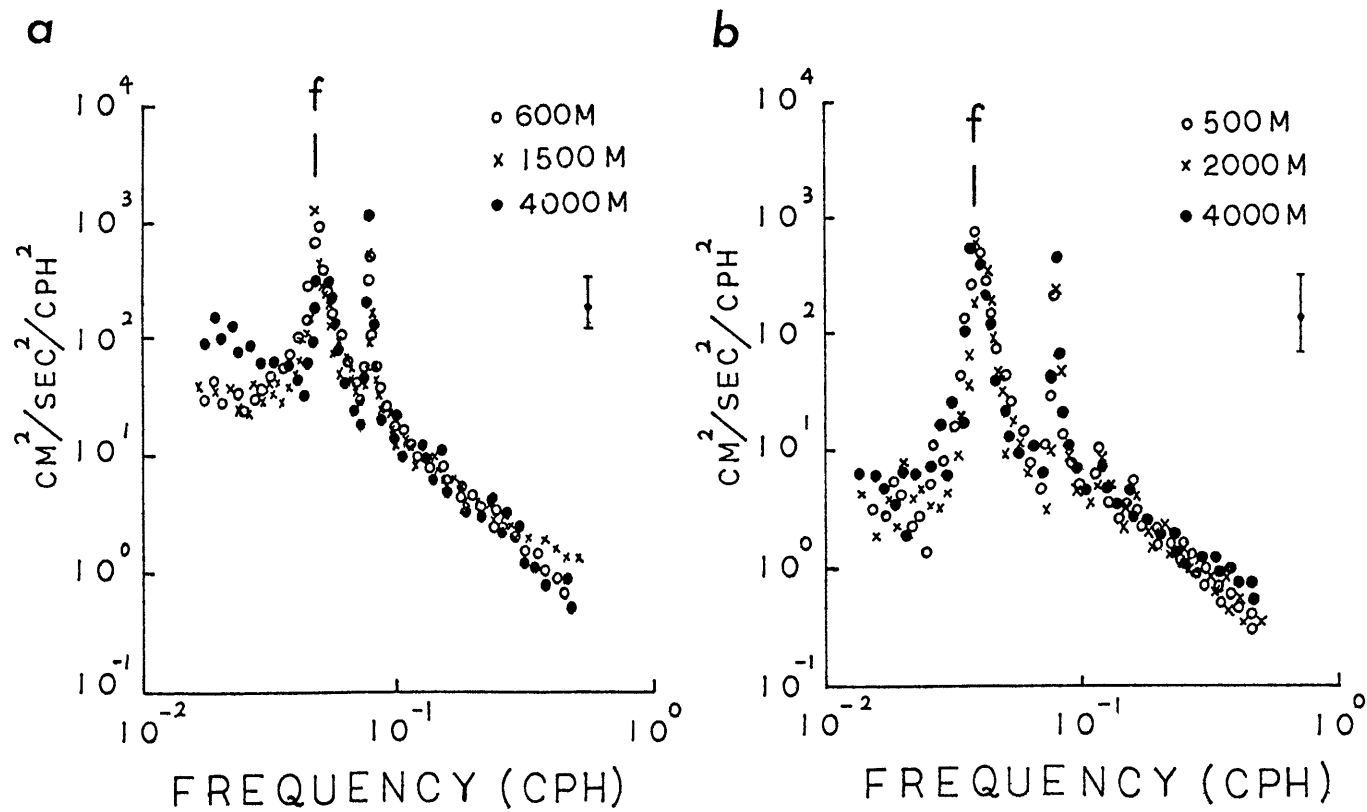
Figure 2.3   Normalized horizontal kinetic energy spectra at (a)
Station 3 of the PMII (smooth topography) and (b) Station 546 of
the PMI (rough topography). Error bar is 95 % confidence limit.
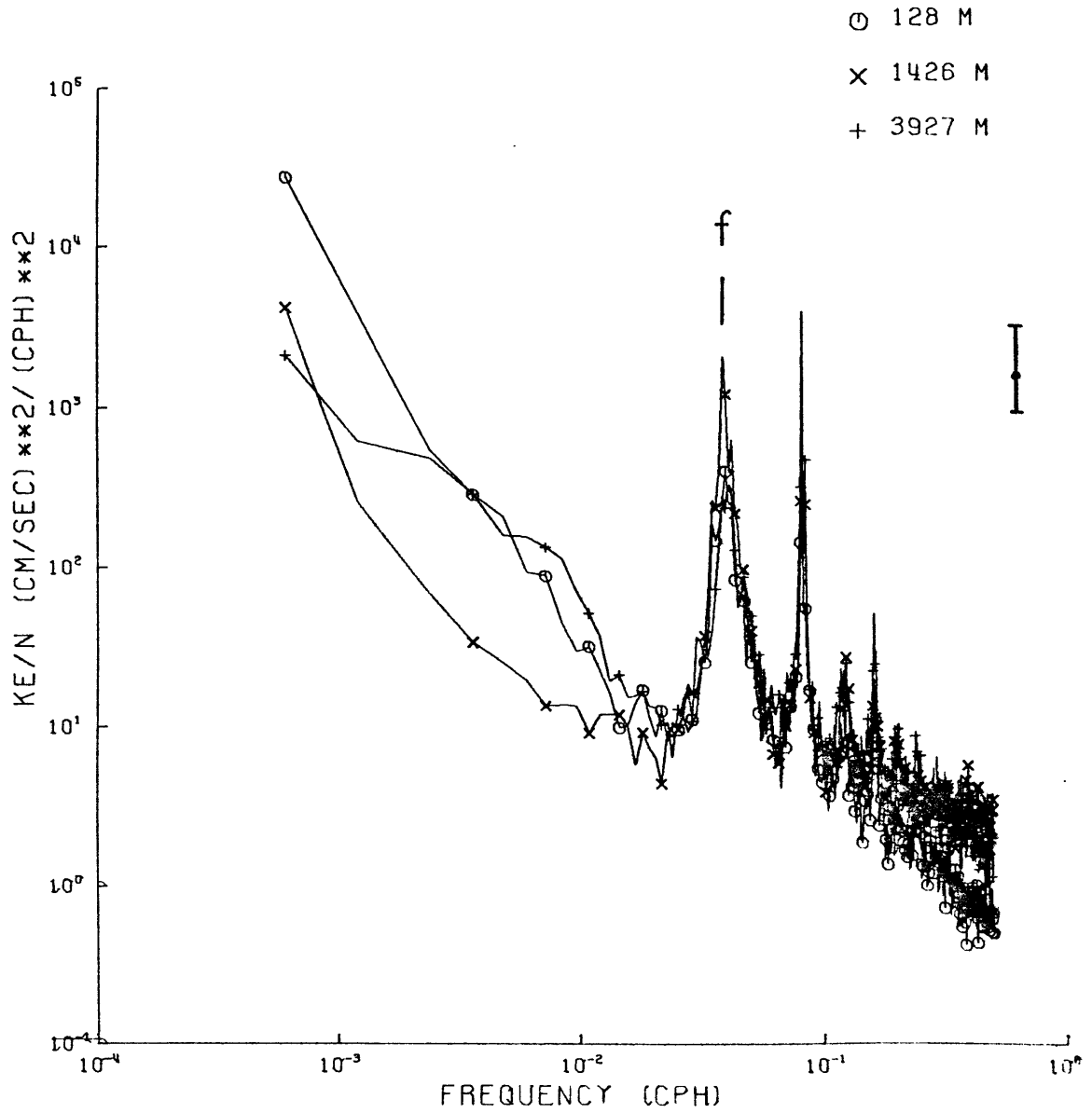
Figure 2.3c As in Fig. 2.3 except at Station 623 of the PMIII cluster B (near the Mid-Atlantic Ridge, very rough topography)

1426 m and 3927 m, p $\approx$ 1 and the normalized high frequency energy is significantly higher than that at 128 m. After further exploration, it was found that the peak height at 4000 m underneath the Gulf Stream (Stations 9, 10, 11, 12) was also about the same as in Fig. 2.3b, although the topography was smooth there. Thus, the different kinds of environment can be roughly grouped into three classes according to their corresponding peak height as follows :

class 1

     nominal depth of 1500 m near the Mid-Atlantic Ridge.

     average PH : 18 db

class 2

     (a) depth less than 2000 m (excluding class 1);

     (b) depth greater than 2000 m over rough topography ;

     (c) nominal depth of 4000 m underneath the Gulf Stream.

     average PH : 11.5 db

class 3

     depth greater than 2000 m over smooth topography.

     (excluding class 2c)

     average PH : 7.5 db

The classification of each record has been noted in Tables 2.1 and 2.2. Displayed in Fig. 2.4 is the histogram of the distribution of peak height of all the records examined, with contributions from different classes properly labeled. The substantial overlap between class 1 and class 2 is basically caused by the ambiguity in identifying the class for some smooth areas which are adjacent (within about 100 km) to rough

Figure 2.4   Histogram of the peak height (PH) distribution.
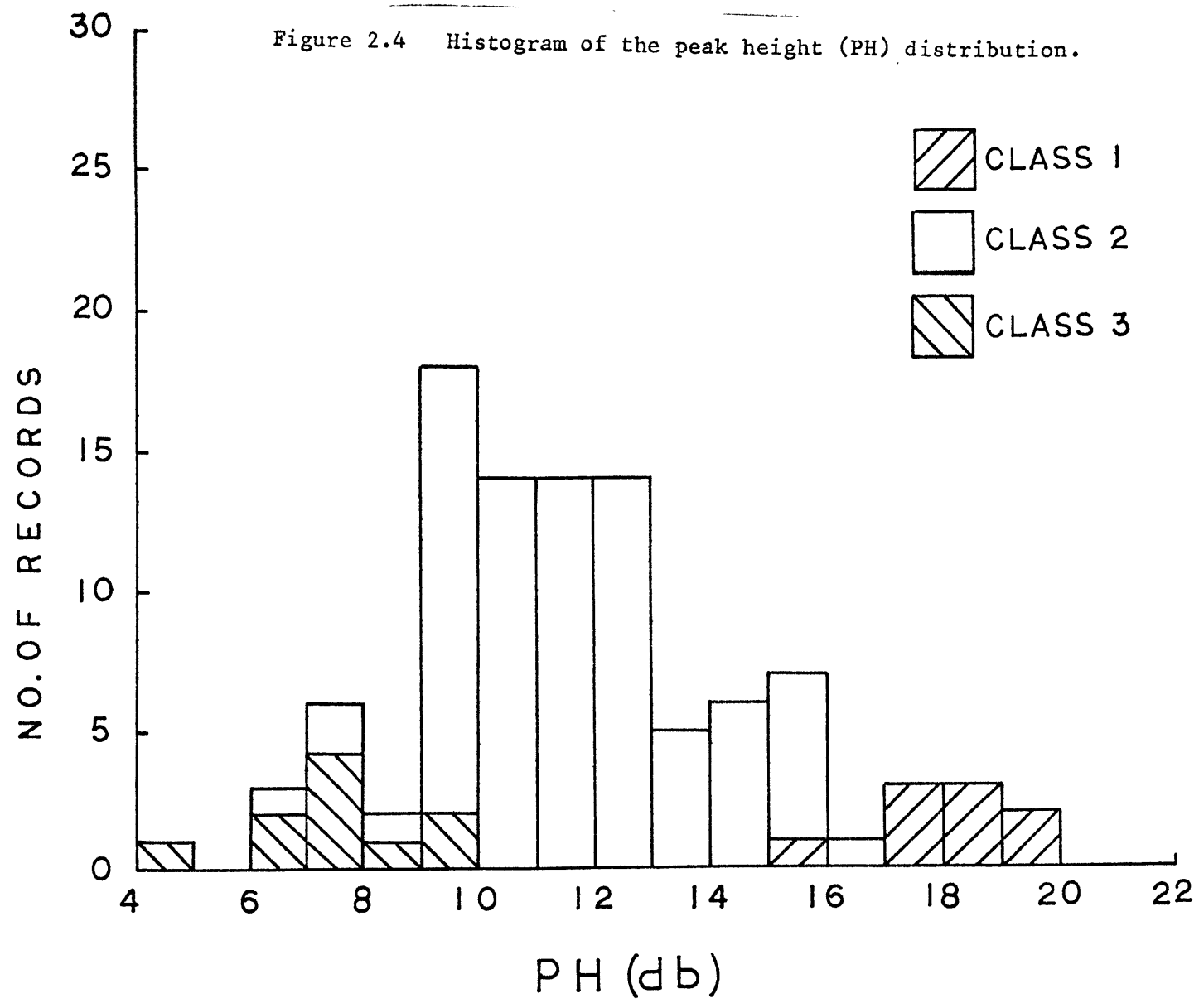
areas. Due to the propagation of inertial waves, the influence of rough topography can easily spread to nearby areas. Despite some degree of looseness, this scheme of classification does provide a sensible way to describe such a great variability of spectral shape.

The lowest peak height from a class 3 environment is associated with the record at the 4000 m level of Station 6, which is in the midst of the New England Seamount Chain and is partially surrounded by seamounts (about 180° azimuth -- SE, NE, and NW). Normalized kinetic energy spectra of this record are shown in Fig. 2.5. The disappearance of a prominent inertial peak here is a unique feature in the whole data set. It is probably caused by the nearby seamounts (the nearest one is about 50 km away), of which some penetrate to less than 2000 m from the sea surface. However, the record at 3000 m of Station 520 which is only 12 km away from the Muir Seamount, shows a prominent peak of 7.5 db. Therefore the overall influence of seamounts on the spectrum of inertial waves, if any, is not particularly clear.

2.3b Frequency shift of the inertial peak

It is well known now that in the deep ocean the inertial peak usually occurs not right at the local f, but at a frequency slightly above it. Theory suggests that only waves with super-inertial frequencies can propagate downward from the surface layer, which presumably is the major source for deep inertial waves. But does this so-called blue shift occur universally in the deep ocean ? Does it vary with depth and geographical environment and consequently with peak height ?

The ratios of the peak frequency ω_p to f for all the records are
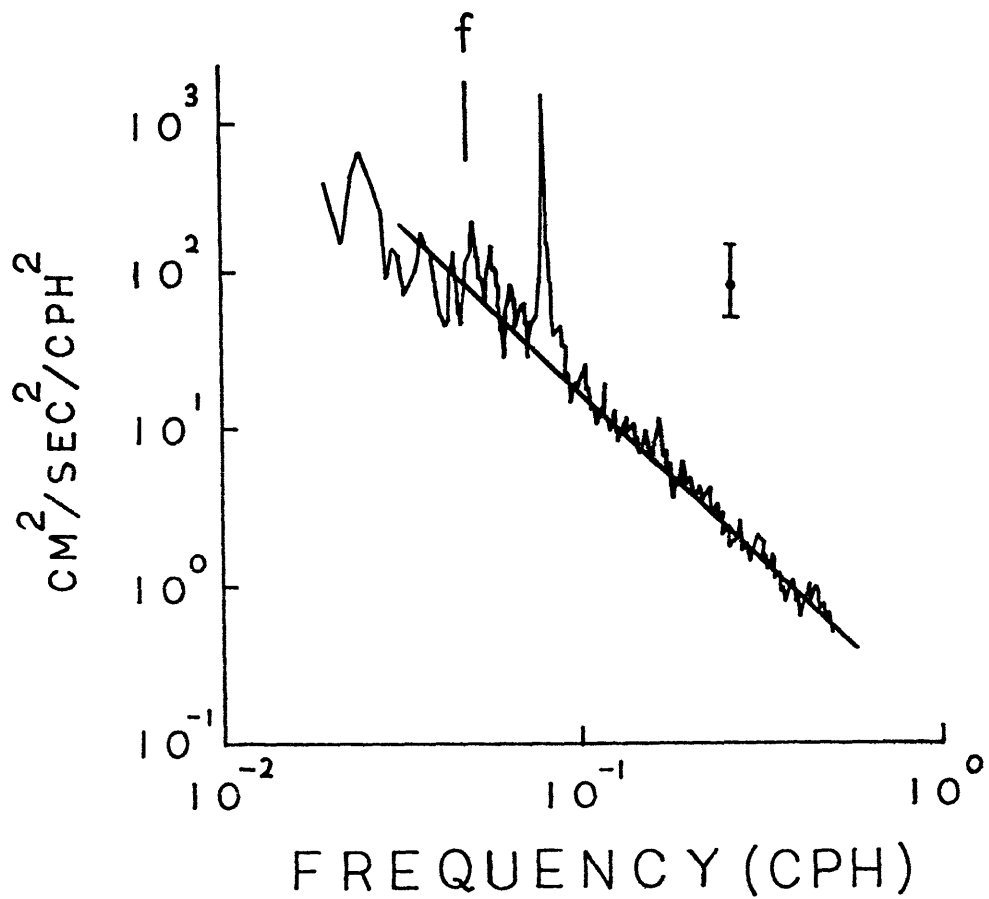
Figure 2.5   Normalized horizontal kinetic energy spectrum at 4000 m, Station 6, PMII. The straight line represents the power law fit. Error bar is 95 % confidence limit.

plotted against depth in Fig. 2.6. The dashed lines represent the limits of the frequency resolution associated with $\omega_p/f = 1$, i.e., ω_p/f is significantly different from 1 for those points outside the strip enclosed by the dashed lines. Over smooth topography, it is clear that a significant blue shift occurs at great depths except near the Gulf Stream, where the peak height is greater. The results over rough topography are mixed; a clear blue shift with depth only occurs at the PMIII cluster C, where the topography is not particularly rough and the corresponding peak height is on the lower side of the class 2 distribution (see Table 2.1). Thus there seems to be some correlation between the blue shift and peak height. In Fig. 2.7 ω_p/f is plotted against peak height for all the 4000 m records except Station 6 where there is no peak. The blue shift is apparently associated with records having lower peak height, which are primarily from the class 3 environment. This result is consistent with the notion that inertial waves in the class 3 environment are free waves coming from elsewhere, whereas those in the class 1 and class 2 are strongly influenced by local sources.

2.3c Bandwidth

The inverse of the bandwidth in a frequency spectrum is a measure of the persistence time scale of a quasi-periodic motion. For instance, if $\Delta\omega/f = 0.1$, then the persistence time scale of inertial waves is about ten inertial periods. From Tables 2.1 and 2.2 $\Delta\omega/f$ has no specific relations with PH but has some weak, if not definite, correlation with latitude. Listed in Table 2.4 is the ensemble average
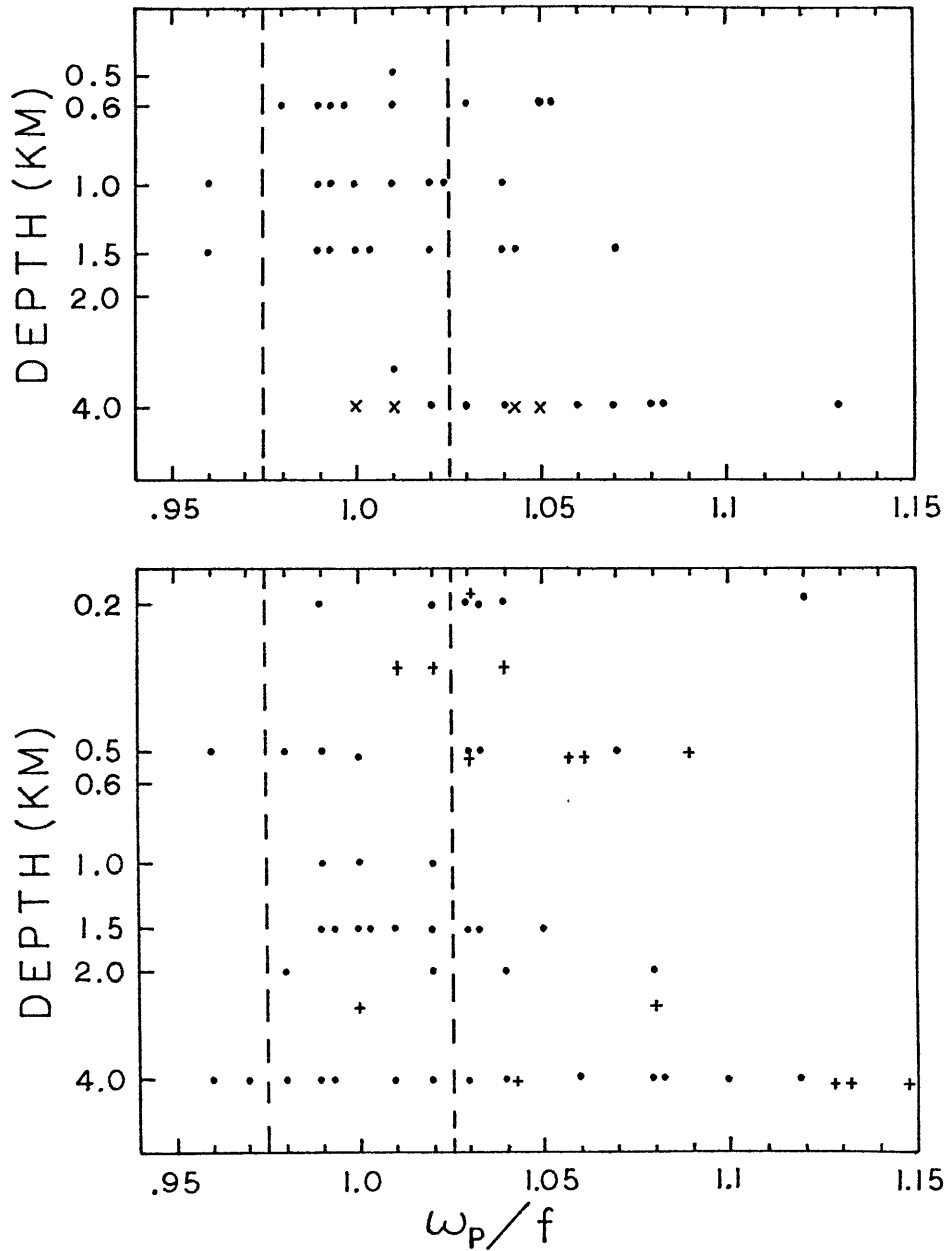
Figure 2.6   Ratio of the peak frequency ω_p to f against instrument depth. Upper panel is for smooth topography areas; lower panel is for rough topography areas. Special symbols :   X -- measurements underneath the Gulf Stream; + -- PMIII C. Dashed lines represent the frequency resolution limits associated with ω_p/f =1.
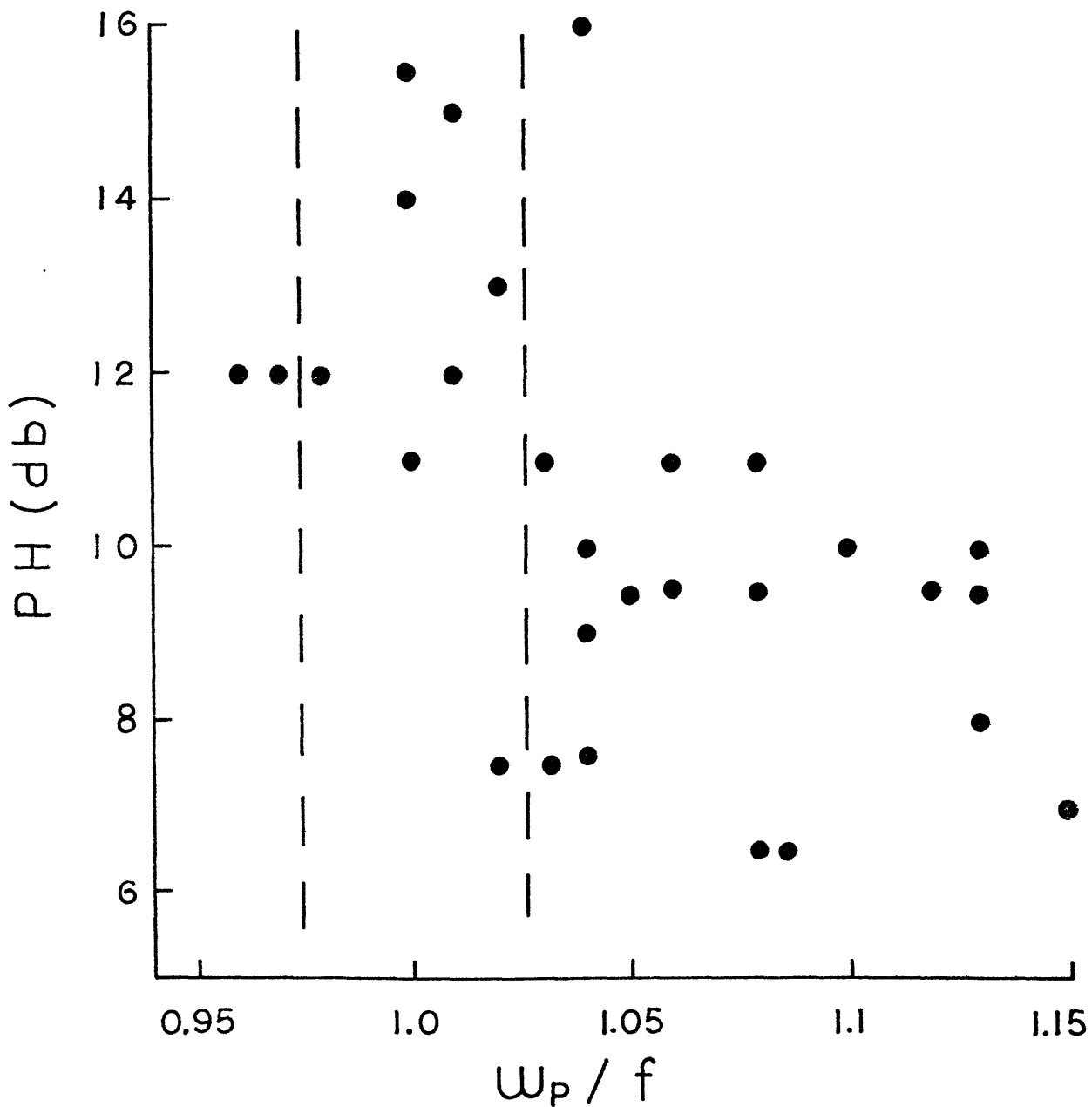
Figure 2.7 ω_p/f against peak height (PH) at 4000 m. Dashed lines are the same as in Fig. 2.6.

of $\Delta\omega/f$ within given latitudinal belt. The value at subtropical latitudes (15° - 20°) is significantly greater than those at mid-latitudes. This result is consistent with the model to be described in chapter 4.

Table 2.4

Average bandwidth (in percentage of f) at various latitudes. Errors are standard deviations.

latitude	average bandwidth
15°-20°	.17 ± .055
25°-30°	.1 ± .044
30°-35°	.095 ± .036
35°-42°	.097 ± .047

2.3d Rotary spectrum

In addition to cartesian components, horizontal kinetic energy also can be decomposed into its rotary components. These have proven useful in separating inertial wave energy from other current components (Gonella, 1972; Mooers, 1973). For the same record shown in Fig. 2.2, the spectra of the two rotary components are shown in Fig. 2.8. The rotational nature of inertial waves is clearly demonstrated by the dominance of the clockwise component spectrum $E_-(\omega)$ over the counter-clockwise component spectrum $E_+(\omega)$. This dominance begins at sub-inertial frequencies, reaches its maximum near f, and continues through the whole internal wave band; on the other hand, $E_+(\omega)$
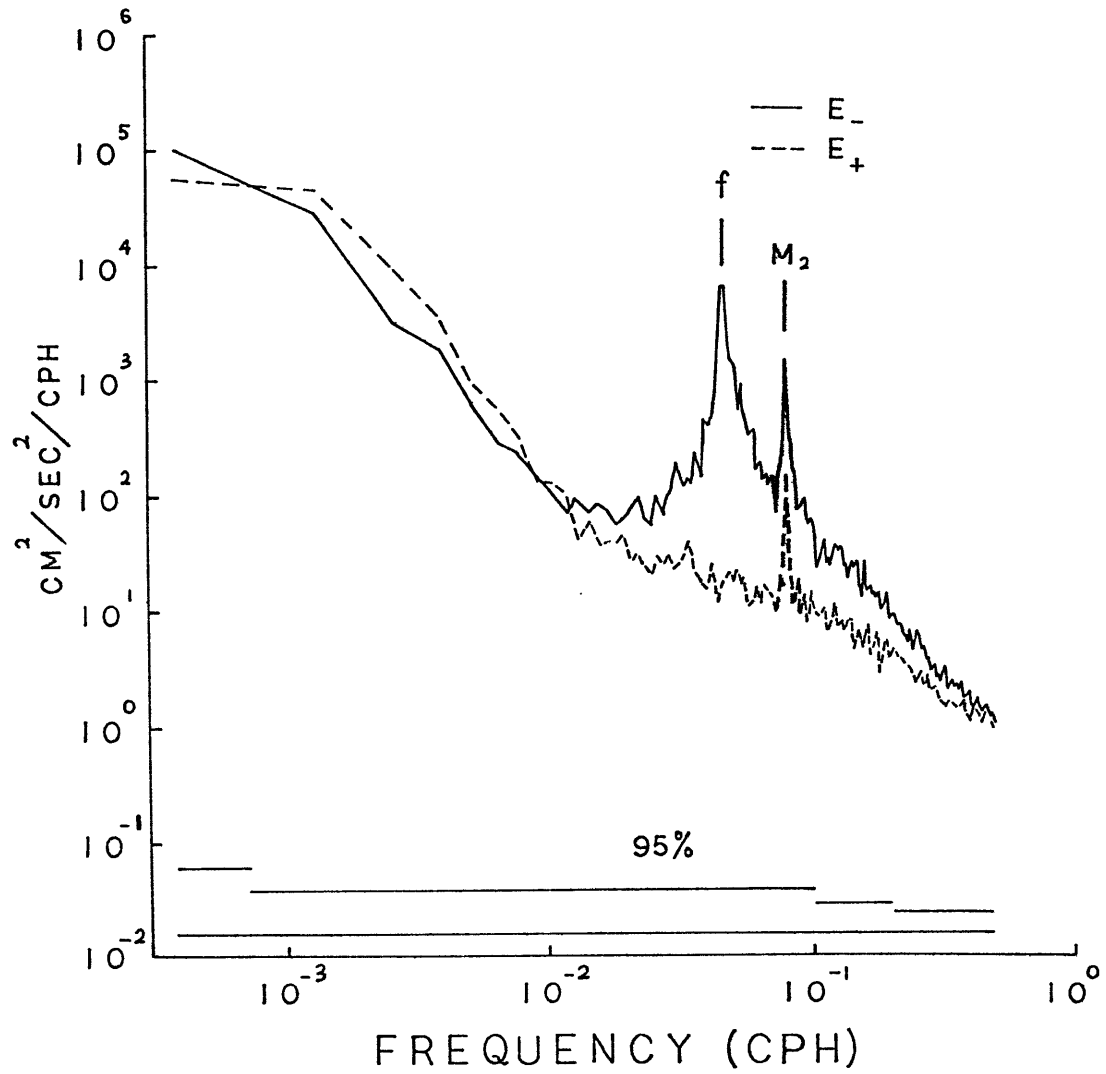
Figure 2.8   Rotary spectra of the same record as in Fig. 2.2.
E_ -- clockwise component; E_+ -- counter-clockwise component.

decreases monotonously and smoothly with frequency. This behavior is typical of all the records and basically consistent with the linear internal wave theory which predicts

$$\frac{E_-(\omega)}{E_+(\omega)} = \left(\frac{\omega + f}{\omega - f}\right)^2 \tag{2.3}$$

Because (2.3) was derived from an f-plane model, the infinite ratio at $\omega = f$ is spurious (see Chapter 4). The cause of the dominance of clockwise energy at sub-inertial frequencies (as low as 0.4 f in Fig. 2.8) is unclear. It may be due to nonlinear interactions between inertial waves and low frequency motions. Otherwise, spectra in this frequency regime presumably is determined by the process of geostrophic turbulence (Charney, 1971), and the coherence between u and v should be zero and hence no clockwise dominance. Because the turbulent cascading would allow certain amount of energy to be transferred from low to high frequencies, until f is reached, inertial waves would be resonantly forced by energy in the clockwise component; however, energy in the counter-clockwise component would continue cascading to higher frequencies and account for part of the observed finite amount of counter-clockwise energy and its smooth spectrum. By this mechanism, low frequency eddies could be potential local sources for inertial waves. However, a model is needed to verify this speculation.

The most important feature of the rotary spectrum near f is the large ratio of $E_-(f)$ to $E_+(f)$. So it is desirable to use the logarithm of this ratio, denoted by Γ, as an index for the description of the rotary spectrum near f. For instance, Γ is 25 db in

Fig. 2.8. As $E_+(\omega)$ decreases smoothly and monotonously with ω, its shape does not vary much from record to record. Thus Γ should be roughly proportional to PH and should have the same variability. In Fig. 2.9 Γ is plotted against PH for all the records except those of the PMIII clusters A and B, which exhibit the same behavior as the other records near 28°N and hence are omitted. A roughly linear correlation between Γ and PH is visible. The systematically low values of Γ near 28°N are probably caused by the closeness of f to the diurnal tidal frequencies; because tides are forced motions, they could have an appreciable amount of counter-clockwise energy.

2.4 Coherences

The calculation of spatial coherence at a particular frequency ω usually yields two kinds of information: from the coherence scale, Δx, defined as the separation distance at which the coherence drops to one half, one can estimate the wavenumber bandwidth, Δk, of the underlying process at ω as $\Delta k = 4/\Delta x$ (c.f. MP, eq.(59)); from the phase difference and separation distance, one can estimate the dominant wavenumber at ω .

2.4a Horizontal separation

There have been few convincing estimates of the horizontal coherence scale for inertial waves in the open ocean. The horizontal spacings of array measurements have usually been either too small ($\lesssim$ O(1 km), e.g., Webster, 1968; Schott, 1970; Briscoe, 1975) or too large. The only conclusion which can be drawn from previous investigations is that the horizontal coherence scale is at least several kilometers. However, the
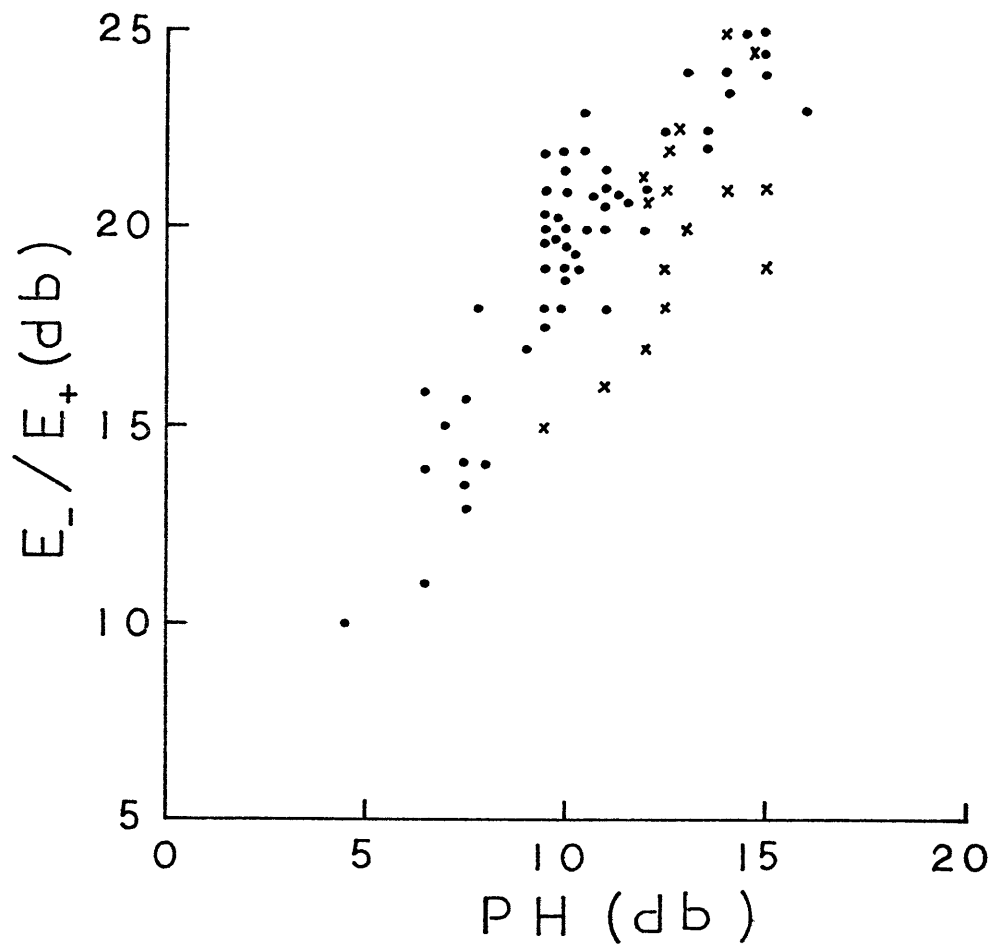
Figure 2.9 E_-/E_+ against peak height (PH). " X " represents the stations roughly along 28°N.

theory of MP suggests that the coherence scale is of the order of tens

of kilometers. There are five clusters of moorings of this size in the

Polymode arrays (see Fig. 2.2) : the central cluster of PMII (36°N,

55°W), the eastern cluster of PMI (28°N, 55° W), the clusters A,

B, and C of PMIII. It is possible now to test the theory of MP using the

coherences estimated from these clusters. Because the major concerns are

inertial waves, all the coherences discussed below are between the

clockwise components of horizontal velocity.

Fig. 2.10 shows the coherence and phase at 600 m between Stations 1

and 2 of the PMII; these moorings are 30 km apart in the zonal

direction. Within a narrow band centered at the local f, the high

coherence and small phase are quite conspicuous. For each of the five

clusters mentioned above, the coherences in the inertial frequency band

have been calculated between selected stations and plotted against

horizontal separation in Fig. 2.11. Each point represents the highest

coherence estimated in three adjacent frequencies of which the central

one is the local f. The coherence is the result of averaging over eleven

frequencies, so the level of no significance at 95 % confidence is about

0.51. In the upper ocean the coherence drops with increasing separation,

yielding a coherence scale of approximately 60 km, which is not

inconsistent with the prediction of MP. So the estimated bandwidth is

1/15 radians/km. In the deep ocean the coherence does not vary so

systematically with separation, and the coherence scale seems to be less

than that in the upper ocean (some high values with large separations

are probably not significant).
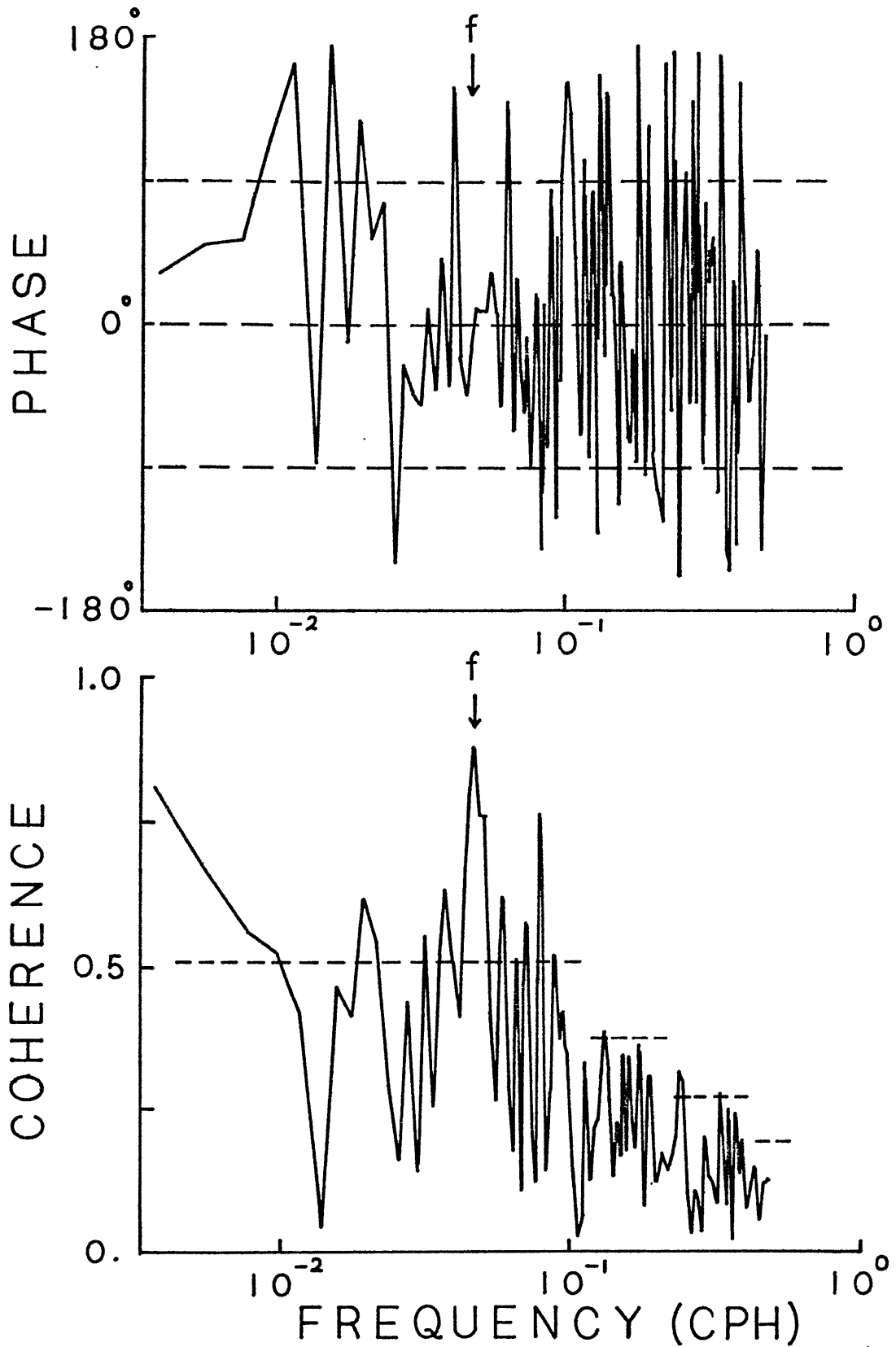
Figure 2.10 Clockwise component coherence and phase between Stations 1 and 2 of the PMII at 600 m. Arrows represent the location of f. Dashed lines in the coherence plot are the 95 % confidence levels of no significance.
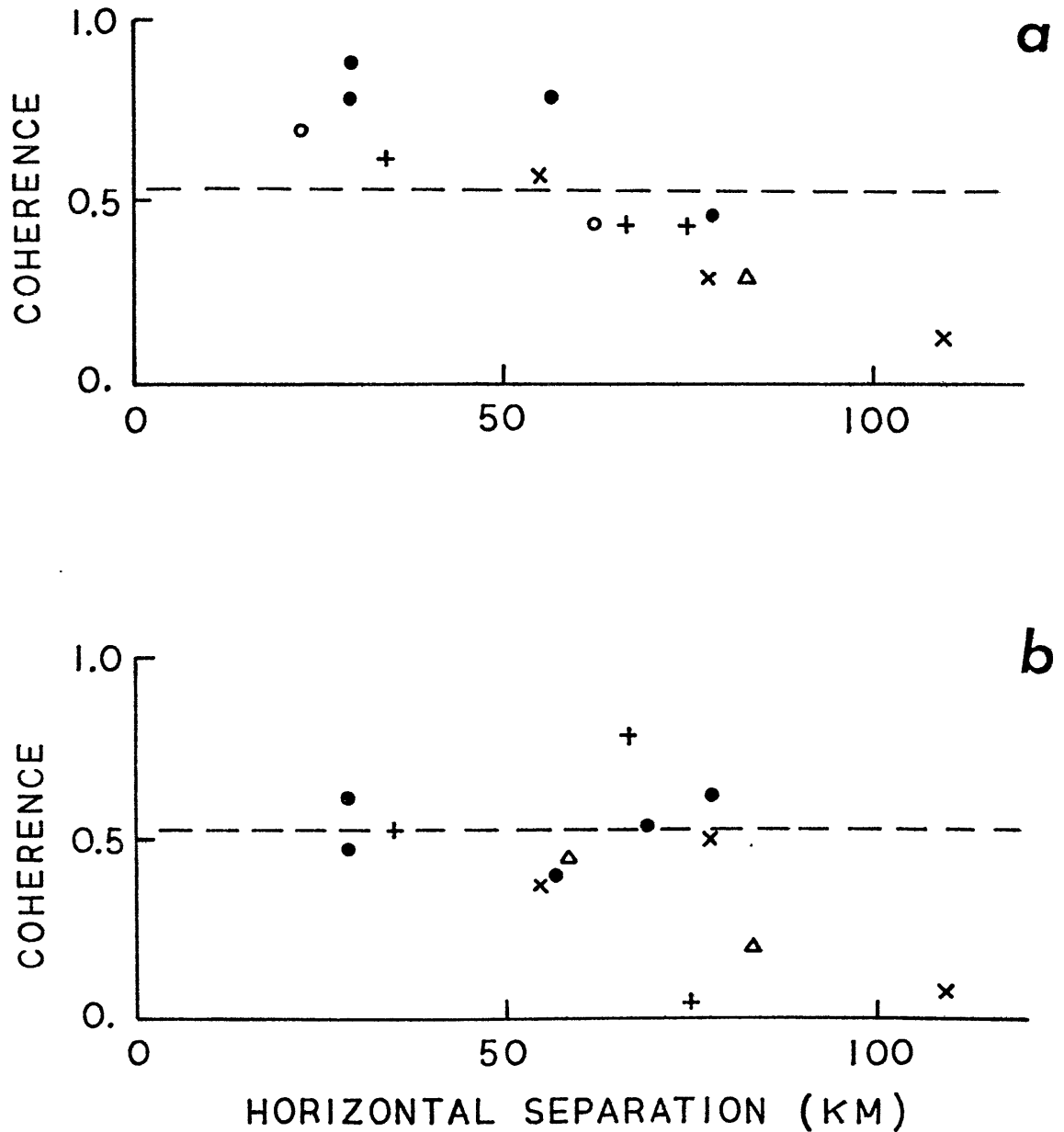
Figure 2.11 Clockwise component coherence against horizontal
separation : (a) at upper levels from 200 m to 600 m; (b) at 4000 m.
Special symbols : + -- PMI ; ● -- PMII ; o -- PMIII A ; Δ -- PMIII B ;
✗ -- PMIII C. Dashed lines are the 95 % confidence levels of no
significance.

The estimates of coherence and phase difference at different depths
for the three closest stations of the central cluster of PMII are listed
in Table 2.5. Horizontal wavenumber spectra have been calculated at each
frequency using these coherence and phase estimates (for the method, see
Wunsch and Hendry, 1972). Due to inadequate array size, the results do
not yield any dominant wavenumbers which are significantly different
from zero and its aliased values. However, recent profiler observations
suggest a horizontal wavelength of the order of 60 km (Sanford, 1979;
personal communication).

2.4b Vertical separation

There have been more reports of the vertical coherence of inertial
waves than of the horizontal one. For example, Webster (1968) reported a
low coherence of 0.3 over 80 meters vertical separation in the upper 100
meters at Site D; Perkins (1970) reported significant coherences even
over 1500 meters separation below the mixed layer in the Mediterranean;
Fomin and Savin (1973) reported that above the main thermocline in the
Black Sea, the coherence decreased rapidly over a distance from 20 to 30
meters, and that below the thermocline, it decreased relatively slowly
with alternating maxima and minima. However, it is generally believed
that below the mixed layer in the open ocean, the vertical coherence
scale of inertial waves is O(70-140m) (Müller et al, 1978). The large
values found in the Mediterranean are probably caused by the atypical
dominance of low modes; indeed, Perkins (1970) showed that the vertical
structure of inertial waves in the Mediterranean could be well described
by the third vertical mode.

Table 2.5

Tabulation of Clockwise Component Coherence Between Horizontally Separated Instruments
    at Three Period Bands of Which the Central One is the Inertial Period.
Parenthetical Values are Phase Differences in Deg. with 95% Confidence Error Bars.

Station pair (separation in km)	Instrument Depth (m)	Coherence		
		21.51 h	20.61 h	19.78 h
1 - 2 (29)	600	.79 (−45 + 21)	.88 (−13 + 15)	.76 (10 + 24)
	1500	.56 (−49 + 44)	.88 (2 + 15)	.76 (10 + 24)
	4000	.16 (−46)	.62 (2 + 36)	.48 (18 + 58)
1 - 3 (29)	600	.51 (42 + 52)	.6 (37 + 38)	.78 (−3 + 22)
	1500	.35 (49)	.72 (31 + 27)	.39 (−18)
	4000	.44 (−86 + 72)	.22 (−26)	.48 (−57 + 58)
2 - 3 (57)	600	.53 (41 + 48)	.71 (55 + 28)	.79 (−11 + 21)
	1500	.69 (143 + 29)	.73 (41 + 26)	.3 (−78)
	4000	.4 (92)	.37 (−119)	.19 (−64)

54

The third mooring at Station 7 (31.6°N, 55°W) was heavily
instrumented below the main thermocline: three additional instruments
were set at 800 m, 950 m, and 1000 m. Clockwise component coherences at
three adjacent frequencies centered at f for these three instruments and
the one at 1500m are listed in Table 2.6. The estimated coherence scale
is of the order of 200 meters. The phase estimates differ significantly
from zero and do not change much from frequency band 1 to band 2, but
drop substantially in band 3; moreover, they are approximately
proportional to the separation distance, suggesting a dominant upward
phase propagation with "local wavelength" about 450 m in bands 1 and 2
and 1100 m in band 3. It should be noted that for the clockwise
component, phase propagation is from the lagging station to the leading
one. From the dispersion relation for internal waves (c.f. Phillips,
1977), upward phase propagation implies downward energy propagation.
This result is consistent with the findings of Leaman and Sanford (1975).

The coherence scale, $\Delta Z_{\frac{1}{2}}$, is related to the "equivalent vertical
wavenumber bandwidth," β_e, or its equivalent mode number, j_e, as
follows (c.f. Müller et al, 1978):

$$\Delta Z_{\frac{1}{2}} = \frac{2}{\beta_e} = \frac{2\,b\,N_o}{j_e\,\pi\,N(z)} \qquad (2.3)$$

where b is the scale of the variation of buoyancy frequency and N_o the
buoyancy frequency at the top of the thermocline. Using the values from
IWEX profile which is not significantly different from that at Station
7, we have bN_o = 5500 m.cph, $N(900m) \approx 2.2$ cph. With $\Delta Z_{\frac{1}{2}}$ = 200m, we
obtain $j_e \approx 8$, which is closer to $j_e = 9$ of Cairns and Williams
(1976) than $j_e = 11$ of Garrett and Munk (1975)(c.f. Müller et al,
1978, Table 1).

Table 2.6

As Table 2.5 Except For Vertically Separated Instruments at Station 7 of the PMII.

Instrument Pair	Coherence		
	24.2 h(#1)	23.1 h(#2)	22.2 h(#3)
800m-950m	.68(92 $\pm$ 30)	.79(106 $\pm$ 21)	.48(57 $\pm$ 58)
950m-1000m	.7(77 $\pm$ 28)	.82(44 $\pm$ 14)	.93(13 $\pm$ 11)
800m-1000m	.64(160 $\pm$ 34)	.83(162 $\pm$ 19)	.43(62 $\pm$ 78)
1000m-1500m	.28(20)	.3(130)	.2(-174)

2.5 Summary

There is no universal spectrum near f, but the deep ocean environment in the Western North Atlantic can be roughly divided into three classes according to the height of the inertial peak above the power law which best fits the high frequency portion of the internal wave spectrum (from 0.1 cph to 0.8 N) : class 1 is the 1500 m level near the Mid-Atlantic Ridge, with the greatest peak height of 18 db; class 2 includes (a) the upper ocean (depth less than 2000 m), (b) the deep ocean (depth greater than 2000 m) over rough topography, and (c) the deep ocean underneath the Gulf Stream, with intermediate peak height of 11.5 db; class 3 is the deep ocean over smooth topography, with the lowest peak height of 7.5 db.

Substantial blue shift of the inertial peak is basically associated with low values of peak height at great depths. The bandwidth near 15°N ($\sim$ 0.17 f) is greater than that north of 25° ($\sim$ 0.1 f).

For horizontal separation, the coherence scale in the inertial frequency band is of the order of 60 km at depths from 200 m to 600 m, and probably less than this value at great depths. The order of magnitude is consistent with the prediction of Munk and Phillips (1968). The wavenumbers estimated from phase differences tend to be indistinguishable from zero. For vertical separation, the coherence scale is of the order of 200 m just below the main thermocline and the phase differences suggest an upward phase (downward energy) propagation. The estimated vertical wavenumber bandwidth is in close agreement with the result of Cairns and Williams (1976).

Interpretation of the results summarized above is the central theme

of later chapters, especially the answer to the following question: Can we describe the differences among the three classes of observations in terms of the proposed global and local wave models ?

Chapter 3   Theory of Low Frequency Internal Waves on a

Rotating Sphere

3.1 Dynamical equations

An approximation to the dynamics of internal waves is most easily

formulated using the equations of motion on an f-plane (e.g., Phillips,

1977), under the assumption that the horizontal wavelengths are so small

that the variation of f will not be "felt". This is essentially the WKBJ

approximation to the horizontal wave equation. From the dispersion

relation

$$\alpha = \frac{m\left(\omega^2 - f^2\right)^{\frac{1}{2}}}{\left(N^2 - \omega^2\right)^{\frac{1}{2}}} \quad , \tag{3.1}$$

where α and m are the horizontal and vertical wavenumbers respectively,

we can clearly see the breakdown of the WKBJ approximation when ω =f,

resulting in an infinite horizontal wavelength. To resolve this problem,

we have to resort to the theory of planetary waves which takes the

sphericity of the earth into account. In order to obtain a tractable set

of equations of motion, the usual assumptions made about the earth's

oceans and atmosphere are

(i)   small perturbations relative to a uniformly rotating spherical

earth,

(ii)   a uniform gravity field,

(iii) radial variation of the metrical coefficients is negligible,

(iv)   the depth of the atmosphere and/or ocean is constant and small

when compared to the earth's radius,

(v)   Boussinesq approximation for the stratification.

The validity of (i)--(iv) was discussed by Miles (1974), and that of (v) was discussed by Spiegel and Veronis (1960). Then the perturbation equations can be written as (c.f. Eckart, 1960)

$$\frac{\partial u}{\partial t} - 2\Omega \sin\phi \, v - 2\Omega \cos\phi \, w = -\frac{1}{R\cos\phi} \frac{\partial P}{\partial \lambda} \tag{3.2}$$

$$\frac{\partial v}{\partial t} + 2\Omega \sin\phi \, u = -\frac{1}{R} \frac{\partial P}{\partial \phi} \tag{3.3}$$

$$\frac{\partial w}{\partial t} + 2\Omega \cos\phi \, u = -\frac{\partial P}{\partial z^*} - g\frac{\rho}{\rho_0} \tag{3.4}$$

$$\frac{1}{R\cos\phi} \left[\frac{\partial u}{\partial \lambda} + \frac{\partial}{\partial \phi}(v\cos\phi) \right] + \frac{\partial w}{\partial z^*} = 0 \tag{3.5}$$

$$\frac{\partial \rho}{\partial t} - \frac{\rho_0}{g} N^2(z^*) \, w = 0 \tag{3.6}$$

where u, v, w, are the zonal, meridional, and radial components of velocity; p is the pressure; ρ and ρ_0 are the perturbation and mean density; g is the gravity constant; $N(z^*)$ is the buoyancy frequency at depth z^*; R and Ω are the radius and rotational frequency of the earth; ϕ and λ are the latitude and longitude.

Because the inertial frequency is usually much smaller than the buoyancy frequency in the ocean, the acceleration of vertical velocity can be neglected in (3.4) for inertial waves -- the hydrostatic approximation. For wave motions of small vertical extent, which is the case of large scale waves as a consequence of condition (iv), the vertical velocity is smaller than the horizontal ones by a factor of

order (H/R), where H is the ocean depth. Therefore the term $2\Omega \cos\phi$ w

in (3.2) can be neglected on this ground. The term $2\Omega \cos\phi$ u in (3.4) is

almost always neglected for the convenience of maintaining a self-adjoint

system (Eckart, 1960). Phillips (1966) showed that these two terms had

to be neglected in Eqs. (3.2)-(3.6) in order to satisfy the conservation

of angular momentum (also see Veronis, 1968). The approximation

associated with the neglect of the horizontal component of the earth's

rotation is usually called the "traditional approximation", which makes

the solutions to (3.2) — (3.6) separable.

3.2 The traditional approximation

Among the various approximations mentioned above, the traditional

approximation is the most controversial one and satisfactory

justification is hard to find in the literature. The neglect of the

terms involving $2\Omega \cos\phi$ is formally correct in the limit $H/R \rightarrow 0$. For

a homogeneous fluid, the resulting equations are the famous Laplace's

tidal equations (LTE hereafter; c.f. Lamb, 1932). Stewartson and Rickard

(1969) carried out a formal expansion in powers of H/R, in which the

first term was the Longuet-Higgins' solution of the LTE (1968). They

found that, near the inertial latitudes where $\sin\phi = \pm\frac{\omega}{2\Omega}$, there was an

unintegrable singularity in the second order terms. After developing an

inner expansion around the inertial latitudes, they could not match the

inner and outer solutions and described the perturbation solutions as

"pathological". Moreover, the pathological solutions were not confined

within the neighborhood of inertial latitudes, but spread over the whole

sphere. By introducing a constant weak stratification N and making a

double expansion in H/R and $(N/\Omega)^2(H/R)^2$, Stewartson and Walton (1976)

were able to resolve the matching problem and obtained regular solutions

for $1 \gg (N/\Omega)^2 (H/R)^2 \gg (H/R)^{3/2}$. However, these solutions are still

pathological in the sense that the scale of the second order motion is

order $(N/\Omega)(H/R)$ smaller than that of the basic motion and vanishes as

$H/R \to 0$. This leads to an infinite velocity shear as $H/R \to 0$. Miles

(1974) pointed out that the fundamental problem of Stewartson and

Walton's expansion was the failure of the solutions of the LTE for

homogeneous fluid (the first order terms) to provide an adequate

description of the characteristics of the primitive equation in the

hyperbolic domain. He showed that, by retaining stratification in the

basic equations, the resulting double infinity of modes (i.e., the

barotropic and an infinite set of baroclinic modes) could be used as

expansion functions to obtain uniformly valid second order solutions.

The barotropic and baroclinic modes are coupled by the horizontal

component of the earth's rotation at the second order. This coupling

decreases with increasing stratification. The inhibiting effect of

stratification on the influence of the horizontal component of the

earth's rotation was also noted by Phillips (1968), Needler and LeBlond

(1973), Kamenkovich and Kulakov (1977).

Miles (1974) showed that, for free oscillations with frequency

$\omega < 2\Omega < N$, the partial differential equation resulting from

(3.2)--(3.6) is elliptic (hyperbolic) poleward (equatorward) of the two

critical latitudes satisfying

$$\sin\phi = \frac{\omega}{2\Omega}\left[1 + \frac{4\Omega^2}{N^2}\left(1 - \frac{\omega^2}{4\Omega^2}\right)\right]$$

In general, the critical latitudes are greater than $\pm \sin^{-1}\left(\frac{\omega}{2\Omega}\right)$,the

inertial latitudes. For strong stratification such that $\frac{4\Omega^2}{N^2} \ll 1$, the

critical latitudes tend to coincide with the inertial latitudes, and the

traditional approximation is formally valid. In the deep ocean

where $\frac{4\Omega^2}{N^2} \lesssim .1$, then one may find some appreciable sub-inertial energy

due to this broadening of internal wave frequency band.

3.3 Asymptotic solutions

It is well-known that packets of internal waves in the ocean

propagate along ray paths which undergo reflections at the vertical

boundaries and the turning latitudes where the latitudinal wavenumber

vanishes. A linear random wave field is represented by the superposition

of ray paths of different frequencies and wavenumbers. However, the

statistical behavior of the wave field also can be described by a set of

equivalent modes as proposed by Garrett and Munk (1972). Because modal

solutions are more easily obtained than ray solutions, we proceed based

on periodic solutions which have modal structure in depth and are

separable in each coordinate as follows:

$$
\begin{Bmatrix} u\cos\phi \\ v\cos\phi \\ p \end{Bmatrix} = A\,\text{Real}\left\{ F(z^*)\exp\left[i(k\lambda - \omega t)\right] \begin{Bmatrix} U(\phi) \\ i\,V(\phi) \\ 2\Omega R\,P(\phi) \end{Bmatrix} \right\} \tag{3.7}
$$

$$
\begin{pmatrix} P \\ \\ W \end{pmatrix} = A \, \mathrm{Real} \left\{ W(z^*) \, \exp\left[i \, (k\lambda - \omega t) \right] \begin{bmatrix} \dfrac{\rho_o \, N^2(z^*)}{g \, \omega} \\ \\ -i \end{bmatrix} P(\phi) \right\} \qquad 3.8)
$$

where U, V, P, F, W are dimensionless functions, and A is a

normalization factor with the dimension of velocity. Defining the

dimensionless depth z = z*/H, frequency $\sigma = \omega / 2\Omega$, and buoyancy

frequency $\tilde{N}(z)$ = N(z*)/N$_o$, the substitution of (3.7) and (3.8) into

(3.2) — (3.6) yields

$$
\sigma U \; + \; \sin\phi \; V \; = \; k \, P \tag{3.9}
$$

$$
\sin\phi \, U \; + \; \sigma \, V \; = \; - \cos\phi \; \frac{d \, P}{d \, \phi} \tag{3.10}
$$

$$
\frac{d \, F}{d \, z} \; + \; \frac{N_o^2 \, H}{4 \, \Omega^2 \, R \, \sigma} \; \tilde{N}^2(z) \, W \; = \; 0 \tag{3.11}
$$

$$
\frac{1}{\sigma \cos^2\!\phi \, P} \left[k \, U + \cos\phi \, \frac{d \, V}{d \, \phi} \right] \; = \; \frac{R}{H \sigma \, F} \; \frac{d \, W}{d \, z} \; = \; \epsilon \tag{3.12}
$$

where the hydrostatic and traditional approximations have been used. Eq.

(3.12) states the condition of separability, where ϵ is the separation

constant which is related to the equivalent depth h (Lindzen, 1967) by

$$
\epsilon \; = \; \frac{4 \, \Omega^2 \, R^2}{g \, h} \tag{3.13}
$$

The vertical equation can be obtained from (3.11) and (3.12),

$$\frac{d^2 W}{d z^2} + \epsilon S^2 \tilde{N}^2(z) W = 0 \quad , \tag{3.14}$$

where $S = N_0 H / 2\Omega R$. The boundary conditions are

$$W = 0 \qquad \text{at } z = 0, -1 \tag{3.15}$$

Because the specific form of N(z) is not crucial to the qualitative

results, we use the same N(z) of Garrett and Munk (1972),

$$N(z) = N_0 \exp(-zH/b) \quad , \tag{3.16}$$

where $N_0 = 3$ cph, $b = 1.3$ km, and $H = 4.5$ km. The solutions of the

eigenvalue problem posed by (3.14) and (3.15) are readily obtained and

the eigenvalues are

$$\epsilon_1 = 1.63 \times 10^5 \, ,$$

$$\epsilon_2 = 7.39 \times 10^5 \, ,$$

$$\epsilon_j = 1.96 \times 10^5 \times j^2 \, , \quad (j \geq 3)$$

where the subscripts are the vertical mode numbers. For high modes, the

WKBJ solutions for F(z) and W(z) are

$$W_j(z) = \frac{-2\Omega\sigma}{N_0} \epsilon_j^{1/2} \tilde{N}^{-1/2} \exp\left[i \int_{-1}^{z} \epsilon_j^{1/2} S \tilde{N}(z') dz' + \frac{\pi}{2} \right]$$

$$F_j(z) = \tilde{N}^{1/2} \exp\left[i \int_{-1}^{z} \epsilon_j^{1/2} S \tilde{N}(z') dz' \right] \tag{3.17}$$

The latitudinal equation can be obtained by eliminating U from (3.10) and (3.12), yielding

$$\cos\phi \frac{dP}{d\phi} + \frac{k\sin\phi}{\sigma} P = \left(\frac{\sin^2\phi}{\sigma} - \sigma\right) V \tag{3.18}$$

$$\cos\phi \frac{dV}{d\phi} - \frac{k}{\sigma} \sin\phi\, V = \left(\epsilon\sigma\cos^2\phi - \frac{k^2}{\sigma}\right) P \tag{3.19}$$

Eliminating P from (3.18) and (3.19), we have the LTE in terms of V:

$$\cos\phi \frac{d}{d\phi}\left(\cos\phi \frac{dV}{d\phi}\right) + \left[\epsilon\cos^2\phi\,(\sigma^2 - \sin^2\phi) - \frac{k}{\sigma}\cos^2\phi - k^2\right] V$$

$$= \frac{2\epsilon\cos^2\phi\sin\phi\left[\frac{k}{\sigma}\sin\phi\, V - \cos\phi \frac{dV}{d\phi}\right]}{\epsilon\cos^2\phi - \frac{k^2}{\sigma^2}} \tag{3..20}$$

Longuet-Higgins (1965) showed that, for large ϵ , the right-hand side of (3.20) can be neglected with an error $O(\epsilon^{-1/2})$ of the left-hand side. As pointed out in MP, this error is not uniform in ϕ , and becomes $O(\epsilon^{-1/3})$ near the inertial latitudes ($\sin\phi = \pm\sigma$).

But another more serious non-uniformity associated with the apparent singularity at $\cos\phi = \frac{k}{\sigma\epsilon^{1/2}}$, where the denominator in (3.20) vanishes, has not been discussed. For inertial waves, k $\lesssim$ $O(\epsilon^{1/3})$ (see MP); hence $\frac{k}{\sigma\epsilon^{1/2}} \ll 1$ if $\sigma \sim O(1)$. The singular latitude is near the poles which is far from the turning latitudes of mid-latitude inertial waves. Because the wave amplitudes are virtually vanishing there, this singularity is of no importance. But for low-latitude inertial waves with $\sigma \ll 1$, this singularity would occur equatorward

of their turning latitudes and seriously affects the solutions. The lower limit in latitude for the validity of neglecting the right-hand side of (3.20) is about 4° for the first baroclinic mode and decreases with mode number. Thus the following discussion is restricted to latitudes greater than 4° and the right-hand side of (3.20) is neglected for now. It is shown in Chapter 4 that, however, the validity of one turning point solutions on which our model is based is restricted to latitudes at least greater than 10°.

The following derivation of the asymptotic solutions basically follows MP. Introducing the Mercator coordinate μ which is defined as

$$\mu = \int_0^\phi \sec \phi' \, d\phi' \tag{3.21}$$

we can eliminate the first derivative term in (3.20) and obtain the spheroidal wave equation in the following form,

$$\frac{d^2 V}{d\mu^2} + \ell^2 V = 0 \tag{3.22}$$

where

$$\ell^2 = \epsilon \cos^2\phi \, (\sigma^2 - \sin^2\phi) - \frac{k}{\sigma} \cos^2\phi - k^2 \tag{3.23}$$

It is clear that ℓ is equivalent to a latitudinal wavenumber. The turning latitude ϕ_s is then defined as the latitude where $\ell = 0$. From (3.23) we have

$$2 \sin^2\phi_s = 1 + \sigma^2 - \frac{k}{\sigma\epsilon} - \left[(1 - \sigma^2 + \frac{k}{\sigma\epsilon})^2 + \frac{4k^2}{\epsilon} \right]^{\frac{1}{2}} \tag{3.24}$$

It can be seen from (3.22) that ϕ_s is the boundary between the

evanescent (poleward) and oscillatory (equatorward) domain of the solution. It is also the latitude where the wave rays reflect back to the equator (Longuet-Higgins, 1965). Hence the basic behavior of the solution is controlled by the location of ϕ_s. In Fig. 3.1, ϕ_s is shown as a function of $2\pi/k$ for different vertical modes with $\sigma = 0.5878$. In general, ϕ_s approaches the inertial latitude with increasing ϵ and/or $2\pi/k$.

In terms of ϕ_s, (3.23) can be written as

$$\ell^2 = \left(\sin^2\phi_s - \sin^2\phi \right)\left(\epsilon \cos^2\phi + k^2 \sec^2\phi_s \right) \tag{3.25}$$

With the Langer transformation in ϕ,

$$\frac{2}{3}\, \xi^{3/2} = \int_\phi^{\phi_s} \left(\sin^2\phi_s - \sin\phi' \right)^{1/2} d\phi' , \tag{3.26}$$

a uniformly valid asymptotic solution of (3.22) is obtained :

$$V = \left(\frac{d\xi}{d\mu} \right)^{-1/2} Ai\left(-\epsilon^{1/3}\xi\right) \left[1 + O\left(\epsilon^{-1/2}\right) \right] , \tag{3.27}$$

where Ai is the Airy function which satisfies the boundary condition V = 0 at ∞. Because we are considering a one turning point problem, the boundary conditions at the other turning latitude can be ignored, and a continuous spectrum in k is allowed. The solutions for U and P can be readily obtained by substituting (3.27) into (3.9) and (3.19). The integral of (3.26) can be evaluated in terms of elliptic functions (see Appendix B). When $\phi \approx \phi_s$, the Taylor expansion of (3.26) is
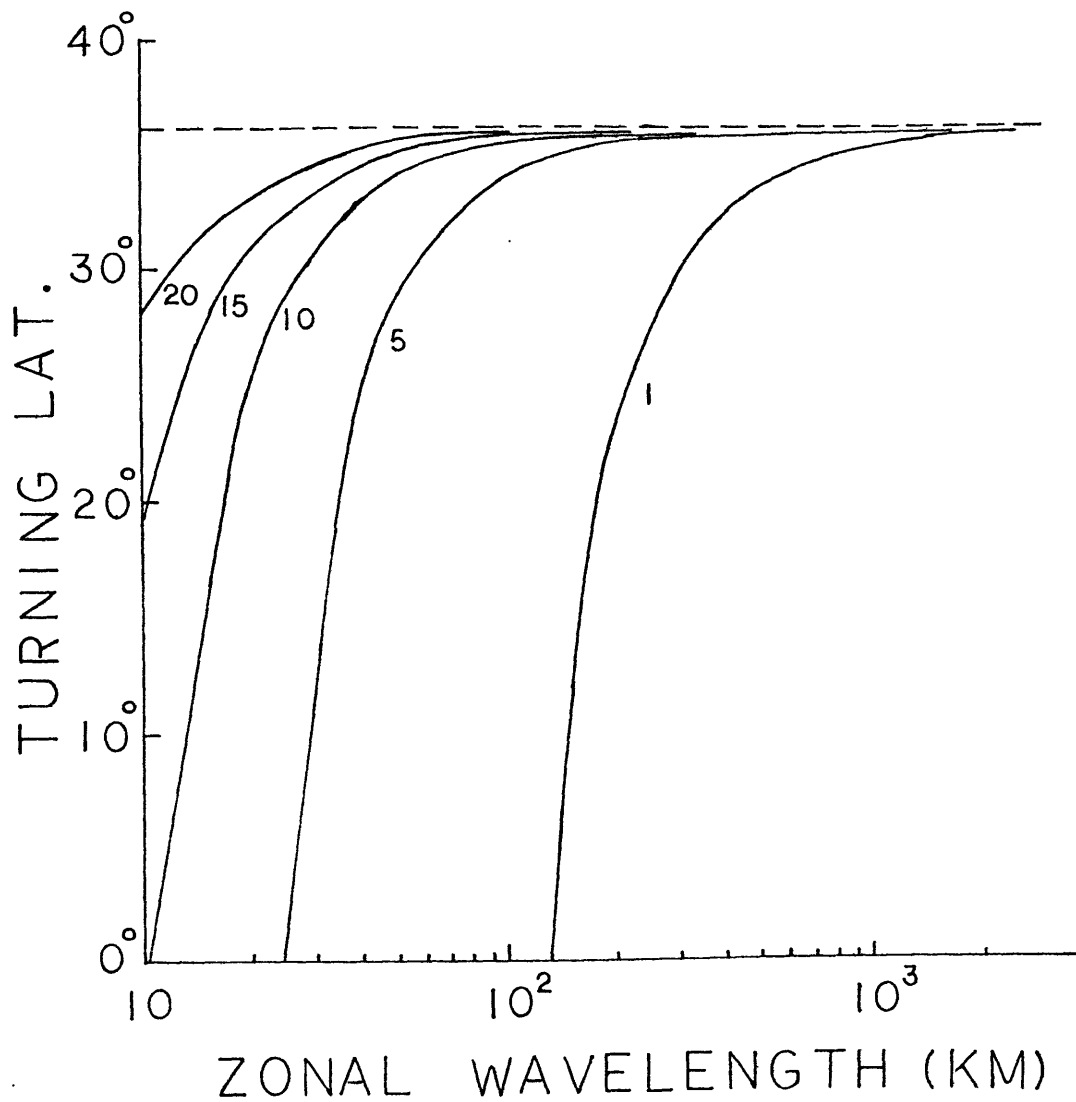
Figure 3.1   Turning latitudes of waves with σ =0.5878 as
functions of zonal wavelength for different vertical modes. The
number next to each curve is the mode.number. Dashed line indicates
the inertial latitude (36o).

$$\xi = \left(\sin 2\phi_s\right)^{1/3} (\phi_s - \phi)\left[1 - \frac{1}{5} \cot 2\phi_s \, (\phi_s - \phi) + \cdots \cdots\right] \tag{3.28}$$

The controlling scale near ϕ_s is the "Airy scale" defined as

$$L = \left(\epsilon \sin 2\phi_s\right)^{-1/3}, \tag{3.29}$$

whose values for the first and tenth vertical modes at selected latitudes are shown in Table 3.1. L is symmetrical about the latitude of 45°, and approaches infinity near the poles and the equator, where this scale becomes irrelevant. Fig. 3.2 shows schematically the

Table 3.1

Airy scales for the 1st and 10th vertical modes.

Parenthetical values are in km.

Latitude(deg)	L_1	L_{10}
5	.033 (210)	.0066 (42)
15	.023 (146)	.0046 (30)
30	.019 (121)	.0039 (25)
45	.018 (115)	.0037 (24)

variation of the solutions represented by (3.27) with respect to k and ϵ . For latitudinally propagating waves with k = 0, ϕ_s is equal to

(a)

$\epsilon = \epsilon_{10}$
$k = 0$

$\sin\phi$

σ

O

(b)

$\epsilon = \epsilon_{10}$
$k \nearrow$

$\sin\phi$

σ

O

(c)

$\epsilon \nearrow$
$k = 0$

$\sin\phi$

σ

O
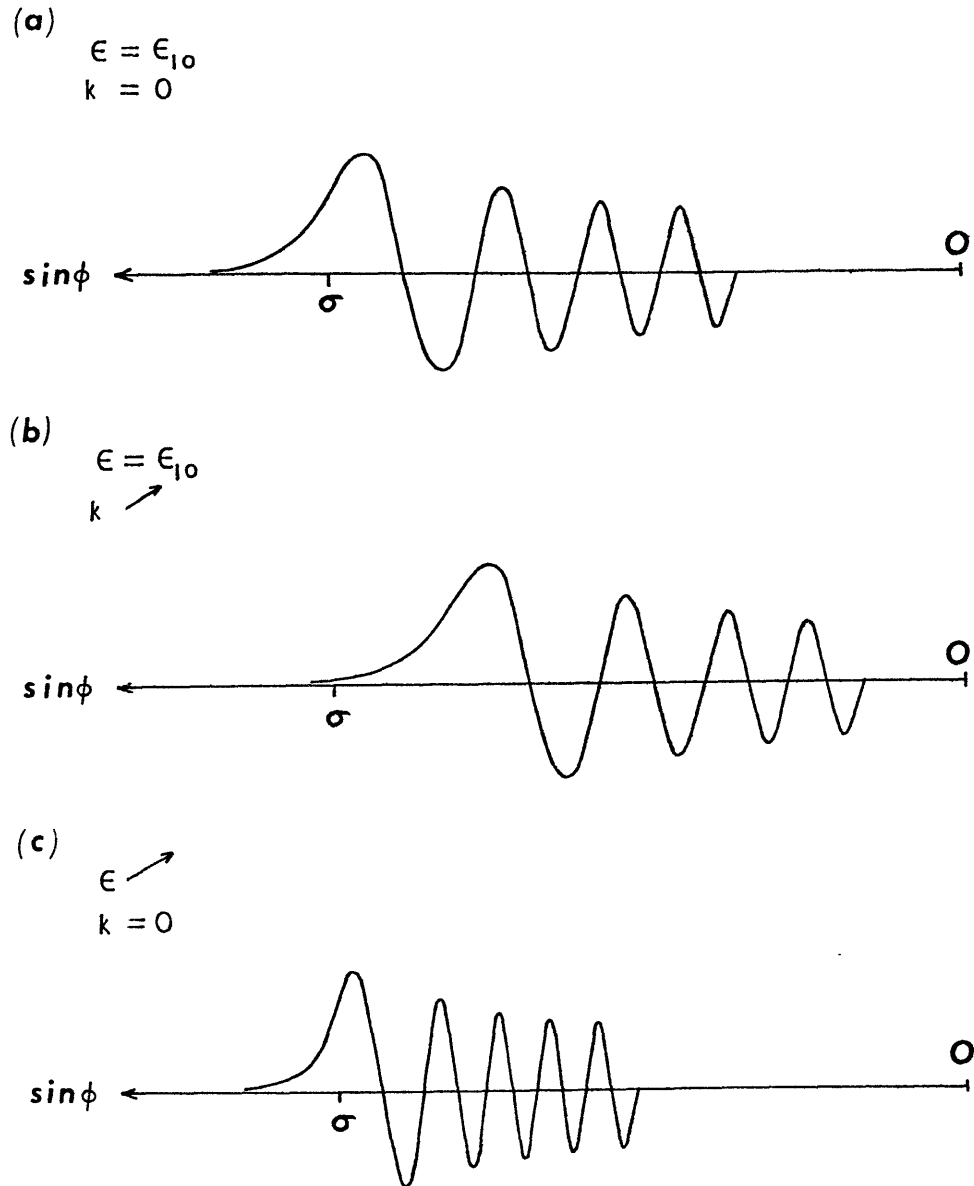
Figure 3.2   Schematic diagram showing the variation of the wave function V with respect to k and ϵ . Horizontal axis is the sine of latitude; σ corresponds to the inertial latitude. k $\nearrow$ means increasing the value of k.

$\sin^{-1}(\sigma)$. An increase in k tends to shift ϕ_s equatorward of

$\sin^{-1}(\sigma)$; an increase in ϵ tends to decrease the latitudinal scale

as implied in Eq. (3.29). Therefore, the observations of inertial peak

only a few percent above f imply a fairly large zonal wavelength. For

instance, assuming that the dominant wave has a tenth-mode vertical

structure, then the observation of an inertial peak with 2.5 % blue

shift at 35° implies that ϕ_s should be 35.3°. From Fig. 3.1, we can

infer that the zonal wavelength is of the order of 100 km.

3.4 The WKBJ approximation

For high frequency internal waves, $\sigma \gg \sin\phi$, we can apply the

WKBJ approximation to (3.22) and obtain the zero order solutions used in

the GM model. But how much greater than $\sin\phi$ should σ be for the

WKBJ solutions to be valid ? To answer this question, we have to look

into the error terms in detail. In general, the error of the WKBJ

solutions, denoted by δ , is growing when approaching turning points.

For Eq. (3.22), δ can be written as (Mathews and Walker, 1970, p.27)

$$\delta = \frac{\dfrac{d(\ell^2)}{d\mu}}{(\ell^2)^{3/2}} \qquad (3.30)$$

Then from (3.25), we have

$$\delta = \frac{2\sin\phi\cos^2\phi\left[1 - 2\sin^2\phi + \sin^2\phi_s + \dfrac{k^2}{\epsilon\cos^2\phi_s}\right]}{\epsilon^{1/2}\left[(\sin^2\phi_s - \sin^2\phi)(\cos^2\phi + \dfrac{k^2}{\epsilon\cos^2\phi_s})\right]^{3/2}} \qquad (3.31)$$

For given ϕ , ϵ , and k, we can find from (3.31) a frequency σ_c beyond

which δ is less than some pre-specified value, say, 0.1. In general, σ_c

is the root of a nonlinear algebraic equation. However, when k = 0, σ_c can be approximated by

$$\sigma_c \approx \sin\phi \left(1 + 10\, L \cot\phi \right) , \tag{3.32}$$

where L is the Airy scale at ϕ . Because for given ϕ , ϵ , and σ , δ is minimum when k = 0, the σ_c given by (3.32) represents a lower bound for frequency below which the WKBJ solutions are invalid for any value of k. The values of σ_c calculated using (3.32) for the first and tenth modes at selected latitudes are shown in Table 3.2. Since the observed vertical wavenumber spectrum (Leaman and Sanford, 1975) suggests that most of the internal wave energy is contained in low modes, σ_c of the tenth mode is probably the lower bound for the validity of the WKBJ approximation and the GM model.

Table 3.2

Values of the critical frequency of the 1st and
10th vertical modes.

Latitude (deg)	$\frac{\sigma_c}{\sin\phi}$ (j=1)	$\frac{\sigma_c}{\sin\phi}$ (j=10)
5	4.75	1.75
15	1.86	1.17
30	1.33	1.07
45	1.18	1.04
60	1.11	1.02

3.5 Discussion

At latitudes sufficiently away from the equator ($\gtrsim 4°$), the asymptotic solutions to the spheroidal wave equation as obtained by MP are valid with an error no greater than $O(\epsilon^{-1/3})$. The WKBJ solutions used in the GM model are valid for frequencies higher than a critical value σ_c , which is dependent on vertical mode numbers. The value of σ_c corresponding to the tenth vertical mode is used as a critical frequency in the calculation of wave functions in the next chapter : for frequencies higher than σ_c , the WKBJ solutions will be used; for frequencies lower than σ_c , the spheroidal wave solutions will be used.

Chapter 4   A Model Spectrum for the Global Inertial Wave Field

4.1 Introduction

In the light of the observations presented in Chapter 2, whatever
mechanisms are responsible for the universality of the internal wave
spectrum at high frequencies do not seem to apply near f. The spectral
shape near f has a strong dependence on geographical location,
suggesting a strong influence of local sources and/or sinks. Presumably
the internal wave spectrum is determined by the radiation balance
equation which involves generation, dissipation, propagation and
nonlinear interaction (c.f. Müller and Olbers, 1975). Because low mode
waves contain most of the energy, they have a dominant influence on the
frequency spectrum. McComas and Bretherton (1977) reported that near f
the interaction time scales for low mode waves are very long as compared
to their periods. Therefore nonlinear interactions may not be important
for the existence of the inertial peak. Major dissipation of these waves
is probably taking place only at the ocean bottom, and it will be shown
in Chapter 6 that the resulting reflection coefficient is near unity and
hence the dissipation rate is small. Therefore the main cause for the
observed inertial peak is likely to be a combination of the generation
and propagation of internal waves in the open ocean.

Low frequency internal waves randomly generated at lower latitudes
can propagate to their inertial latitude and become, by definition,
inertial waves, as long as their zonal wavenumbers are small enough. The
inertial wave field of this origin is defined in Chapter 1 as the global

wave field. In addition, there are several possible local forcing

mechanisms for inertial waves : wind forcing, energy cascades from

sub-inertial frequencies, interactions between low frequency eddies and

rough topography, etc. Among these, the wind forcing is probably the

best understood and also the most important source. In the mixed layer,

inertial currents are forced as a direct response to local winds and

could propagate along ray paths to the deep ocean nearby with possibly

appreciable amplitudes (Kroll, 1975). This would result in a

predominantly downward propagating wave field which is defined in

Chapter 1 as the local wave field. To distinguish the local wave field

from the global wave field in the observed spectra is the major task of

this chapter. Determination of the spectrum of wind forced inertial

waves requires detailed knowledge of the wind spectrum which is poorly

known near the inertial frequency. Furthermore, boundary layer dynamics

near the inertial frequency are also poorly understood. We will

therefore proceed in the other direction -- first determining the global

wave spectrum and then ascribe the residual to local forcing.

Because the f-w spectrum of the global wave field is well described

by the GM model at lower latitudes where the WKBJ approximation is

valid, the frequency spectrum near f can be obtained by using the GM

model and the wave functions derived in Chapter 3. Thus the difference

between the global wave spectrum and the observed spectrum can be

interpreted as the result of locally forced waves.

4.2 The Garrett and Munk Model

Under the assumption of stationarity and homogeneity of internal

waves in the ocean, Garrett and Munk (1972) patched together a great number of observations of different origins, trying to seek a universal f-w spectrum. In their work, the following additional assumptions were made :

(1) the observed motion is interpreted as linear superposition of internal waves with random phase relations.

(2) horizontal isotropy and vertical symmetry, i.e., there is no preferred directionality.

(3) the WKBJ approximations for the wave functions in both the vertical and latitudinal variable.

Then the energy density can be written as E(α, ω) , which depends only on two variables : the frequency ω and horizontal wavenumber α . Because the observed vertical coherences were independent of frequency, they proposed the following separable form for E(α, ω) :

$$E(\alpha, \omega) = E_c \, A(\lambda) \, B(\omega) \, , \tag{4.1}$$

where $\quad \lambda = \dfrac{\alpha}{\alpha_*} \quad , \quad \alpha_* = j_* \pi \, (\omega^2 - f^2)^{\frac{1}{2}} \quad , \quad j_* = 20 \quad , \tag{4.2}$

$$A(\lambda) = \frac{1}{\alpha_*} \quad (\lambda \le 1) \; ; \quad 0 \; (\lambda > 1) \tag{4.3}$$

$$B(\omega) = \frac{2}{\pi} f \, \omega^{2S-2} \, (\omega^2 - f^2)^{-S} \quad , \quad S = \frac{1}{2} \tag{4.4}$$

The spectrum represented by (4.1)--(4.4) is usually referred as "GM72". The wavenumber spectrum A(λ) is of top hat shape with cutoff mode number j_* deduced from vertical coherence measurements. The particular

form of $B(\omega)$ is chosen to behave like ω^{-2} when $\omega \gg$ f and also to have an integrable cusp at f. The ω^{-2} behavior when $\omega \gg$ f is supported by observations in most parts of the deep ocean. But the cusp with s = 1/2 is arbitrary, and is there only to satisfy the condition of integrability which requires $0 < s < 1$. After admitting that observed motions with relatively high wavenumbers are indeed internal waves rather than fine structures, Garrett and Munk (1975) modified $A(\lambda)$ so that it falls off smoothly with a high wavenumber slope,

$$A(\lambda) = (t-1)(1+\lambda)^{-t} / \alpha_* \quad , \tag{4.5}$$

where t = 2.5, and α_* corresponds to $j_* = 6$. The model with this modification is usually referred as "GM75". Using relatively less contaminated observations from a mid-water float, Cairns and Williams (1976) showed that t = 2 and $j_* = 3$ are probably better fits.

With normalized wave functions of horizontal velocity $X(\not{z}, \omega)$, and vertical displacement $Z(\not{z}, \omega)$, the corresponding frequency spectra are

$$\int_{-\infty}^{\infty} \left[X^2(z, \omega) , \ Z^2(z, \omega) \right] E(\alpha, \omega) \, d\alpha \tag{4.6}$$

As a consequence of the underlying WKBJ approximations for X and Z, the above description applies only for f $\ll \omega \ll$ N(z). Analytical representations of various spectral quantities based on GM75 were derived by Desaubies (1976).

4.3 The global inertial wave model

4.3a Normalization

In order to be useful in the spectrum calculations, the wave functions derived in 3.3 have to be normalized at some low latitude where the WKBJ approximation is valid. Quite naturally and conveniently, we choose the equator for formal normalization. The observed small vertical coherence scales near the equator (Wunsch and Webb, 1979) suggest that the wavenumber bandwidth there is greater than what is given by the GM model, but this is irrelevant because the model is not applied on the equator. The normalization condition requires that

$$\int_{-1}^{0} \left[\frac{1}{2} (u^2 + v^2 + w^2) + \frac{1}{2} \frac{g^2 \rho^2}{\rho_0^2 N^2} \right] dz = 1 \qquad (4.7)$$

at the equator. After substituting (3.7) and (3.8) into (4.7), we have

$$A^2 \int_{-1}^{0} \left[\frac{1}{2} \overline{F^2} (U^2 + V^2) + \frac{1}{2} \overline{W^2} \left(1 + \frac{N^2}{\omega^2} \right) P^2 \right] dz = 1 \qquad (4.8)$$

where $\overline{F^2}$ and $\overline{W^2}$ are the squares of F(z) and W(z) averaged over depth. From (3.17), we have

$$\overline{W^2} = \frac{4 \Omega^2 \sigma^2}{N_0^2} \epsilon \, \tilde{N}^{-1}(z)$$

and

$$\overline{F^2} = \tilde{N}(z)$$

Using the solutions obtained in 3.3 for U, V, and P, and their

asymptotic approximations at $\phi = 0$, the following results are obtained :

$$A^2 = \frac{\epsilon^{1/6} \sin\phi_s}{J \left\{ 1 + \frac{\sin^2\phi_s (\sigma^2 + \frac{k^2}{\epsilon})}{(\sigma^2 - \frac{k^2}{\epsilon})^2} \right\}} + O(\epsilon^{-1/3}) \quad , \qquad (4.9)$$

where

$$J = \frac{b(1 - e^{-H/b})}{2\pi H}$$

4.3b Construction of frequency spectra

With wave functions given by (3.7), (3.8), and (4.9), the frequency spectra of v component velocity and density at latitude ϕ and depth z can be written as

$$E_v(\omega, \phi, z) = \sum_{j=1}^{m} \int_{-\infty}^{\infty} G(k, j, \omega) \left| v(k, \epsilon_j, \omega, \phi, z) \right|^2 dk$$

$$E_\rho(\omega, \phi, z) = \sum_{j=1}^{m} \int_{-\infty}^{\infty} G(k, j, \omega) \left| \rho(k, \epsilon_j, \omega, \phi, z) \right|^2 dk \quad , \qquad (4.10)$$

where j is the vertical mode number, m is the maximum mode number, and ω is the frequency. G(k, j, ω) is the f-w spectrum of the following form :

$$G(k, j, \omega) = E_o \left(\frac{\omega}{\omega_o}\right)^{-2} C(j) D(k, j, \omega) \quad ; \qquad (4.11a)$$

where $C(j) = \dfrac{(1 + j/j*)^{-t}}{\sum\limits_{j=1}^{m} (1 + j/j*)^{-t}}$ $\qquad$ (4.11b)

and E_o is the total energy per unit mass per cph averaged over depth at the equator. The frequency and vertical mode distributions have the same forms as those of GM75, but we need some arguments to choose a proper zonal wavenumber spectrum $D(k, j, \omega)$ for given ω and j.

For $\omega \gg f$, the assumption of horizontal isotropy requires that energy density be a function of total wavenumber α only, which is defined as

$$\alpha = (k^2 + \ell^2)^{1/2},$$

where ℓ is given by Eq.(3.23). It can be shown that for $\omega \gg f$,

$$\alpha \approx \epsilon^{\frac{1}{2}} \cos\phi \; \frac{(\omega^2 - f^2)^{\frac{1}{2}}}{2\Omega} \; \sim \; O(\epsilon^{\frac{1}{2}}) \; . \tag{4.12}$$

Because

$$k = \alpha \cos\theta$$

and

$$D(k, j, \omega) \, dk = \frac{1}{2\pi} \, d\theta \; ,$$

where θ is the azimuthal angle, we have

$$D(k, j, \omega) = \frac{1}{\pi\alpha} \left[1 - \left(\frac{k}{\alpha}\right)^2 \right]^{-1/2} \qquad (\omega \gg f) \tag{4.13}$$

For $\omega \approx f$, we can no longer interpret ℓ as a local latitudinal wavenumber, because the wave functions are no longer periodic in latitude; the direction of propagation is primarily zonal, and we do not have a clear definition of horizontal isotropy for inertial waves. The

following two models are therefore proposed for D(k, j, ω) when $\omega \approx f$:

Model 1

Let us first find the range of k for given ω and j, i.e., the cutoff wavenumbers $-k_1$ and k_2 which satisfy the following equation :

$$2 \sin^2(\phi - L_j) = 1 + \sigma^2 - \frac{k}{\sigma \epsilon_j} - \left[(1 - \sigma^2 + \frac{k}{\sigma \epsilon_j})^2 + \frac{4k^2}{\epsilon_j} \right]^{\frac{1}{2}} , \tag{4.14}$$

which are obtained from (3.24) by setting $\phi_s = \phi - L_j$. Thus $-k_1$ and k_2 are the zonal wavenumbers for which the jth mode wave with frequency σ will turn at $\phi - L_j$. The reason for setting $\phi_s = \phi - L_j$ instead of $\phi_s = \phi$ is that, the wave amplitude is appreciable to latitudes one Airy scale north of the turning latitude (see Fig. 3.2). The solutions of (4.14) are

$$\left. \begin{array}{c} -k_1 \\ k_2 \end{array} \right\} = \frac{-\cos\theta}{4\sigma} \mp \frac{\epsilon_j^{\frac{1}{2}} \cos\theta}{\sigma} \left(\sigma^4 - \sigma^2 \sin^2\theta + \frac{\cos^2 2\theta}{16 \epsilon_j \cos^2\theta} \right)^{\frac{1}{2}} ,$$

where $\theta = \phi - L_j$. For $\omega \approx$ f, the above expression can be approximated by

$$\left. \begin{array}{c} -k_1 \\ k_2 \end{array} \right\} = \mp k_0 + O(1) \tag{4.15a}$$

where $k_0 = \cos\phi \, L_j^{-3/2} \left[\frac{\omega - f}{2\Omega \cos\phi} + L_j \right]^{\frac{1}{2}} \sim O(\epsilon^{1/3})$ \quad (4.15b)

Thus the zonal wavenumber of inertial waves is restricted to $-k_0 < k < k_0$. If inertial waves, as in the case of global generation, are propagating from equatorward of their turning latitudes where D(k, j, ω)

\

is given by Eq. (4.13), we must have (when $w \approx f$)

$$D(k, j, w) \propto \left[1 - (\frac{k}{\alpha})^2 \right]^{-\frac{1}{2}} \qquad \text{with } |k| \leq k_o,$$

because k is conserved along ray paths. From Eqs. (4.15b) and (4.12), we have

$$\frac{k}{\alpha} \sim O(\epsilon^{-\frac{1}{6}})$$

and

$$D(k, j, w) \propto 1 + O(\epsilon^{-\frac{1}{3}}) .$$

Hence $D(k, j, w)$ can be approximated by a constant when $|k| \leq k_o$, and the Model 1 for $D(k, j, w)$ is formally defined as

$$\begin{aligned} D(k, j, w) &= \frac{1}{2k_o} && \text{for } |k| \leq k_o , & (4.16) \\ &= 0 && \text{for } |k| > k_o . \end{aligned}$$

Eq. (4.16) therefore represents the zonal wavenumber spectrum of an inertial wave field which can be mapped onto an isotropic internal wave field at lower latitudes.

Model 2

Although there is no latitudinal propagation when $w \approx f$, we can still think of $(k^2 + \ell^2)^{1/2}$, which is equal to k_o as given by (4.15b), as a total wavenumber and define $D(k, j, w)$ according to Eq. (4.13) as follows :

$$D(k, \, j, \, \omega) = \frac{1}{\pi k_0 \left[1 - \left(\frac{k}{k_0} \right)^2 \right]^{1/2}} \qquad \text{for } |k| \leq k_0 \qquad\qquad (4.17)$$

$$= 0 \qquad\qquad\qquad \text{otherwise.}$$

This is actually an artificial definition of horizontal isotropy for inertial waves which can propagate only in the zonal direction. There is not any physical ground for the Model 2 except using the same form of $D(k, \, j, \, \omega)$ at all frequencies. Fig. 4.1 shows the zonal wavenumber spectra corresponding to these two models.

With these two models for $D(k, \, j, \, \omega)$, the integrals in (4.10) were calculated numerically up to the critical frequency σ_c of the tenth vertical mode as discussed in Section 3.4, where the spectra can be matched with GM75. The accuracy of the results was assured when no significant improvements were observed by reducing the integration step.

4.3c Model results and their sensitivity

Because of the nearly circular motion of inertial waves, the spectra of the two horizontal velocity components, $E_u(\omega)$ and $E_v(\omega)$, are the same, and the result for $E_v(\omega)$ can be viewed as the horizontal kinetic energy (H.K.E.) spectrum. The potential energy (P.E.) spectrum can be derived from $E_p(\omega)$ as

$$E_{PE}(\omega) = \frac{1}{2} \frac{g^2 E_p(\omega)}{\rho_0^2 N^2} \qquad\qquad (4.18)$$

Because of the WKBJ approximation in the vertical wave functions, E_v and E_{PE} are proportional to $N(z)$.

a

$D(k,j,\omega)$

$-k_o$ 0 k_o k

b

$D(k,j,\omega)$

$-k_o$ 0 k_o k
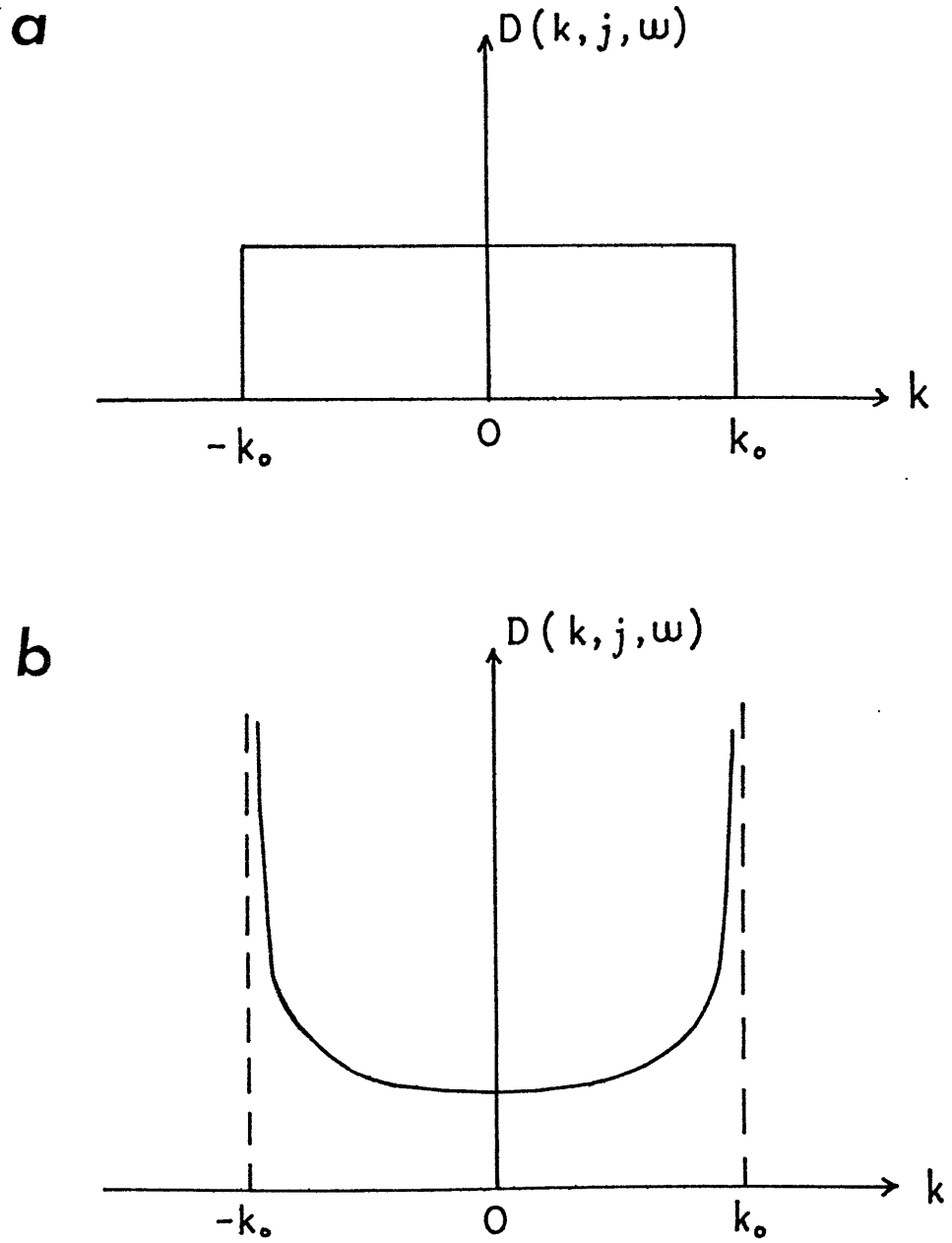
Figure 4.1   Schematic representation of the zonal wavenumber spectra of (a) Model 1 and (b) Model 2.

With $D(k, j, \omega)$ given by Model 1, m = 20, t = 2.5, and $j_{*} = 6$,

$E_V(\omega)/N(z)$ and $E_{PE}(\omega)/N(z)$ were calculated at five selected

latitudes, of which some were chosen to be where there were

observations. The results are shown in Fig. 4.2, where the scale of the

ordinate corresponds to $E_0/N_0 = 0.03$ $cm^2/sec^2/cph^2$, an estimate

from the comparisons with observations to be discussed later in 4.4.

Using the same values for j_*, t, m, and E_0/N_0, the normalized

energy spectra at 32° with $D(k, j, \omega)$ given by Model 2 are shown in

Fig. 4.3. Because the latitudinal dependence is the same as in Fig. 4.2,

the spectra at other latitudes are not shown. The only difference

between these two models is a slightly weaker peak in the kinetic energy

spectrum of Model 2 -- 4.5 db as compared to 7 db. Because such a small

difference -- a factor less than two -- is very difficult to distinguish

in the observations, only Model 1 will be used from hereon.

Fig.4.2 thus describes a mapping of the GM spectrum from the equator

onto higher latitudes. The changes in spectral shape and energy level

with latitude are simply due to the properties of wave functions on a

rotating sphere. The most encouraging result is the presence of

prominent inertial peaks in the velocity spectra, whereas there are no

such peaks in the potential energy spectra. The reason for the formation

of the inertial peaks in the velocity spectra is the constructive

interference of velocity wave functions near their turning latitudes;

however, note that each individual wave function does not have a sharp

peak near its turning latitude (see Fig. 3.2). The corresponding peak

height, peak frequency, and bandwidth of the velocity spectrum at each

latitude are listed in Table 4.1. The blue shift and bandwidth decrease
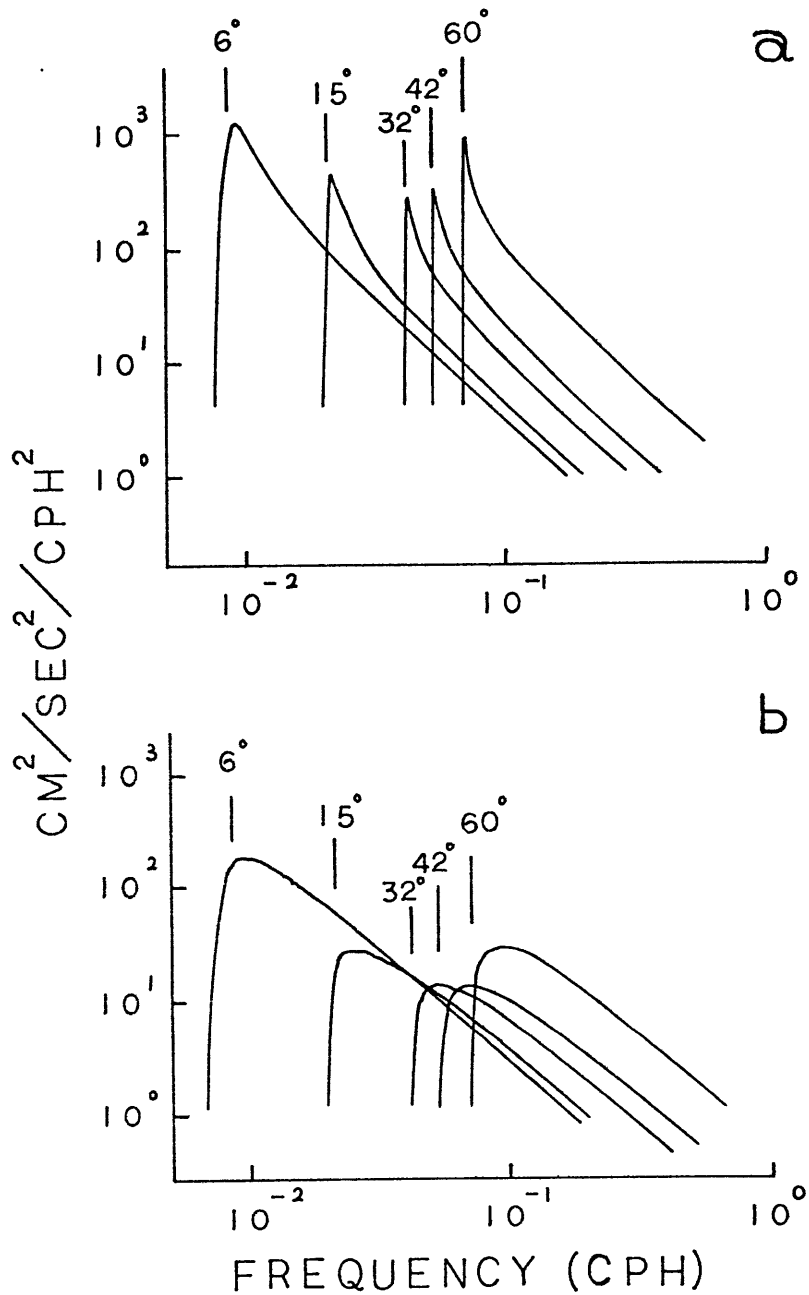
Figure 4.2   Model normalized spectra of (a) horizontal kinetic energy and (b) potential energy at five latitudes, with D(k, j, ω) given by Model 1, m = 20, $j_* = 6$, t = 2.5, and E_o/N_o =0.03 $cm^2/sec^2/cph^2$. The numbers are latitudes in deg.; the vertical bars indicate the locations of f.
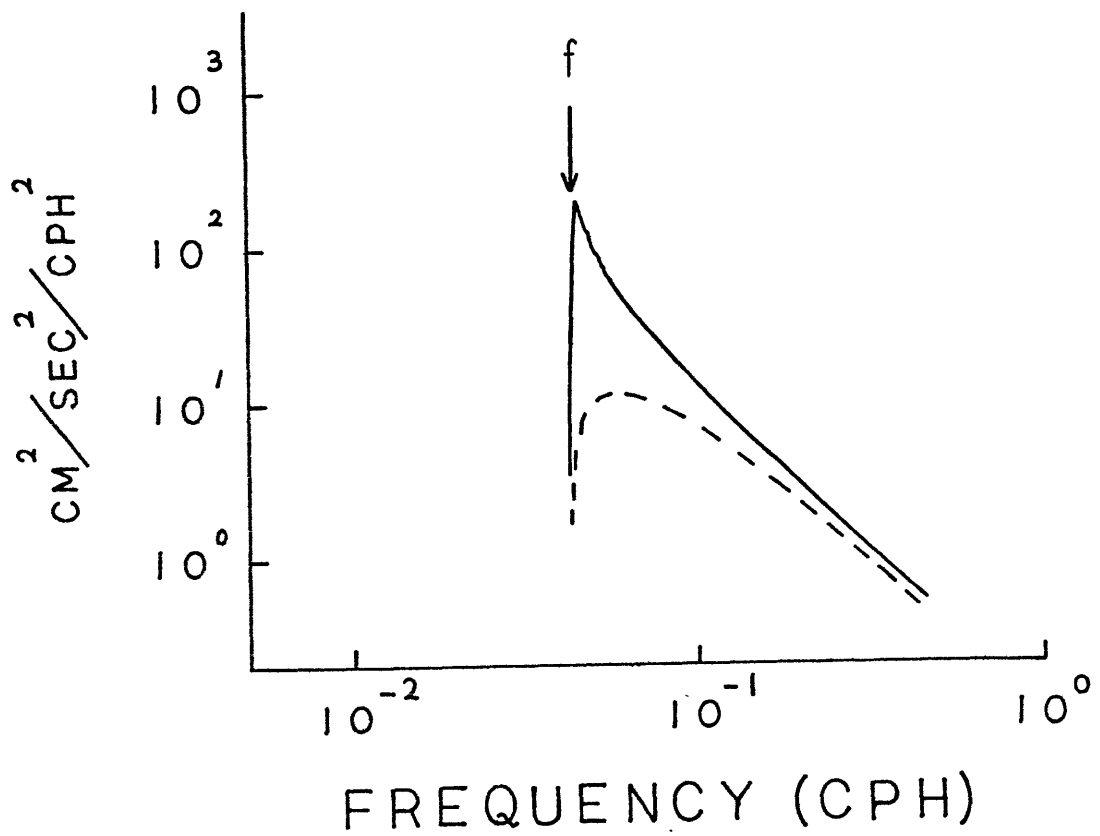
Figure 4.3   Model normalized spectra of horizontal kinetic energy
(solid line) and potential energy (dashed line) at 32°, with
D(k, j, ω) given by Model 2 and the other parameters the same as
in Fig. 4.2.

Table 4.1

Spectral characteristics of the model spectra shown in

Fig. 4.2. Peak height is in db above the ω^{-2} spectrum,

bandwidth in percentage of f.

Latitude(deg)	$\dfrac{\omega p}{f}$	Peak Height	bandwith
6	1.07	4.5	31.5 %
15	1.03	7.	14 %
31.6	1.01	7.	7 %
41.5	1.006	7.	5 %
60	1.004	6.5	3.5%

Table 4.2

Values of frequency scale L_σ for the 1st and 10th

modes at various latitudes.

Latitude(deg)	L_σ	
	j=1	j=10
5	.376	.076
15	.086	.017
30	.033	.0067
45	.018	.0036
60	.011	.0022
75	.006	.0012

with latitude, and this can be explained as follows. As $\phi \approx \phi_s$ and $\sigma \approx$

$\sin \phi$, the argument of the Airy function in (3.27) can be approximated

by (Eq.(39), MP)

$$\epsilon^{1/3} \xi = - \frac{\sigma - \sin\phi}{(\epsilon \sin 2\phi)^{-1/3} \cos\phi} + k^2 L^2 .$$

For given $\dfrac{\sigma}{\sin\phi}$, the controlling frequency scale L_σ is given by

$$L_\sigma = \frac{(\epsilon \sin 2\phi)^{-1/3} \cos\phi}{\sin\phi} \qquad\qquad (4.19)$$

which decreases with latitude as shown in Table 4.2. After superposition

of many modes, L_σ determines the latitudinal dependence of the blue

shift and bandwidth of the resulting spectrum.

In Fig. 4.2, note that the energy level at a particular frequency

increases with latitude, and this can be explained as follows: When a

wave packet propagates poleward, the conservation of wave action (c.f.

Bretherton and Garrett, 1969), A, defined as (wave energy)/frequency,

requires that

$$\frac{\partial A}{\partial t} + \nabla \cdot (\vec{C_g} A) = 0 ,$$

or

$$\left(\frac{\partial}{\partial t} + \vec{C_g} \cdot \nabla \right) A = - A \nabla \cdot \vec{C_g} ,$$

where $\vec{C_g}$ is the group velocity of the wave packet. Because wave rays

converge with increasing latitude, from the equations above, A increases

with latitude. Thus the background spectral level increases with

latitude. Now we can explain why the energy level of the inertial peak

varies with latitude as shown in Fig. 4.2. Because the peak height is almost independent of latitude and the background spectrum is red, the peak energy would decrease monotonously with latitude if the background spectral level were independent of latitude. At low latitudes, the poleward increase of the background spectral level is relatively slow while the poleward increase of the inertial frequency is relatively fast, so the peak energy decreases with latitude. At high latitudes, the situation is reversed, so the peak energy begins to increase with latitude; the minimum occurs at about 30°.

Fig. 4.4 shows the ratio of P.E. to H.K.E. at the same five latitudes together with the curve representing

$$\frac{P.E.}{H.K.E.} = \frac{(\omega^2 - f^2)}{(\omega^2 + f^2)} \quad , \tag{4.20}$$

the result of the WKBJ approximation (Garrett and Munk, 1972). The range of the validity of the WKBJ approximation in frequency increases with latitude as described in Table 3.2. Significant deviations occur at low latitudes. The approximation is a good one down to 1.02 f at mid-latitudes, where Fofonoff (1969) showed that Eq. (4.20) was consistent with observations at frequencies very close to f. The minimum ratio of P.E. to H.K.E. near f varies from 0.125 at 6° to 0.006 at 60°.

Displayed in Fig. 4.5 are the rotary spectra at 32°. When $\omega \approx f$, E_{+} is finite rather than zero as would result from an f-plane model. The latitudinal dependence of $\Gamma(\omega)$, defined in Chapter 2 as $\log(E_{-}/E_{+})$, is shown in Fig. 4.6 together with the WKBJ approximation (c.f. Eq.(2.3)). The behavior of the deviations from the WKBJ result is the same as in Fig. 4.4 as expected.
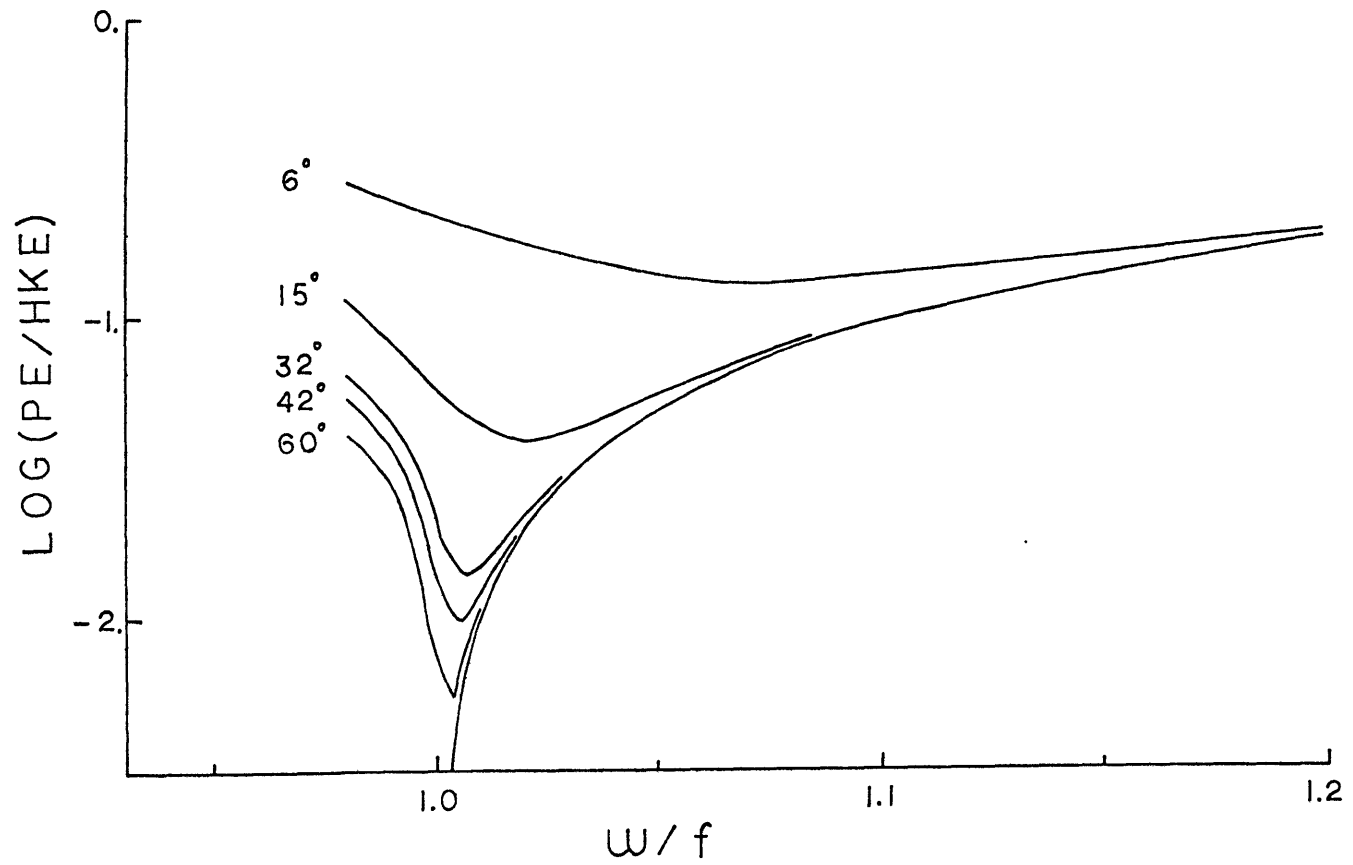
Figure 4.4   Model results of Log(P.E./H.K.E.) at the same
latitudes and with the same model parameters as in Fig. 4.2. The
envelope of the curves represents the WKBJ result.
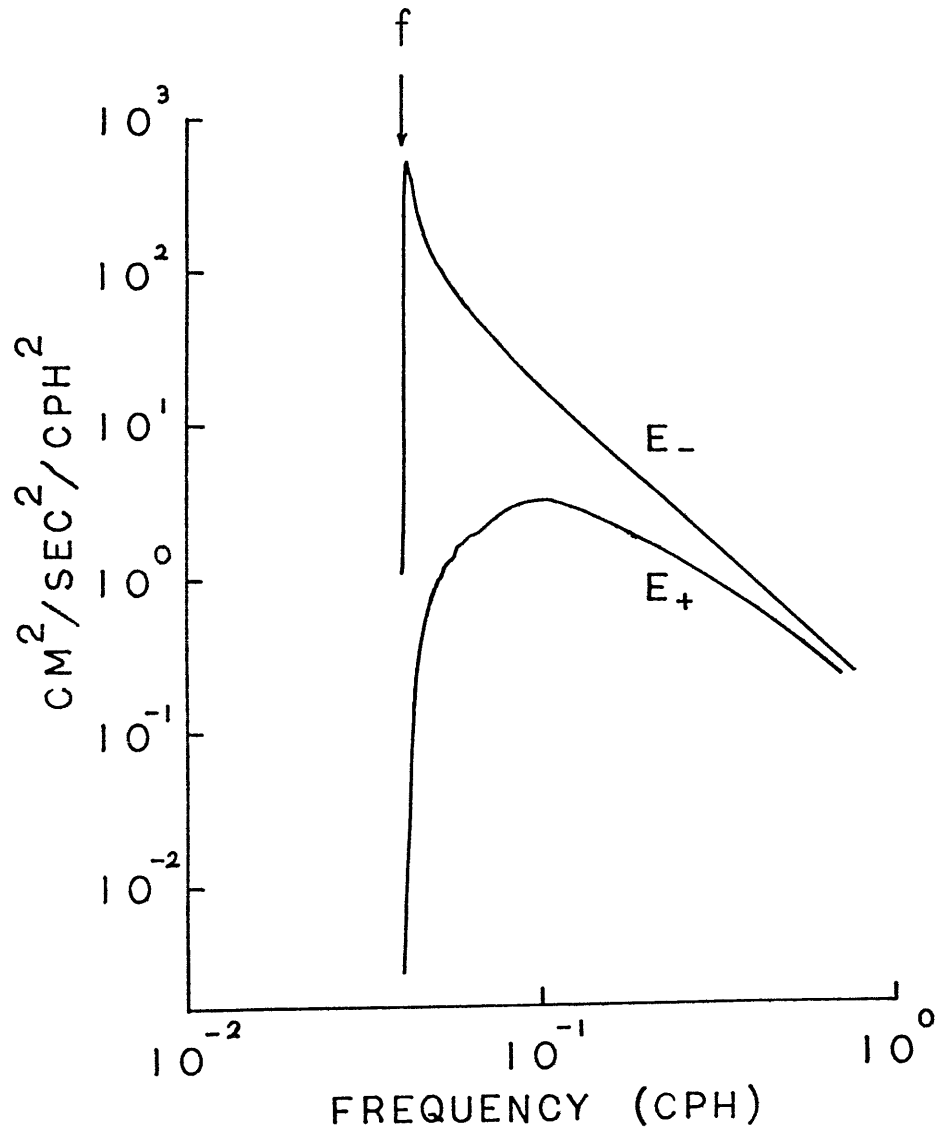
Figure 4.5   Model rotary spectra at 32° with the same model
parameters as in Fig. 4.2

Figure 4.6   Model results of Log(E_/E_+), i.e., Γ , at the
same latitudes and with the same model parameters as in Fig. 4.2.
The envelope curve is the WKBJ result.
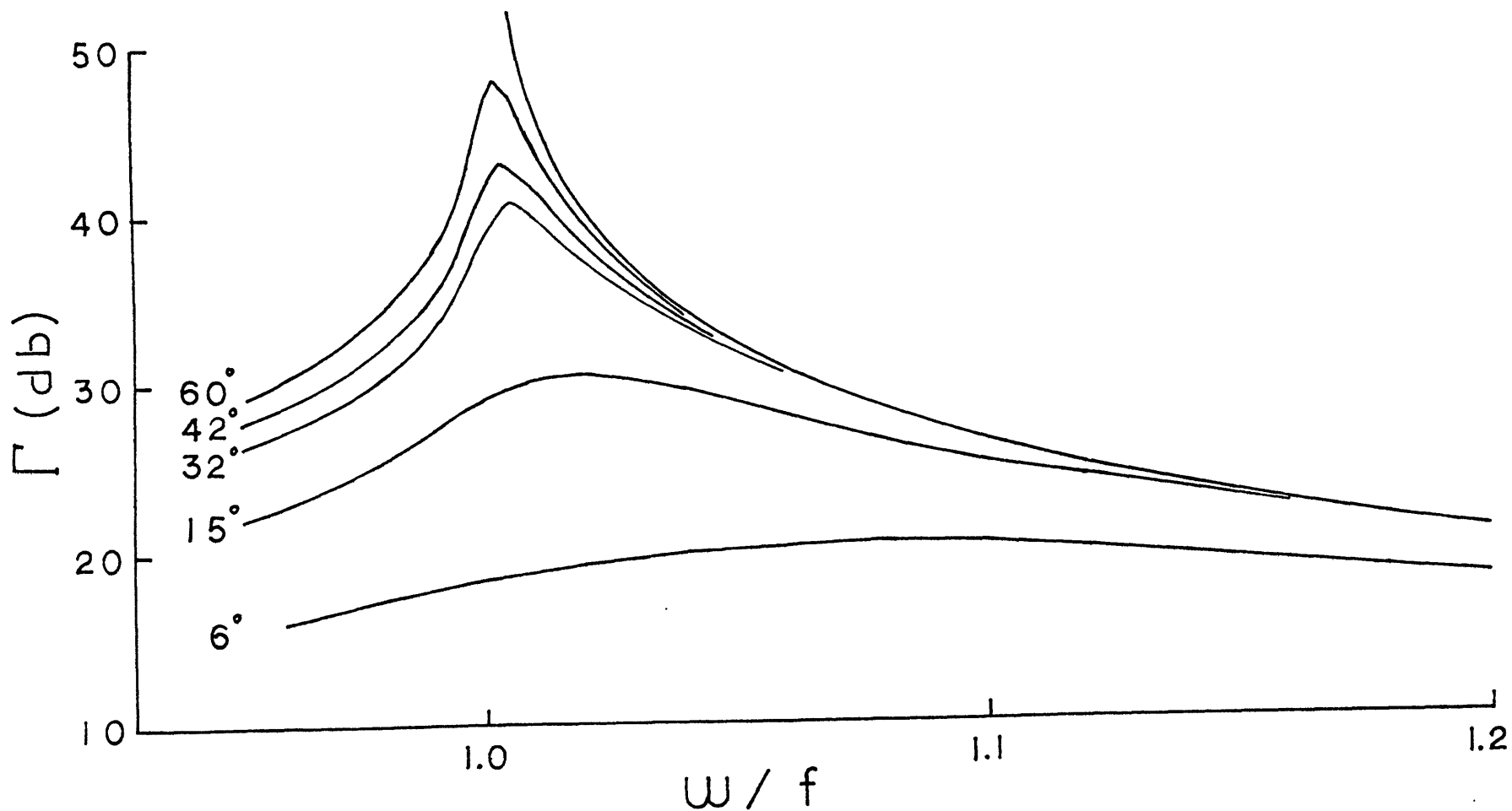
Although the results presented above are encouraging in some respects, it remains to be seen whether they are sensitive to the parameters j_*, t, and m in the vertical wavenumber spectrum A(j) and the special assumptions about D(k, j, ω).

The variation of the spectrum of H.K.E. with respect to j_*, t, and m is shown in Figs. 4.7, 4.8, and 4.9 respectively. There are only a slight increase in peak height and a decrease in blue shift with either increasing j_* or decreasing t -- both are equivalent to increasing the "equivalent band width" as discussed by Müller et al (1978). This reflects the wavenumber dependence of the horizontal wave functions. The case with $j_* = \infty$ corresponds to the top hat spectrum of GM72. Fig. 4.9 reveals that, for m > j_*, the results are virtually insensitive to m, the number of modes used in the calculations. Thus the results discussed in the previous section are not particularly sensitive to the model parameters.

As indicated in Fig. 3.2, the magnitude of the blue shift should be most sensitive to the zonal wavenumber content of the wave field. Because the turning latitude of a single wave decreases with increasing zonal wavenumber, one would expect an increase in the blue shift of the inertial peak if there exists a low wavenumber cutoff k_c, i.e., D(k, j, ω) = 0 for $|k| < k_c$. The model spectra at 32° were calculated with two values of k_c : 100 (340 km wavelength) and 400 (90 km wavelength). The results are not particularly sensitive to k_c in this range. When k_c = 100, the peak frequency is essentially unchanged, i.e., 1.01 f; when k_c = 400, it increases to 1.03 f. The other characteristics of the spectra essentially remain the same.
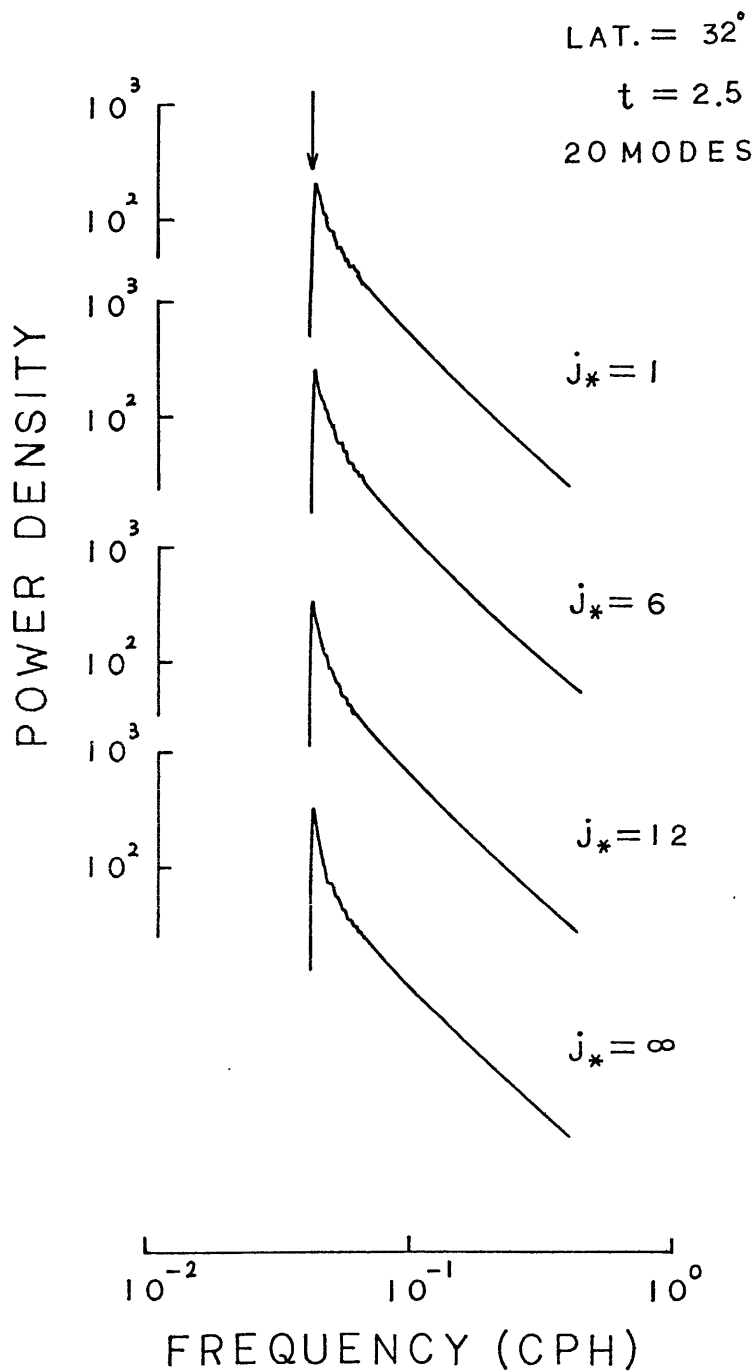
Figure 4.7   Model normalized horizontal kinetic energy spectra at 32° with different values of j*. Other model parameters are the same as in Fig. 4.2. The arrow indicates the local f.
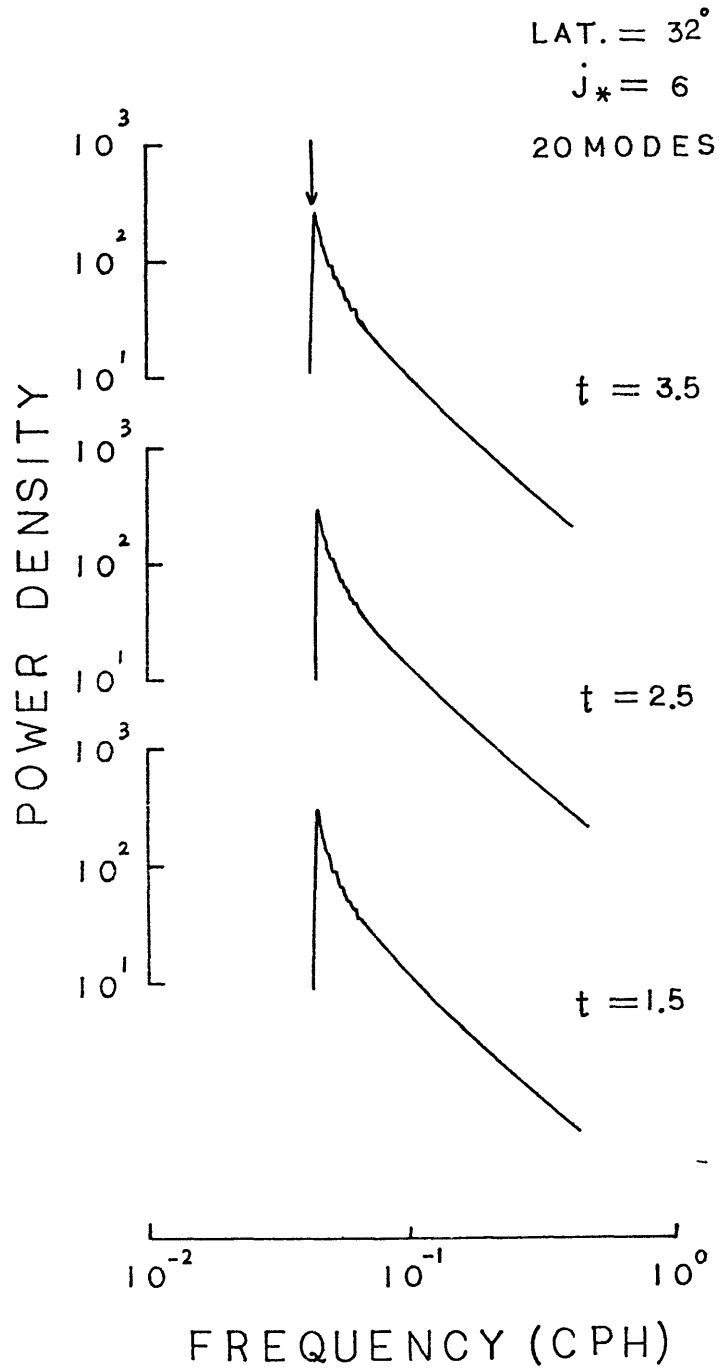
Figure 4.8   As in Fig. 4.7 except for different values of t.
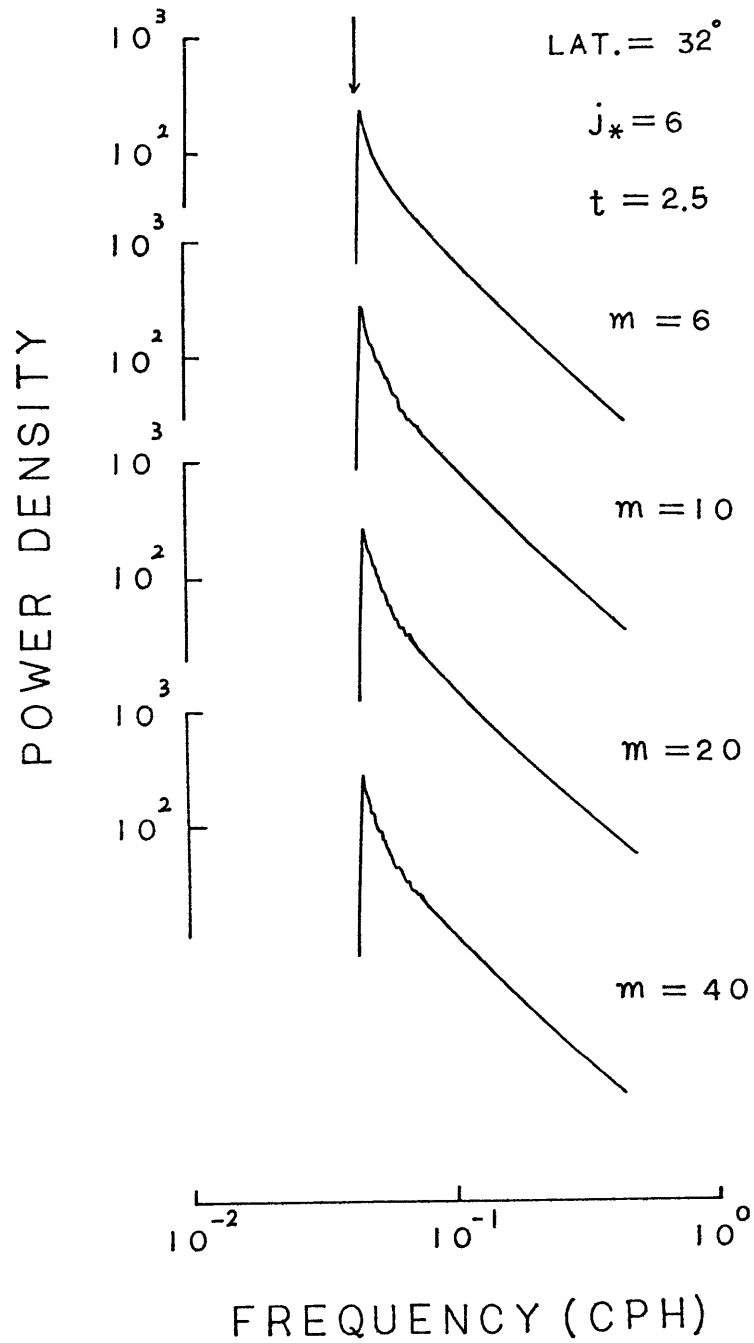
Figure 4.9   As in Fig. 4.7 except for different values of m (number of modes summed).

4.4 Comparisons with observations

4.4a Horizontal kinetic energy spectrum

As noted in Table 4.1, the peak height of the model spectrum is of the right order to account for observations from the class 3 environment, i.e., the deep ocean over smooth topography far from strong currents, where there are no apparent local sources. With the energy level E_o/N_o as an adjustable parameter and other assumptions the same as used in Fig. 4.2, the model was fitted to the deep observations at six latitudes by requiring that the peak value of H.K.E. be equal to the observed value at each latitude. The results for E_o/N_o are listed in Table 4.3. These six records belong to class 3 except those at 15° and 41.5^o, which are classified as class 2 in Chapter 2 with some ambiguity. The average of the estimates for E_o/N_o is 0.03 $cm^2/sec^2/cph^2$ with 15 % standard deviation. Fig. 4.10 shows the

Table 4.3

Estimated values of E_o/N_o for six records at 4000 m. The latitudes and classification of the records are as indicated.

Latitude(deg)	E_o/N_o	Class
15	.035	2b
28	.022	3
31.6	.033	3
35.6	.0267	3
37.5	.031	3
39.5	.033	2c

Figure 4.10 Model (smooth curves) and observed normalized spectra
of H.K.E. at 4000 m. Latitude, station number, and 95 % confidence
error bar for each record are shown.

a

PIIIC 4000M
LAT.= 15.0

b

WH5427 4000M
LAT.= 28.0

c

#7 PMII 4000M
LAT.= 31.6

d

#3 PMII 4000M
LAT.= 35.6

e

#8 PMII 4000M
LAT.= 37.5

f

#10 PMII 4000M
LAT.= 39.5
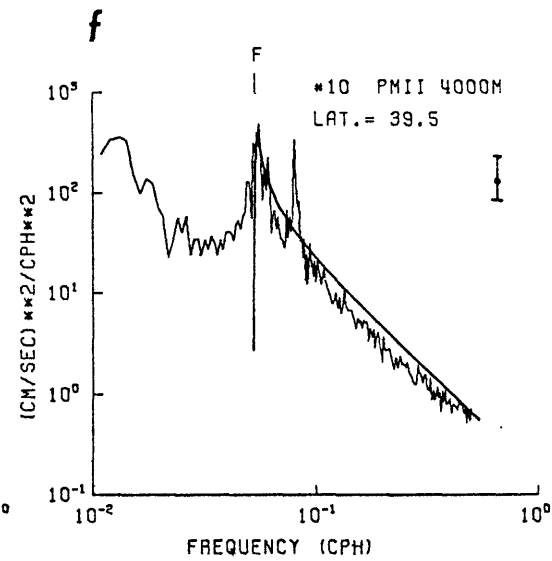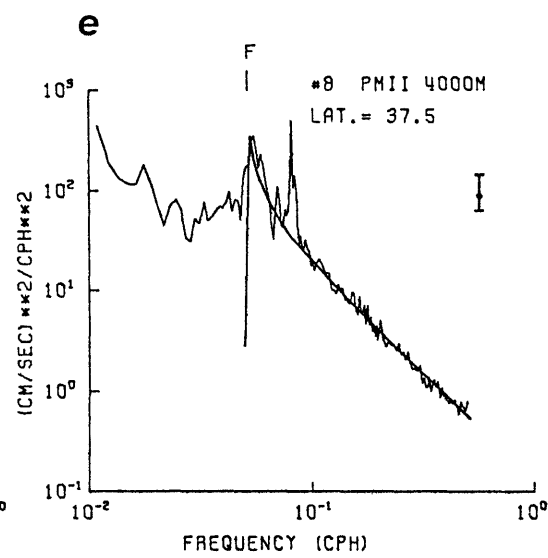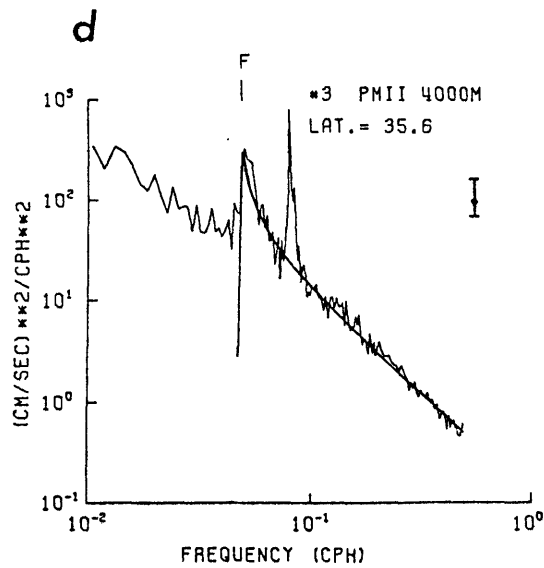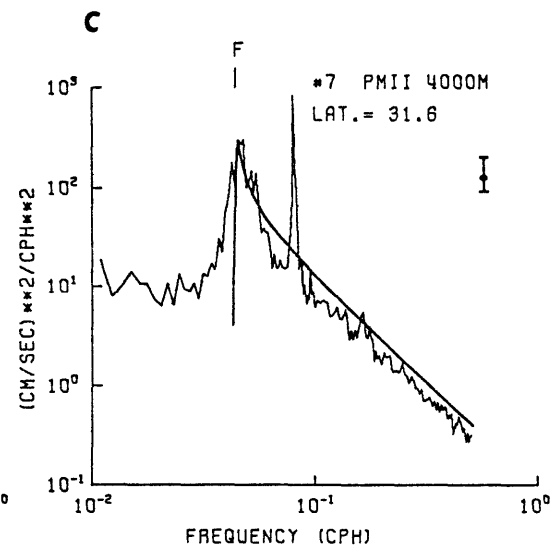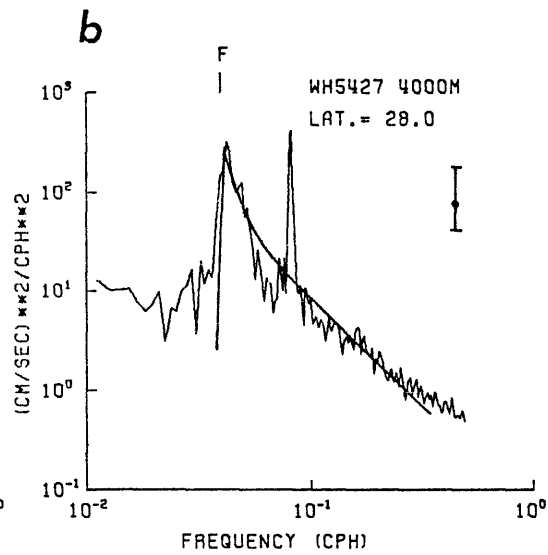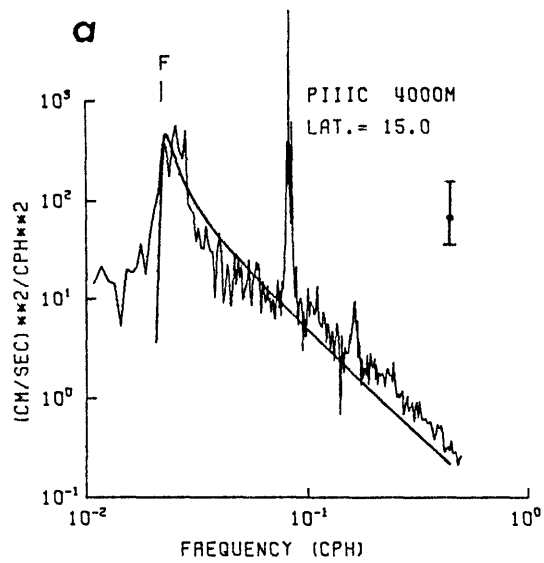
comparisons of the H.K.E. spectra between the model with E_o/N_o given

above and the corresponding observations. The agreement is fairly good,

indicating that the inertial wave field here is consistent with the

global model.

The estimated value for E_o/N_o can be compared with direct

equatorial observations. An "eyeball fit" of an energy spectrum of the

form $E_T \, \omega^{-2}$ to the observations of Eriksen (1979, Fig. 3), with the

assumption of equi-partition of H.K.E. and P.E., yields $E_T = 5.2$ x

10^{-2} cm^2/sec^2/cph^2. From the relation

$$\int_{-1}^{0} E_T \, N(z) \, dz \; = \; E_o$$

and the N(z) given by (3.16), we obtain

$$E_o/N_o = 0.0146 \text{cm}^2/\text{sec}^2/\text{cph}^2,$$

which is about a factor of two less than the extrapolation from

mid-latitude observations. This difference seems to be within the

uncertainty of the estimation of N(z), considering the difference in

N(z) at mid-latitudes and equatorial region.

We have now obtained a reference energy level for the global wave

field -- 7 db higher than the ω^{-2} spectrum extrapolated from high

frequencies, and identified the observations of class 3 with this

category. The average peak height of the class 2 observations is 12 db,

indicating that the energy level is about three times the value given by

the model. Thus the partition of inertial wave energy of the class 2

observations is likely to be the following : one third of the total

energy is due to global generation and two thirds local generation.

Assuming that all the local waves are generated at the surface and propagate downward, which is the case relevant to smooth topography areas, then the vertical wavenumber spectrum of the class 2 observations is such that 5/6 of the energy is travelling downward and 1/6 upward, because the global wave field is vertically symmetric (one half upward and one half downward) as a consequence of the underlying GM model. From a recent observation of Sanford (personal communication, 1979), about 72 % of the inertial wave energy is travelling downward, and 28 % upward; this differs from the above interpretation by about 11 % of the total energy, probably within the estimation errors.

The order of magnitude variation of energy levels with latitude at super-inertial frequencies (Fig. 4.1) seems contradictory to observations, because Wunsch and Webb (1977) reported nearly constant energy levels at 5-hour period regardless of latitude. However, Eriksen (1979) reported that near the equator, there is always a jump in energy level across the M_2 tidal frequency. Thus, if the super-M_2 energy level is constant, the sub-M_2 energy level near the equator must be less than that at higher latitudes, consistent with the model. For high frequency waves, nonlinear interactions are important in determining the spectrum; for a mid-latitude model see McComas and Bretherton (1977).

As noted in Table 4.1, the blue shift predicted by the model is smaller than the observed values in the class 3 environment (generally greater than 3 % of f). As discussed in the previous section, a low zonal wavenumber cutoff with $k_c \gtrsim 0(400)$ is therefore required to account for the observed magnitude of the blue shift. Because the spectral shape is not affected by the value of k_c, we can freely

adjust k_c to fit the observed blue shift for each individual record. However, such a "tuning" was not attempted in Fig. 4.10.

The decrease of the bandwidth with latitude as indicated in Table 4.1 is consistent with observations (see Table 2.4). The predicted values of the bandwidth are generally less than the observed values; however, the differences are probably not significant, i.e., not substantially greater than the frequency resolution limit. On the other hand, the pressence of a low frequency current can cause the broadening of the inertial peak through two mechanisms. Firstly, a uniform mean current could cause a Doppler shift of the inertial frequency (White, 1972). For example, a uniform current of 10 cm/sec would result in a Doppler shift with magnitude of 8 % of f at 30°, provided that the wavelength of the inertial waves is 100 km. Secondly, Fomin (1973) and Mooers(1975) have shown that a horizontal shear can cause an "effective inertial frequency" defined as

$$f_e = (f(f + \zeta))^{1/2},$$

where ζ is the vertical component of the relative vorticity of the mean current. For a relatively strong eddy with $\left|\dfrac{\zeta}{f}\right| \sim 0.05$, we have $\left|f_e - f\right| = 0.025f$. This effect has been observed at Site D by Perkins (1976). The result of these two mechanisms is to broaden the observed inertial bandwidth in long-term measurements by an amount of the order of 10 % of f, which is large enough to account for the difference between observations and the model results.

In summary, by assuming a low zonal wavenumber cutoff with

$k_c \gtrsim 400$ (1/90 cycle/km) in the Model 1 for $D(k, j, w)$, the H.K.E. of

the class 3 observations can be well-described by the model in terms of

both the peak height and blue shift. The slight difference between

observed and calculated bandwidth can be attributed to the kinematic

effects of mean flow on inertial waves.

4.4b Potential energy spectrum

When multiplied by $\frac{1}{2}(\frac{d\rho}{dT})^2 \frac{g^2}{\rho_0^2 N^2}$, observed temperature spectra can be

converted to P.E. spectra and compared with the model. Fig. 4.11 shows

the results at the same latitudes. Here the model cannot account for the

observed apparent inertial peaks. As mentioned earlier, temperature

signals in the inertial band are subject to contaminations (see Appendix

A), and the inconsistency between the observed H.K.E. and P.E. near f is

not unexpected. Using the measurements of isotherm depth from a

mid-water float, Cairns and Williams (1976) reported a vertical

displacement spectrum without inertial peaks similar to the model.

4.4c Rotary spectrum

Although the counter-clockwise energy level E_+ at the inertial

frequency predicted by the model is finite rather than zero (see Fig.

4.5), it is still much smaller than the observed values (see Fig. 2.8).

At mid-latitudes the calculated $\Gamma(f)$ is about 40 db, as compared to 15

db in the observed class 3 spectra (c.f. Fig. 2.9). This implies that

there is an excess of counter-clockwise energy which must be accounted

for by other mechanisms; local energy cascade from low frequency motions

is a possible candidate (see Section 2.3d).

4.5 Latitudinal limits of the model

Because the poles are singular points of Eq. (3.20), a special

Figure 4.11 As in Fig. 4.10 except for potential energy. 95 %
confidence error bar is the same for each record.

a

F

PIIIC 4000M
LAT.= 15.0

10^2

10^1

10^0

10^{-1}

10^{-2}

(CM/SEC) **2/CPH**2

10^{-2} 10^{-1} 10^0
FREQUENCY (CPH)

b

F

WH5428 4000M
LAT.= 28.0

10^2

10^1

10^0

10^{-1}

10^{-2}

(CM/SEC) **2/CPH**2

10^{-2} 10^{-1} 10^0
FREQUENCY (CPH)

c

F

#7 PMII3 4000M
LAT.= 31.6

10^2

10^1

10^0

10^{-1}

10^{-2}

(CM/SEC) **2/CPH**2

10^{-2} 10^{-1} 10^0
FREQUENCY (CPH)

d

F

#3 PMII3 4000M
LAT.= 35.6

10^2

10^1

10^0

10^{-1}

10^{-2}

(CM/SEC) **2/CPH**2

10^{-2} 10^{-1} 10^0
FREQUENCY (CPH)

e

F

#8 PMII3 4000M
LAT.= 37.5

10^2

10^1

10^0

10^{-1}

10^{-2}

(CM/SEC) **2/CPH**2

10^{-2} 10^{-1} 10^0
FREQUENCY (CPH)

f

F

#10 PMII3 4000M
LAT.= 39.5

10^2

10^1

10^0

10^{-1}

10^{-2}

(CM/SEC) **2/CPH**2

10^{-2} 10^{-1} 10^0
FREQUENCY (CPH)

expansion is needed to obtain valid wave functions there. Consequently, the model discussed above breaks down when $\phi \approx \pm 90°$. But how close to $\pm$ 90° is the model formally valid ? The validity of the Airy solution represented by (3.27) depends on the implicit assumption that $|\phi_s| < 90°$, i.e., there must be a turning latitude between 0° and 90°. For $\sigma > 1$, there is no turning latitude; the Airy solution is not applicable. However, at latitudes far from $\pm$ 90°, the Airy solutions can be replaced by the WKBJ solutions when $\sigma \gtrsim 1$ because σ_c there is well below unity (see 3.4); hence the model is valid at all frequencies. Thus the poleward limits of ϕ for the validity of the model are the latitudes where $\sigma_c = 1$. From (3.32), these are approximately $\pm$ 68°.

On the other hand, when $\phi \approx 0°$, the latitudinal equatorial modes for low frequency waves are likely to be established (Matsuno, 1966), and the continuous wavenumber spectrum underlying the model is irrelevant. The question about where the transition from the one turning point problem to the two turning point problem occurs is not easy to answer. Presumably for each vertical mode m, there exists a maximum latitudinal mode number n_{max} such that no equatorial modes exist with mode number $n > n_{max}$. Then the turning latitude of mode n_{max} is the transition latitude in question for the particular vertical mode m. Hence the answer is dependent on the wavenumber spectrum. Because the first vertical mode is usually the most energetic one, we proceed to discuss, based on m = 1, some possible implications from equatorial wave dynamics and observations.

Near the equator, Eq. (3.23) can be approximated by

$$\ell^2 = \epsilon_m (\sigma^2 - \phi^2) - \frac{k}{\sigma} - k^2 \tag{4.21}$$

The condition for the establishment of equatorial modes requires (Matsuno, 1966)

$$\sigma^2 \epsilon_m - \frac{k}{\sigma} - k^2 = \epsilon_m^{1/2} (2n+1) \quad, \tag{4.22}$$

where $n = 0, 1, 2, \ldots\ldots$. Then the turning latitude ϕ_{sn} for mode n is

$$\phi_{sn} = \epsilon_m^{-1/4} (2n+1)^{1/2} \quad. \tag{4.23}$$

We do not have a theory to determine n_{max}; presumably it depends on the dissipation and the time T which is required to establish the mode. With the latitudinal group velocity denoted by c_g, T can be written

$$T = 2 \int_{-\phi_{sn}}^{\phi_{sn}} \frac{d\phi}{c_g} \quad, \tag{4.24}$$

the time it takes a wave packet to make a complete excursion in the wave guide. From (4.21) and (4.22) we have

$$c_g = \frac{\partial \sigma}{\partial \ell} = \frac{2 \left[\epsilon_m^{1/2} (2n+1) - \epsilon_m \phi^2 \right]^{1/2}}{2 \sigma \epsilon_m + \frac{k}{\sigma^2}} \tag{4.25}$$

For simplicity, we assume that k = 0 in (4.25) and obtain

$$C_g = \left(\sigma \, \epsilon_m^{\frac{1}{2}} \right)^{-1} \left[\epsilon_m^{-\frac{1}{2}} (2n+1) - \phi^2 \right]^{\frac{1}{2}}$$

$$= \left(\sigma \, \epsilon_m^{\frac{1}{2}} \right)^{-1} \left(\sigma^2 - \phi^2 \right)^{\frac{1}{2}} \tag{4.26}$$

Substituting (4.26) into (4.24), we have

$$T = \pi \, \epsilon_m^{\frac{1}{4}} \left(2n+1 \right)^{\frac{1}{2}} \tag{4.27}$$

The values of ϵ_m are related to c_m, the gravity wave phase speed for vertical mode m, as follows:

$$\epsilon_m = \frac{4 \Omega^2 R^2}{c_m^2}$$

With c_1 = 2.6 m/sec as used by Wunsch and Gill (1976), we have $\epsilon_1 = 1.27 \times 10^5$. The values of ϕ_{sn} and T for m = 1 and some selected n's are tabulated in Table 4.4. The increase of T with n implies that higher modes are more difficult to set up as we expected. Wunsch and Gill (1976) showed clear evidence for the existence of equatorial modes up to n = 4 in the Pacific; Considering the increase of T with n, the value of n_{max} is likely O(5) and the transition occurs at O(10°). For higher vertical modes, T increases and ϕ_{sn} decreases; 10° is probably an upper bound for the relevance of a two turning point model.

Using discrete modal solutions on an equatorial beta plane, Eriksen (1979) developed a model spectrum for equatorially trapped waves. He found that there were no apparent inertial peaks at $\phi \approx 0^o$, and that a weak peak first showed up at about 3° with the blue shift equal

Table 4.4

Tabulation of ϕ_{sn} and T of the 1st baroclinic mode

equatorially trapped gravity waves for selected

meridional mode numbers n. Parenthetical values of T

are in wave periods.

n	ϕ_{sn}(deg.)	T(days)	
1	5.3°	103	(19)
2	6.8°	133	(31)
3	8.0°	157	(44)
4	9.1°	178	(57)
5	10.°	197	(69)
6	11.°	214	(82)
10	14.°	272	(132)

to 23 % of f. At 6° the blue shift predicted by his model is 18 % as

compared to 7 % by our model; hence the amount of the blue shift is a

good parameter to distinguish these two models. The observation at

7° N quoted by Eriksen (1979) showed a 10 % blue shift, which lies

between the predictions of these two models, implying only part of the

wave field (presumably the low vertical modes) has equatorial modal

structure. This supports the speculation that 10° is an upper bound

for the existence of equatorial gravity modes.

4.6 Summary and discussion

A model spectrum for the global inertial waves randomly forced at

lower latitudes has been developed. The model results vary with latitude. In general, there is a peak a few percent above f in the horizontal kinetic energy spectrum, with peak height a few decibels above the extrapolation of the spectrum at high frequencies; there is no distinct peak in the corresponding potential energy spectrum whose shape is very similar to the result of the GM model. The normalized energy level at the inertial frequency has its minimum at mid-latitudes (approximately $30°$) with variation less than one order of magnitude; the normalized energy level at super-inertial frequencies increases with latitude monotonously, yielding a difference greater than one order of magnitude between low and high latitudes. The general model results are not particularly sensitive to the model configuration and parameters. However, the assumption of a low zonal wavenumber cutoff slightly increases the blue shift.

Except at very low latitudes (less than $10°$), the peak height of the H.K.E. spectra is about 7 decibels and accounts for the observations in the deep ocean over smooth topography far from strong currents (class 3). With the difference between the model results and the upper ocean observations (class 2a) attributed to a downward propagating local wave field, we have estimated an energy budget in terms of upward and downward travelling wave energy; the result is fairly consistent with recent observations. A forced model is proposed in Chapter 5 to describe this local wave field.

The model predicts a slight decrease in both the bandwidth and blue shift with latitude, which is consistent with observations. In order to produce the observed magnitude of the blue shift, a low zonal wavenumber

cutoff of 1/90 cycle/km is required, i.e., the wavelength is required to be less than 90 km. The frequency bandwidth predicted by the model is slightly less than what is observed, but this difference can be accounted for by the kinematic effects of low frequency motions.

The latitudinal range of the validity of the model is roughly from 10° to 68°.

Chapter 5   A Forced Model for the Local Inertial Wave Field

5.1 Introduction

The purpose of this chapter is to study the oceanic response to a

localized forcing mechanism in the inertial frequency band. As the

details of the forcing spectrum near f are essentially unknown, we

consider an idealized model which is as simple as possible. Our focus is

on the following question : Can we show qualitatively that the observed

spectral characteristics which cannot be described by the global model,

are the results of local forcing ? Quantitative results in this chapter

are only suggestive, not conclusive.

The forcing is imposed through boundary conditions of the vertical

velocity field w_b at the base (or top) of the surface (or bottom)

mixed layer. In the surface layer w_b could be produced by either the

convergence and divergence of inertial currents in the mixed layer, or

the advection of its large scale corrugations by mean surface currents.

In the bottom layer w_b could be produced as a result of the

interaction between low frequency eddies and rough topography. But the

details of the boundary layer dynamics will not be pursued here.

At any particular latitude ϕ_b , we consider the response only in a

narrow frequency band around the local f, in which the forcing spectrum

can be simply modeled as white noise. Furthermore, we assume that the

corresponding spatial structure is localized and not varying with

frequency. The assumption of localness does not imply that remote

forcing with frequencies in this particular range does not exist, but

that it has been already accounted for by the global model.

In order to describe the transition of wave functions from evanescent when $w < f$ to oscillatory when $w > f$, as noted in Chapter 1, the variation of f with latitude must be taken into account in the governing equations. The simplest approximation of this kind is the equatorial beta plane approximation with $f = \beta y$; however, this aproximation is not strictly valid for the problem of mid-latitude inertial waves (see Lindzen, 1967). With $f = f_o + \beta y$ at mid-latitudes, the resulting equation is the Weber equation whose solutions are not particularly easy to handle. The recent developments in asymptotic solutions of the LTE (e.g., Kamenkovich and Tsybaneva, 1975 a, b) have provided a feasible way to deal with the LTE directly. With proper boundary conditions, the eigensolutions of the LTE form a complete set (Longuet-Higgins, 1968) which can be used to expand the latitudinal structure of the forcing function. Then the problem remaining is to solve the vertical equation for each latitudinal mode subject to specific boundary conditions. At the forced boundary, the vertical velocity is given, but the other boundary condition needs some arguments. Should we let the waves reflect from the vertical boundaries with the possibility that they form normal modes with the incident waves? The answer depends on the travel time to take a wave packet through a vertical round trip in the ocean. In Kroll's model (1975) of the ray paths of internal waves on a beta plane, it was implied that the travel time was of the order of 60 days for those rays which had encountered their turning points, and of the order of 10 days for those which had not. Because the travel time is longer than the time scale of the forcing (usually less than a week), it seems appropriate to neglect the

reflected waves. This conclusion also can be reached by considering the nearly horizontal propagation of the rays when $\omega \approx f$. With the mid-latitude beta plane approximation, the equation for the amplitude of the velocity v, which is proportional to $\exp(\ i\ (k\lambda - \omega t))$ can be written as (c.f. Philander, 1978)

$$V_{yy} - (\ k^2 + \beta \frac{k}{\omega}\ ) V\ +\ (\ f^2 - \omega^2\ )\frac{\partial}{\partial z}\ (\ \frac{1}{N^2}\ \frac{\partial V}{\partial z}\ )\ =\ 0 \qquad (5.1)$$

where $f = f_0 + \beta y$, $\beta = \dfrac{df}{dy}$, and $y = R\phi$. If, for simplicity, we assume k = 0, the ray paths lie in the y-z plane and can be represented by

$$\pm \int_0^z N(z)dz\ =\ \frac{1}{\beta}\ \int_{f_0}^{f(y)} (\ \omega^2 - f^2\ )^{1/2}\ df \qquad (5.2)$$

Then for a surface-generated wave packet reflecting back to the surface, the latitudinal distance it travels, d, can be estimated by repeated uses of (5.2). For H = 5 km, and ϕ_0 = 30°, we obtain d $\approx$ 500 km. If the latitudinal scale of the forcing is less than 500 km, the reflected waves will be out of the forced region and can then be neglected in the local dynamics. Based on these two considerations, it seems justified in a local model to assume that the ocean is infinitely deep and that the waves never reflect; hence we should use appropriate radiation boundary conditions whenever they are relevant. So the model configuration is basically the same as that used by Wunsch (1977) in his study of the

equatorial Indian Ocean. But where does the energy go ? Presumably part of it is lost through friction and/or redistributed through nonlinear interactions; the remaining energy will eventually become, through "remote reflections," part of the internal wave field equatorward of the forced region.

In order to put this model into its proper perspective, we briefly review some previous models with emphasis on their differences from this one. The purpose of the model of Pollard (1970) was to study the oceanic response to a wind event of finite duration as an initial value problem. It was an f-plane model with vertical modal decomposition and its focus was on the amplitudes and structures of wind forced inertial waves. The model of Hendershott (1973), on the other hand, studied the response to periodic forcing with the diurnal tidal frequency; its focus was on the response at this particular frequency as a function of latitude. The procedure for obtaining a solution is similar to that used in our model, but it involved vertical modes rather than propagating waves, and the beta plane equations rather than the LTE. The model of Kroll (1975) was used to study the propagation of inertial waves from the surface mixed layer to the deep ocean based on ray theory; its focus was on the ray paths at a particular frequency near f and the variation of amplitude along them. For the ray solutions, however, it is generally difficult to obtain their Eulerian representations which can most easily be compared with field observations. Furthermore, the response at sub-inertial frequencies cannot be adequately described.

The organization of this chapter is as follows : Section 5.2 describes the formulation of the model and methods of solution; Section

5.3 presents an asymptotic expansion procedure for the LTE in the parameter regime of inertial waves; Section 5.4 presents the model results; Section 5.5 is a summary.

5.2 The model and methods of solution

At a particular position (λ_o , ϕ_o), the local forcing generally can be represented as a Fourier integral in frequency space as follows:

$$W_b(\lambda,\phi,t) = \frac{1}{\sqrt{2\pi}} \, Real \int_{-\infty}^{\infty} \hat{W}_b(\lambda,\phi,\sigma) \, exp(-i\sigma t) \, d\sigma \, , \qquad (5.3)$$

with
$$\hat{W}_b = \frac{s(\lambda,\phi)}{\left(2\,|\sigma_2 - \sigma_1|\right)^{1/2}} \qquad for \quad \sigma_2 > |\sigma| > \sigma_1 > 0 \qquad (5.4)$$

$$= 0 \qquad \qquad otherwise,$$

where $\sigma_2 > \dfrac{f_o}{2\Omega} > \sigma_1$, and $f_o = 2\Omega \sin \phi_o$. Thus the forcing energy is evenly distributed in a narrow frequency band centered on $\pm f_o$, and $\left| s(\lambda,\phi) \right|$ represents the spatial distribution of its root mean square amplitude. In particular, we consider $s(\lambda,\phi)$ of the following form :

$$S(\lambda,\phi) = S_o \, exp\left[i\,k_o\,(\lambda - \lambda_o) - \frac{(\phi - \phi_o)^2\,R^2}{L^2} \right] \, , \qquad (5.5a)$$

where
$$k_o = \frac{R\cos\phi_o}{L} \qquad \qquad (5.5b)$$

and L is a length scale. Eqs. (5.5a) and (5.5b) represent a disturbance

of which the latitudinal dependence is a Gaussian distribution centered at ϕ_0 with scale L, and the zonal dependence is sinusoidal with dimensional wavenumber equal to 1/L. With s(λ , ϕ) given by (5.5a) and (5.5b), Eq. (5.3) represents a group of zonally propagating waves whose amplitudes are localized in latitude with scales comparable to their zonal wavelengths. This is the simplest model for a latitudinally localized forcing.

Now the solutions of all the field variables can be written as

$$
\begin{bmatrix} u(\lambda,\phi,z,t) \\ v(\lambda,\phi,z,t) \\ w(\lambda,\phi,z,t) \\ p(\lambda,\phi,z,t) \\ \rho(\lambda,\phi,z,t) \end{bmatrix} = \frac{1}{\sqrt{2\pi}} \, Real \int_{-\infty}^{\infty} d\sigma \begin{bmatrix} \hat{u}(\phi,z,\sigma) \\ \hat{v}(\phi,z,\sigma) \\ \hat{w}(\phi,z,\sigma) \\ \hat{p}(\phi,z,\sigma) \\ \hat{\rho}(\phi,z,\sigma) \end{bmatrix} exp\left[i(k_0\lambda - \sigma t)\right] \qquad (5.6)
$$

with $\hat{w}(\phi,z,\sigma) = \hat{w}_b$ at the forced boundary and proper radiation conditions at the other. Following Eq. (3.8), $\hat{w}(\phi,z,\sigma)$ generally can be written as the sum of an infinite series of functions separable in z and ϕ as follows:

$$
\hat{w}(\phi,z,\sigma) = \sum_{n=1}^{\infty} -i \, W_{n,\sigma}(z) \, P_{n,\sigma}(\phi) \, . \qquad (5.7)
$$

Each term in (5.7), when multiplied by $exp(i(k_0\lambda - \sigma t))$, is a solution to Eqs. (3.2)-(3.6) with terms involving $2\Omega \cos\phi$ neglected. Similarly, $\hat{v}(\phi, z, \sigma)$ and $\hat{p}(\phi, z, \sigma)$ can be written

$$\hat{v}\,(\phi,\,z\,,\,\sigma\,) \;=\; \frac{i}{\cos\phi} \sum_{n=1}^{\infty} F_{n,\sigma}\,(z)\;V_{n,\sigma}(\phi) \quad, \tag{5.8}$$

$$\hat{p}\,(\phi,\,z\,,\,\sigma\,) \;=\; 2\,\Omega\,R \sum_{n=1}^{\infty} F_{n,\sigma}(z)\;P_{n,\sigma}\,(\phi) \;. \tag{5.9}$$

The latitudinal problem

The equation for $P_{n,\sigma}$ can be obtained by eliminating V from (3.18) and (3.19), yielding the conventional form of the LTE in terms of pressure:

$$(1-\nu^2)\frac{d^2 P_{n,\sigma}}{d\nu^2} + 2\nu\,\frac{1-\sigma^2}{\sigma^2-\nu^2}\,\frac{d P_{n,\sigma}}{d\nu} + \left[\,\epsilon_{n,\sigma}\,(\sigma^2-\nu^2) - \frac{k_0^2}{1-\nu^2} - \frac{k_0}{\sigma}\,\frac{\nu^2+\sigma^2}{\nu^2-\sigma^2}\,\right]P_{n,\sigma} = 0 \tag{5.10}$$

where $\nu = \sin\phi$. With appropriate homogeneous boundary conditions imposed at the latitudinal boundaries, $\pm\,\phi_b$, $\epsilon_{n,\sigma}$ is the eigenvalue for the nth eigensolution $P_{n,\sigma}$. Eq. (5.10) then poses a Sturm-Liouville problem. For given σ and k_0, we have the following orthogonality condition

$$\int_{-\phi_b}^{\phi_b} P_{n,\sigma}(\phi)\;P_{m,\sigma}(\phi)\;d\phi \;=\; \delta_{m,n} \tag{5.11}$$

Moreover, $P_{n,\sigma}$'s form a complete set in $\left[-\phi_b,\,\phi_b\right]$ (Longuet-Higgins, 1968).

From Eq. (3.18), $V_{n,\sigma}(\phi)$ can be obtained as

$$V_{n,\sigma} \;=\; \frac{\sigma}{\nu^2-\sigma^2}\left[\,(1-\nu^2)\,\frac{d P_{n,\sigma}}{d\nu} + \frac{k_0\nu}{\sigma}\,P_{n,\sigma}\,\right] \tag{5.12}$$

The boundary conditions and corresponding eigensolutions of Eqs. (5.10) and (5.12) are discussed in Section 5.3.

The vertical problem

The vertical equation for $W_{n,\sigma}(z)$ is the same as (3.14) with ϵ replaced by the eigenvalue $\epsilon_{n,\sigma}$:

$$\frac{d^2 W_{n,\sigma}(z)}{d z^2} + \epsilon_{n,\sigma} S^2 \tilde{N}^2(z) W_{n,\sigma}(z) = 0 \qquad (5.13)$$

The boundary condition at the forced boundary can be written

$$\sum_{n=1}^{\infty} - i W_{n,\sigma}(z_b) P_{n,\sigma}(\phi) = \hat{w}_b(\phi) , \qquad (5.14)$$

where $z_b = 0$ for surface forcing,

$\qquad\qquad\quad = -1$ for bottom forcing.

Multiplying both sides of (5.14) by $P_{m,\sigma}(\phi)$ and integrating from $-\phi_b$ to ϕ_b, with the use of (5.11) we obtain

$$W_{n,\sigma}(z_b) = i\, a_{n,\sigma} , \qquad (5.15)$$

where $$a_{n,\sigma} = \int_{-\phi_b}^{\phi_b} P_{n,\sigma}(\phi)\, \hat{w}_b(\phi)\, d\phi \qquad (5.16)$$

From Eq. (3.12) we can obtain $F_{n,\sigma}(z)$ from $W_{n,\sigma}(z)$ as follows :

$$F_{n,\sigma}(z) = \frac{R}{\epsilon H \sigma} \frac{d W_{n,\sigma}}{d z} \qquad (5.17)$$

Before proceeding to solve the vertical equations, we should choose a suitable $N(z)$. With surface sources, using an exponential $N(z)$ Wunsch (1977) encountered two problems : Firstly, Wunsch (1977) has pointed out that, as $z \rightarrow -\infty$, $N(z)$ eventually becomes smaller than any given frequency σ and waves reflect even in an infinitely deep ocean. Secondly, D. Moore and J. McCreary (personal communication via C. Wunsch) have recently pointed out that the solutions obtained by Wunsch (1977) in terms of Hankel functions are erroneous because the argument of the Hankel functions in his problem is small in the far-field ($z \rightarrow -\infty$) where the radiation condition should be applied, and the asymptotic behavior (upward phase propagation to produce downward energy propagation) invoked is not correct. Both problems can be resolved, however, by assuming the following form of $\tilde{N}(z)$:

$$\tilde{N}(z) = N_b/N_o + \exp(zH/b) \qquad (5.18)$$

where N_b is a constant representing a nearly uniform stratification as $z \rightarrow -\infty$. If the value of N_b is chosen to be at least several times greater than f (usually the case in the deep ocean), inertial waves would not reflect and the WKBJ solutions are valid as $z \rightarrow -\infty$. Hence the appropriate solutions are those with upward phase propagation, as the consequence of requiring downward energy propagation. The parameter H, defined as the ocean depth before, is an arbitrary scale for z now, because we have assumed that the ocean is infinitely deep. However, for the problem of bottom forcing, we will assume that the source is located at $z = -1$ (or $z^* = -H$), and let the ocean extend to $z \rightarrow +\infty$.

With $\tilde{N}(z)$ given by (5.18) and boundary condition given by (5.15), the WKBJ solutions can be readily obtained from Eq. (3.17). Defining

$$\gamma = \frac{S'b}{H} |\epsilon|^{1/2} \qquad (5.19)$$

and

$$\theta(z) = \frac{N_b}{N_0} (z+1) S' |\epsilon|^{1/2} + \gamma (e^{zH/b} - e^{-H/b}), \qquad (5.20)$$

the results for both surface and bottom forcing are written as follows :

Surface forcing

(i) $\underline{\epsilon_{n,\sigma} > 0}$

$$W_{n,\sigma}(z) = A_{n,\sigma} \tilde{N}(z)^{-1/2} \exp[i\theta(z)], \qquad (5.21)$$

$$F_{n,\sigma}(z) = \frac{iN_0}{2\Omega\sigma} |\epsilon_{n,\sigma}|^{-1/2} A_{n,\sigma} \tilde{N}(z)^{1/2} \exp[i\theta(z)], \qquad (5.22)$$

where

$$A_{n,\sigma} = \left\{ \tilde{N}(0)^{-1/2} \exp[i\theta(0)] \right\}^{-1} (ia_{n,\sigma}) \qquad (5.23)$$

When multiplied by $\exp(-i\sigma t)$, Eqs. (5.21)-(5.23) represent a wave solution with upward phase (downward energy) propagation.

(ii) $\underline{\epsilon_{n,\sigma} < 0}$

$$W_{n,\sigma}(z) = B_{n,\sigma} \tilde{N}(z)^{-1/2} \exp[\theta(z)], \qquad (5.24)$$

$$F_{n,\sigma}(z) = \frac{-N_0}{2\Omega\sigma} |\epsilon_{n,\sigma}|^{-1/2} B_{n,\sigma} \tilde{N}(z)^{1/2} \exp[\theta(z)] \qquad (5.25)$$

where

$$B_{n,\sigma} = \left\{ [\tilde{N}(0)]^{-1/2} \exp[\theta(0)] \right\}^{-1} (ia_{n,\sigma}) \qquad (5.26)$$

Eqs. (5.24)-(5.26) represent an evanescent solution trapped to the surface (z = 0).

Bottom forcing

(i) $\epsilon_{n,\sigma} > 0$

$$W_{n,\sigma}(z) = C_{n,\sigma}\, \tilde{N}(z)^{-\frac{1}{2}} \exp\left[-i\,\theta(z)\right] \quad , \tag{5.27}$$

$$F_{n,\sigma}(z) = \frac{-i N_0}{2\Omega\sigma} \left|\epsilon_{n,\sigma}\right|^{-\frac{1}{2}} C_{n,\sigma}\, \tilde{N}(z)^{\frac{1}{2}} \exp\left[-i\,\theta(z)\right], \tag{5.28}$$

where

$$C_{n,\sigma} = \left[\tilde{N}(-1)\right]^{\frac{1}{2}} \left(i\, a_{n,\sigma}\right) \tag{5.29}$$

When multiplied by exp(-i σ t), Eqs. (5.27)-(5.29) represent a wave solution with downward phase (upward energy) propagation.

(ii) $\epsilon_{n,\sigma} < 0$

$$W_{n,\sigma}(z) = C_{n,\sigma}\, \tilde{N}(z)^{-\frac{1}{2}} \exp\left[-\theta(z)\right] \quad , \tag{5.30}$$

$$F_{n,\sigma}(z) = \frac{N_0}{2\Omega\sigma} \left|\epsilon_{n,\sigma}\right|^{-\frac{1}{2}} C_{n,\sigma}\, \tilde{N}(z)^{\frac{1}{2}} \exp\left[-\theta(z)\right]. \tag{5.31}$$

Eqs. (5.30)-(5.31) represent an evanescent solution trapped to the bottom (z = -1).

To complete the solutions, we proceed to the latitudinal problem in the next section, solving for the eigenfunctions $P_{n,\sigma}$ and $V_{n,\sigma}$ and their eigenvalues $\epsilon_{n,\sigma}$ for given k_0.

5.3 Asymptotic solutions of the Laplace's tidal equations in the parameter regime of inertial waves

5.3a Introduction

General eigensolutions of the LTE , the so-called Hough functions, were investigated extensively by Flattery (1967) and Longuet-Higgins (1968), but they are global in character and inconvenient to apply in describing a localized, high wavenumber phenomenon such as oceanic inertial waves. Because the non-dimensional parameter of the LTE, $\epsilon = \dfrac{4\Omega^2 R^2}{gh}$, where R is the radius of the earth, h the equivalent depth for a particular mode, g the gravity, is very large ($\gtrsim 10^5$) under oceanic conditions, asymptotic approximations in terms of ϵ have been applied by several investigators. The spheroidal wave equation was applied by Longuet-Higgins (1965), and by Munk and Phillips (1968) to approximate the LTE for large ϵ . Solutions obtained by the latter authors were applied in Chapter 4 to construct the global wave model; however, these solutions are invalid for $\phi \sim \cos^{-1}(\dfrac{k}{\epsilon^{1/2} \sigma}$) (see Section 3.3). For a forced model, we need uniformly valid eigensolutions to expand a given forcing function, therefore the solutions of MP cannot be applied here. Using matched asymptotic expansion methods, Kamenkovich and Tsybaneva (1975 a, b) obtained uniformly valid asymptotic solutions in two limits : (a) k is of order unity; (b) k is of order $\epsilon^{1/2}$. As originally pointed out by MP, the zonal wavenumber of inertial waves is of order $\epsilon^{1/3}$ or less; in this limit, Kamenkovich et al (1977) have derived asymptotic formula for positive ϵ but not for negative ϵ . Miles (1977) has extensively discussed asymptotic eigensolutions of the

LTE with large ϵ ; however, for $\sigma < 1$, his results are formally valid only for $k/\sigma \lesssim O(1)$.

The purpose of this section is to present an asymptotic expansion procedure for the LTE with zonal wavenumber ranging from zero to order $\epsilon^{1/3}$; which includes case (a) of Kamenkovich and Tsybaneva (1975 a) as a limiting case. However, the geometry is different; the ocean is not assumed to cover the whole earth but to be bounded by two latitudes $\pm \phi_b$. The reason for this assumption is to avoid the complexity involved near the poles, which actually are separated from the major oceans. Moreover, the high modes of interest are insensitive to the details of the boundary conditions. To be remote from the mid-latitudes which are our major concern, ϕ_b has been arbitrarily set to be 60°. For given and k, approximate eigensolutions and eigenvalues have been obtained. The results for positive eigenvalues, which are not affected by boundary conditions poleward of the turning latitude, have been compared with Longuet-Higgins' numerical results (1968).

5.3b Solutions

Dropping all the subscripts, we rewrite (5.10) here for reference

$$(1-\nu^2)\frac{d^2 P}{d\nu^2} + 2\nu \frac{1-\sigma^2}{\sigma^2-\nu^2} \frac{dP}{d\nu} \left[\epsilon (\sigma^2- \nu^2) - \frac{k^2}{1-\nu^2} - \frac{k}{\sigma} \frac{\nu^2+ \sigma^2}{\nu^2- \sigma^2} \right] P = 0 \qquad (5.32)$$

The eigenvalue ϵ can be either positive or negative, and we call the corresponding eigensolutions "positive modes" and "negative modes" respectively.

In the parameter regime of oceanic inertial waves, i.e., $|\epsilon| \gg 1$,

$\sigma \lesssim O(1)$, and $k \lesssim O(\epsilon^{1/3})$, from the dispersion diagrams of Longuet-Higgins (1968), only the type 1, type 4, and type 5 waves as classified by him are present. Type 1 waves are inertia-gravity waves with $\epsilon > 0$; type 4 and type 5 waves are westward-going and eastward-going waves respectively with $\epsilon < 0$, which are trapped in the vertical. We shall treat first the case of positive modes.

(i) Positive modes

If we write

$$k = s\,\epsilon^{1/3}, \quad (s \lesssim O(1))$$ (5.33)

and

$$G(\nu) = (\sigma^2 - \nu^2)(1 - \nu^2) - \epsilon^{-1/3} s^2$$ (5.34)

then Eq. (5.32) becomes

$$(1-\nu^2)\frac{d^2 P}{d\nu^2} + 2\nu\frac{1-\sigma^2}{\sigma^2-\nu^2}\frac{dP}{d\nu} + \left[\epsilon\frac{G(\nu)}{1-\nu^2} - \frac{s}{\sigma}\epsilon^{1/3}\frac{\nu^2+\sigma^2}{\nu^2-\sigma^2}\right] = 0$$ (5.35)

there are two positive roots, ν_0 and ν_1, of the equation $G(\nu) = 0$. Assuming that $\nu_0 < \nu_1$, then we have

$$\nu_0 = \sigma\left[1 - \frac{s^2}{2}\epsilon^{-1/3}\frac{1}{\sigma^2(1-\sigma^2)}\right] + O(\epsilon^{-2/3})$$ (5.36)

$$\nu_1 = 1 + \frac{s^2}{2}\epsilon^{-1/3}\frac{1}{1-\sigma^2} + O(\epsilon^{-2/3})$$ (5.37)

The latitudes corresponding to $\pm \nu_0$ are the "turning latitudes," where Eq.(5.35) changes from hyperbolic ($|\nu| < \nu_0$) to elliptic ($|\nu| > \nu_0$).

The latitudinal boundaries, $\pm \phi_b$, are presumably poleward of the turning latitudes; to be specific, we assume that $\left| \sigma - \sin\phi_o \right| \gg \epsilon^{-1/3}$ in what follows. Following the method of matched asymptotic expansion (Nayfeh, 1973), we shall first derive the "turning point solution" which is valid in the vicinity of ν_o , and the "outer solution" which is valid as $\left(\nu - \nu_o \right) \sim O(1)$; then obtain a uniformly valid composite solution using the matching conditions.

Turning point solution (P_i)

In the vicinity of ν_o , we define

$$\xi = \left(\nu - \nu_o \right) \epsilon^{\beta} \tag{5.38}$$

and

$$P_i = B_o + B_1 \epsilon^{\alpha} + B_2 \epsilon^{2\alpha} + \cdots \cdots \tag{5.39}$$

If we substitute (5.38) and (5.39) into (5.35) and equate terms of equal power in ϵ , then the balance among dominant terms yields $\alpha = -1/3$, $\beta = 1/3$ and

$$\frac{d^2 B_o}{d\xi^2} - \frac{1}{\xi - \frac{bs}{2\nu_o}} \frac{dB_o}{d\xi} - \left[c\xi + \frac{b}{\xi - \frac{bs}{2\nu_o}} \right] B_o = 0 \tag{5.40}$$

where

$$c = \frac{2\nu_o \left(\nu_1^2 - \nu_o^2 \right)}{\left(1 - \nu_o^2 \right)^2} \quad , \quad b = \frac{s}{1 - \nu_o^2} \tag{5.41}$$

An approximate solution to (5.40) was found to be

$$\Gamma'(\xi) = r \, Ai \, (c^{1/3}\xi) - c^{1/3} \, Ai'(c^{1/3}\xi), \tag{5.42}$$

where

$$\bar{r} = b \left(\frac{\nu_1^2 - \nu_0^2}{1 - \nu_0^2} \right) \; ; \tag{5.43}$$

Ai and Ai' are the Airy function and its derivative which are bounded at $+ \infty$. $\Gamma(\xi)$ satisfies Eq. (5.40) with the b's replaced by r's. From Eqs. (5.36), (5.37), and (5.43) we have

$$r = b \left[1 + O(\epsilon^{-1/3}) \right] \; ,$$

and consequently

$$\Gamma(\xi) = B_0(\xi) + O(\epsilon^{-1/3}) \; .$$

Therefore $\Gamma(\xi)$ is a consistent first order approximation of P_i, i.e.,

$$P_i = \Gamma(\xi) + O(\epsilon^{-1/3}) \tag{5.44}$$

Outer solution (P_0)

Solutions poleward of the turning latitudes are exponentially small as indicated by the Airy functions in (5.42); hence they have no effects on solutions equatorward of the turning latitudes, and we shall not derive them in detail. For $\nu < \nu_0$, an appropriate expansion was found to be

$$P_0(\nu) = M \left(A_0 + \epsilon^{-1/6} A_1 + \epsilon^{-1/3} A_2 + \epsilon^{-1/2} A_3 + \cdots \right) \exp\left[\pm i \epsilon^{1/2} a(\nu) \right] \tag{5.45}$$

where M is a constant to be determined by the matching conditions. It is clear from (5.44) and (5.45) that we must carry the second order term A_1 in (5.45), in order to obtain a uniformly valid solution. Substituting (5.45) into (5.35) and equating terms of equal power in ϵ, we obtain

$$a(\nu) = \int_{\nu}^{\nu_0} \frac{G^{1/2}}{1 - \nu'^2} \, d\nu' \tag{5.46}$$

$$A_0(\nu) = \left| \frac{\nu_0^2 - \nu^2}{\nu_1^2 - \nu^2} \right|^{1/4} \tag{5.47}$$

$$A_1(\nu) = \mp \frac{iS}{2\nu_0} A_0(\nu) F(\nu) \tag{5.48}$$

where the signs correspond to those in (5.45), and

$$F(\nu) = \frac{\nu^2 + \nu_0^2}{\nu \left| (\nu_0^2 - \nu^2)(\nu_1^2 - \nu^2) \right|^{1/2}} + \int_{\nu}^{\nu_0} \left| \nu_0^2 - \nu'^2 \right|^{-1/2} \frac{d}{d\nu'} f(\nu') \, d\nu' \tag{5.49}$$

$$f(\nu) = \frac{\nu^2 + \nu_0^2}{\nu (\nu_1^2 - \nu^2)^{1/2}} \tag{5.50}$$

We should note here that each term on the right-hand side of Eq. (5.49) is singular when $\nu = 0$, but it can be shown that

$$\lim_{\nu \to 0} F(\nu) = O(1) \; .$$

Composite solution

In the vicinity of ν_0, P_i and P_0 should match each other in the

following sense,

$$\lim_{\nu \to \nu_0} P_0(\nu) = \lim_{\xi \to -\infty} P_i(\xi) \qquad (5.51)$$

Using Eq.(5.44) and the asymptotic behavior of the Airy function, the

right-hand side of (5.51), denoted by P_m, can be written as

$$P_m = \pi^{-\frac{1}{2}} c^{5/12} \epsilon^{1/12} (\nu_0 - \nu)^{1/4} \left\{ \cos \circledH + \epsilon^{-1/6} (\nu_0 - \nu)^{-\frac{1}{2}} \frac{s \sin \circledH}{[2\nu_0 (\nu_i^2 - \nu_0^2)]^{\frac{1}{2}}} \right\} \qquad (5.52a)$$

where

$$\circledH = \frac{2}{3} \epsilon^{1/2} c^{1/2} (\nu_0 - \nu)^{3/2} + \frac{\pi}{4} \qquad (5.52b)$$

Now the constant M in (5.45) can be determined through the use of Eqs.

(5.45)-(5.52), yielding the following result :

$$M = \left(\frac{\nu_i^2 - \nu_0^2}{2\nu_0} \right)^{1/4} \pi^{-\frac{1}{2}} \epsilon^{\frac{1}{12}} c^{\frac{5}{12}} \qquad (5.53)$$

The outer solution which satisfies Eq. (5.51) can be written as

$$P_0 = M A_0(\nu) \left\{ \cos \left[\epsilon^{\frac{1}{2}} a(\nu) + \frac{\pi}{4} \right] + \epsilon^{-1/6} \frac{s}{2\nu_0} F(\nu) \sin \left[\epsilon^{\frac{1}{2}} a(\nu) + \frac{\pi}{4} \right] \right\} + O(\epsilon^{-1/3}) \qquad (5.54)$$

thus a uniformly valid composite solution can be expressed by

$$P = P_o + P_i - P_m \qquad (5.55)$$

Velocity solutions can be obtained from the pressure through the use

of (5.12), which has been rewritten as

$$V = \frac{\sigma}{\nu^2 - \sigma^2} \left[(1 - \nu^2) \frac{dP}{d\nu} + \epsilon^{1/3} \frac{s\nu}{\sigma} P \right] \tag{5.56}$$

From Eqs. (5.44), (5.52), (5.54), (5.55), and (5.56), the following expressions are obtained,

$$V_i = - \epsilon^{2/3} \nu_0 \, Ai(c^{1/3} \xi)$$

$$V_0 = M \left(\frac{1 - \nu_0^2}{\nu_1^2 - \nu_0^2} \right) \epsilon^{1/2} \nu_0 \frac{A_0}{\nu^2 - \nu_0^2} \left\{ G^{1/2} \sin\left[\epsilon^{1/2} a(\nu) + \frac{\pi}{4} \right] \right.$$

$$\left. + \epsilon^{-1/6} \frac{s}{\nu_0} (\nu - \frac{1}{2} G^{1/2} F) \cos\left[\epsilon^{1/2} a(\nu) + \frac{\pi}{4} \right] \right\} \tag{5.57}$$

$$V_m = - \frac{\epsilon^{1/2}}{2} (2\nu_0)^{3/4} (\nu_1^2 - \nu_0^2)^{1/4} (\nu_0 - \nu)^{-1/4} \sin \, \textcircled{H}$$

$$V = V_0 + V_i - V_m$$

The meanings of the subscripts are the same as before.

Eigensolutions

Since the positive modes are either even or odd functions in the interval $[-\phi_b, \phi_b]$, we must have either

$$\left. \frac{dP}{d\nu} \right|_{\nu=0} = 0 \qquad \text{(even)}, \tag{5.58a}$$

or $\quad P(0) = 0 \qquad\qquad \text{(odd)} \tag{5.58b}$

Substituting the asymptotic series for P (Eq. (5.54)) into (5.58a) and (5.58b), the first order approximation to the eigenvalues can be written as

$$\epsilon_n^{1/2} = (n \mp \tfrac{1}{2}) \frac{\pi}{2} \Big/ a(0) + O(\epsilon^{-1/6}) \qquad (5.59)$$

where the upper sign corresponds to k > 0 and the lower sign to k < 0; n is the number of zeros of P(ν) (V(ν)) in the interval $[-\phi_b, \phi_b]$ if k > 0 (k < 0). Eq.(5.59) is equivalent to the result of Kamenkovich et al (1977, Eq.(4)) within O($\epsilon^{-1/6}$). The reason for using the zeros of different variables to label the eigensolutions for eastward and westward waves is the following : The number of zeros of P(ν) (V(ν)) is invariant with respect to ϵ if k > 0 (k < 0) (Longuet-Higgins, 1968); thus we are able to identify the eigen-curves (ϵ_n vs σ for given n and k) calculated using (5.59) with those of Longuet-Higgins (1968) for small and moderate ϵ . The relation between the number of zeros for P and that for V is varying with ϵ_n , so the formula given by Odulo (1972), which is independent of ϵ_n, is not strictly correct (e.g., compare his formula with Longuet-Higgins' Fig.11).

With the eigenvalues given by (5.59), Eqs. (5.58a) and (5.58b) are not satisfied to second order. Hence the eigensolutions represented by (5.55), (5.57), and (5.59) have error terms of order $\epsilon^{-1/6}$, although the proposed asymptotic series could produce solutions accurate to O($\epsilon^{-1/3}$) if the true eigenvalues were known. Second order calculations of ϵ_n are straightforward, but require considerable efforts; however, they are not significant for the problem of inertial waves due to the largeness of ϵ_n.

Since a(0) itself is dependent on ϵ_n , Eq.(5.59) was evaluated using

an iteration method. Comparisons of the eigenvalues obtained form (5.59)
with those taken from Longuet-Higgins' paper (1968) are presented in
Table 5.1. Note that the first order approximations to ϵ_n are degenerate
and lie between the numerical results for positive and negative k. The
error is only about 6 % even when ϵ_n is as small as 23. The accuracy of
Eq. (5.59) has also been confirmed by Kamenkovich et al (1977) using
numerical results. Eigensolutions with $k = \pm 50$, $\sigma = .5878$, $\epsilon_n^{1/2} = 370.2$,
and $n = 63$ $(k > 0)$, $62(k < 0)$, are displayed in Figs. 5.1a and 5.1b.
Note that P has n zeros for $k > 0$ and $(n-1)$ zeros for $k < 0$, while V has
$(n-1)$ zeros for $k > 0$ and n zeros for $k < 0$.

Table 5.1

Positive eigenvalues with $|k| = 5$ (ϵ is from Eq. (5.59), ϵ_+ and ϵ_-
are from Longuet-Higgins' numerical calculation for $k = 5$ and -5
respectively. n_+ and n_- are the numbers of zeros of P for $k > 0$ and
of V for $k < 0$ respectively.

σ	n_+	n_-	$\epsilon_+^{1/2}$	$\epsilon_-^{1/2}$	ϵ
.2303	3	2	102.7	94.3	98.6
.2886	4	3	89.3	84.2	86.8
.3408	5	4	81.	77.5	79.3
.3885	6	5	75.3	72.6	73.9
.4329	7	6	70.9	68.8	69.8
.4859	7	6	56.6	54.6	55.6
.5456	7	6	45.2	43.3	44.3
.6132	7	6	36.2	34.4	35.3
.6902	7	6	29.	27.2	28.3
.78	7	6	23.3	21.6	22.9

Figure 5.1a   Eigensolutions of v-velocity (upper one) and pressure (lower one) with σ = 0.5878, k = 50, n = 63, and $\epsilon_n^{1/2}$ = 370.2.
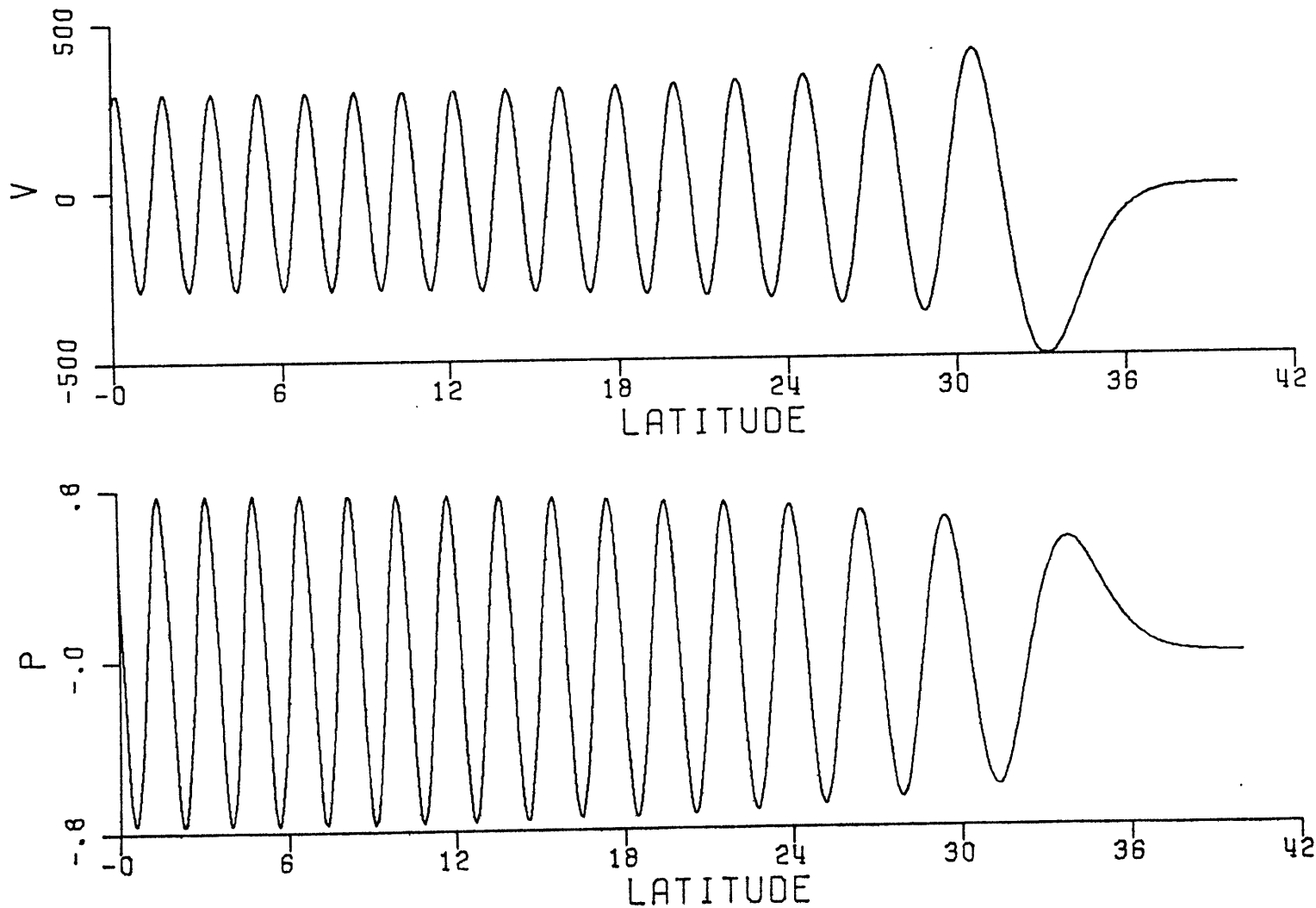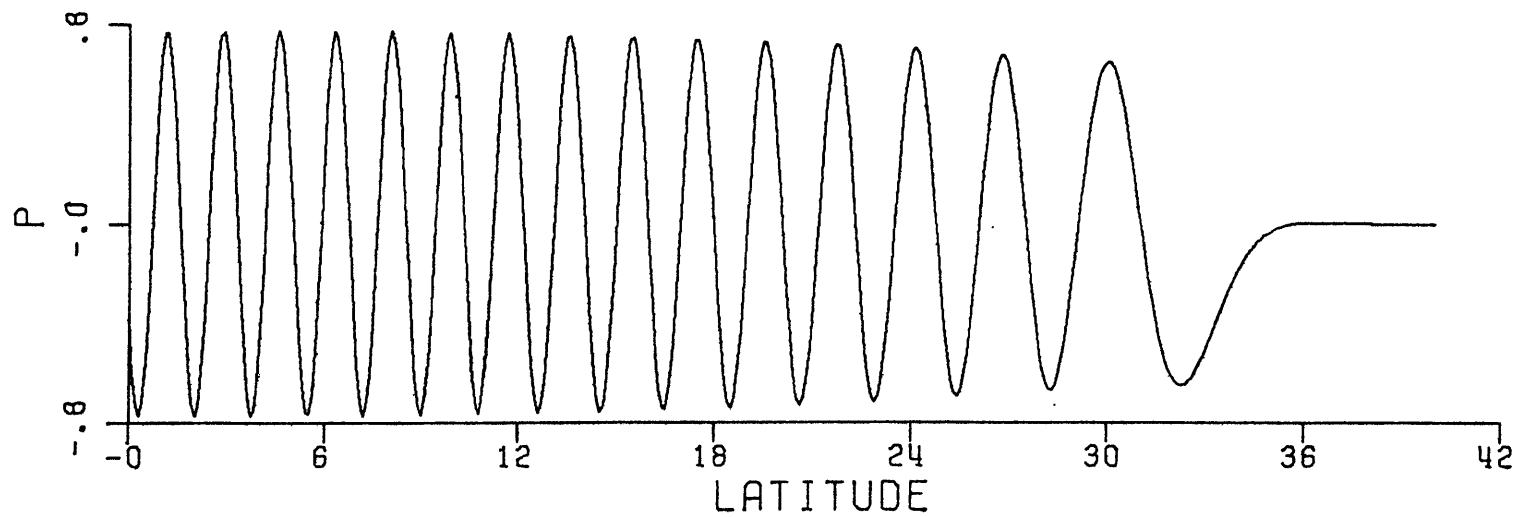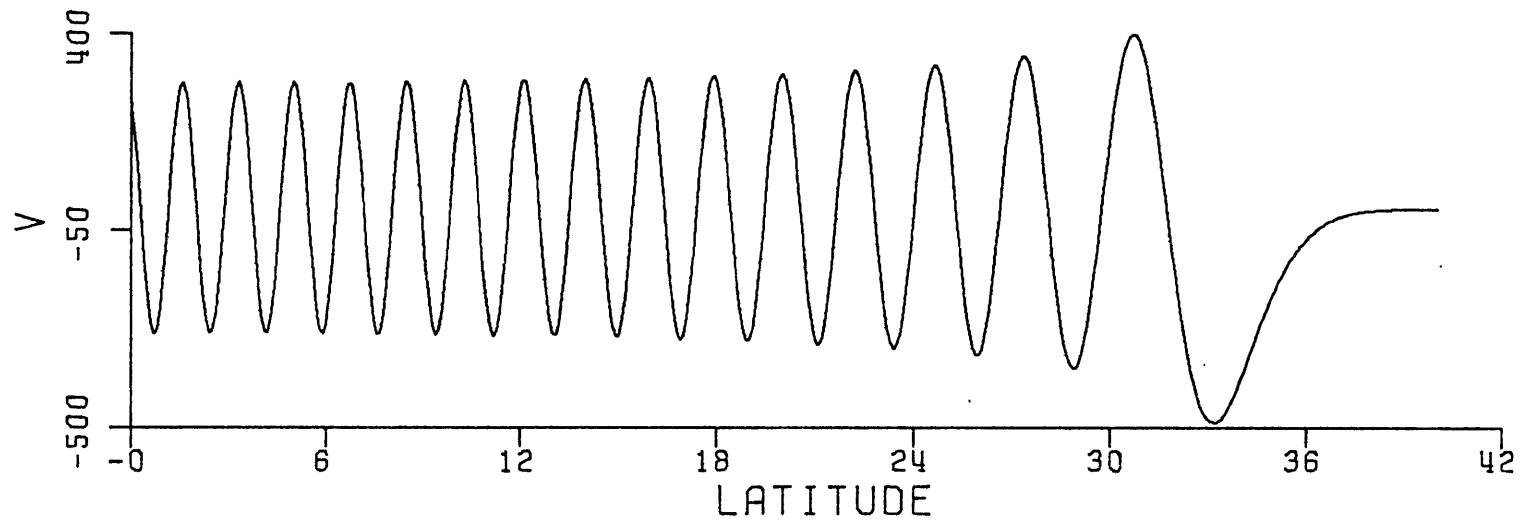
Figure 5.1b As in Fig. 5.1a except that k = -50, and n = 62.

(ii) <u>Negative modes</u>

If we define $\gamma = |\epsilon|$, then Eq. (5.32) becomes

$$(1-\nu^2)\frac{d^2 P}{d\nu^2} + 2\nu \frac{1-\sigma^2}{\sigma^2-\nu^2}\frac{dP}{d\nu} + \left[\gamma \frac{E(\nu)}{1-\nu^2} - \frac{\gamma^{1/3}s}{\sigma}\frac{\nu^2+\sigma^2}{\nu^2-\sigma^2}\right]P = 0$$

where
$$E(\nu) = (\nu^2-\sigma^2)(1-\nu^2) - \gamma^{-1/3}s^2$$

The two positive roots for $E(\nu) = 0$ are

$$\nu_0 = \sigma + \frac{s^2}{2}\gamma^{-1/3}\frac{1}{\sigma(1-\sigma^2)} + O(\gamma^{-2/3})$$

and
$$\nu_1 = 1 - \frac{s^2}{2}\gamma^{-1/3}\frac{1}{1-\sigma^2} + O(\gamma^{-2/3})$$

It is obvious that the solution now is oscillatory between the two turning points ν_0 and ν_1, exponentially decaying equatorward of ν_0, and having a complicated boundary layer between ν_1 and 1. The problem associated with the poles will not be pursued here ; the boundaries we have chosen, $\pm\phi_b'$, are sufficiently distant from the poles to avoid the turning point ν_1 and its boundary layer. Because the expansion procedure is exactly the same as that used in (ii), only the results are presented below.

<u>Pressure</u>

$$P_0 = M A_0(\nu)\left\{\cos\left[\gamma^{1/2}a(\nu)+\frac{\pi}{4}\right] + \gamma^{-1/6}\frac{s}{2\nu_0}F(\nu)\sin\left[\gamma^{1/2}a(\nu)+\frac{\pi}{4}\right]\right\}$$

$$P_1 = -b\,Ai\left[c^{1/3}\gamma^{1/3}(\nu_0-\nu)\right] - c^{1/3}Ai'\left[c^{1/3}\gamma^{1/3}(\nu_0-\nu)\right]$$

(5.60)

$$P_m = \left(\frac{2\nu_0}{\nu_1^2 - \nu_0^2}\right)^{1/4} (\nu - \nu_0)^{1/4} \left\{ \cos \circledH - \gamma^{-1/6} \frac{s \, \sin \circledH}{[2\nu_0(\nu_1^2 - \nu_0^2)]^{1/2}} (\nu - \nu_0)^{-1/2} \right\}$$

where $\circledH = \frac{2}{3} \gamma^{1/2} c^{1/2} (\nu - \nu_0)^{3/2} + \frac{\pi}{4}$

and $\quad a(\nu) = \int_{\nu_0}^{\nu} \frac{E^{1/2}(\nu')}{1 - \nu'^2} \, d\nu'$

The expressions for M, $A_0(\nu)$, b, c, and $F(\nu)$ are the same as before.

Velocity

$$V_0 = -M \left(\frac{1 - \nu_0^2}{\nu_1^2 - \nu_0^2}\right) \gamma^{1/2} \nu_0 \frac{A_0(\nu)}{\nu^2 - \nu_0^2} \left\{ E(\nu)^{1/2} \sin\left[\gamma^{1/2} a(\nu) + \frac{\pi}{4} \right] \right.$$

$$\left. - \gamma^{-1/6} \frac{s}{\nu_0} \left[\nu + \frac{1}{2} E(\nu)^{1/2} F(\nu) \right] \cos\left[\gamma^{1/2} a(\nu) + \frac{\pi}{4} \right] \right\}$$

$$\qquad\qquad\qquad\qquad\qquad\qquad\qquad\qquad (5.61)$$

$$V_i = -\gamma^{2/3} \nu_0 \, Ai\left[c^{1/3} \gamma^{1/3} (\nu_0 - \nu) \right]$$

$$V_m = -\frac{\gamma^{1/2}}{2} (2\nu_0)^{3/4} (\nu_1^2 - \nu_0^2)^{1/4} (\nu - \nu_0)^{-1/4} \sin \circledH$$

Eigenvalues

The boundary conditions at $\pm \phi_b$ are simply V = 0; hence the approximate eigenvalues are

$$\gamma_n^{1/2} = \left(n - \frac{1}{4}\right)\pi \Big/ a(\nu_m) + O(\gamma^{-1/6}),$$

where $\nu_m = \sin\phi_b$; n is the number of zeros of V(ν) in $\left[0, \phi_b\right]$. The

eigensolutions with k = ± 50, σ = .5878, $\gamma_n^{\frac{1}{2}}$ = 573.1, and n = 31, are

displayed in Figs. 5.2a and 5.2b. Now the number of zeros of P

in $\left[0, \phi_b\right]$ is (n-1) for k $>$ 0 and n for k $<$ 0. Solutions in the

Southern Hemisphere, which are not shown here, are either symmetric or

anti-symmetric with their counterparts in the Northern Hemisphere; thus

these two cases are degenerate.

5.4 Results

Our major interests are in finding model spectra of v and w at ϕ_o as

functions of depth, which can be directly compared with the observations

presented in Chapter 2. In other words, for each σ in $\left[\sigma_1, \sigma_2\right]$, we

want to calculate $\left|\hat{w}(\phi_o, z, \sigma)\right|^2$ and $\left|\hat{v}(\phi_o, z, \sigma)\right|^2$. With the

knowledge of $P_{n,\sigma}(\phi)$, $V_{n,\sigma}(\phi)$, $W_{n,\sigma}(z)$, and $F_{n,\sigma}(z)$ as derived in

5.2 and 5.3, the calculation is straightforward using Eqs. (5.7) and

(5.8). To be specific, we choose ϕ_o = 36°, σ_1 = .94 $\sin\phi_o$, and

σ_2 = 1.26 $\sin\phi_o$. For given σ in $\left[\sigma_1, \sigma_2\right]$, we have calculated

$|\hat{w}|^2$ and $|\hat{v}|^2$ with three different forcing scales at the following four

depths : 200 m, 600 m, 1500 m, and 4000 m. Calculations have been made

for both surface and bottom forcing.

For given σ , the first step was to calculate the $a_{n,\sigma}$'s from

(5.16), in which the integration was evaluated numerically using the

trapezoidal rule. For both positive and negative modes, the value of

$a_{n,\sigma}$ initially increases with n ; after reaching a maximum at some

intermediate n, it then decreases with n. In general, the calculation

was truncated at four mode numbers n_1, n_2, n_3, and n_4 such that

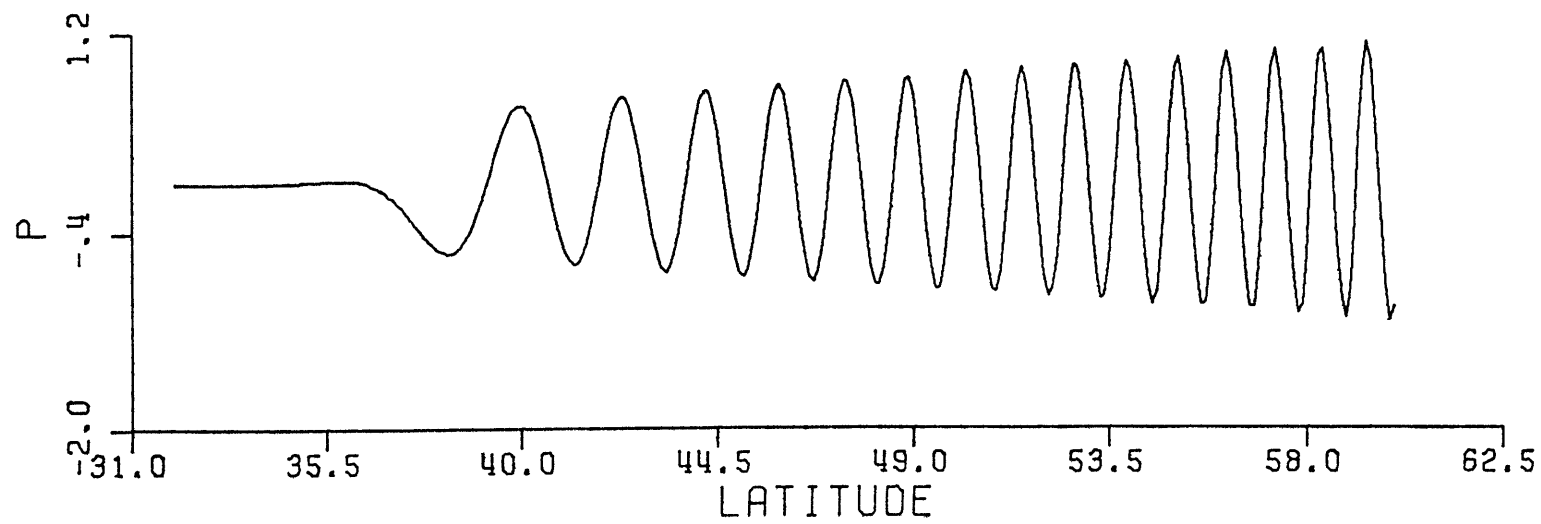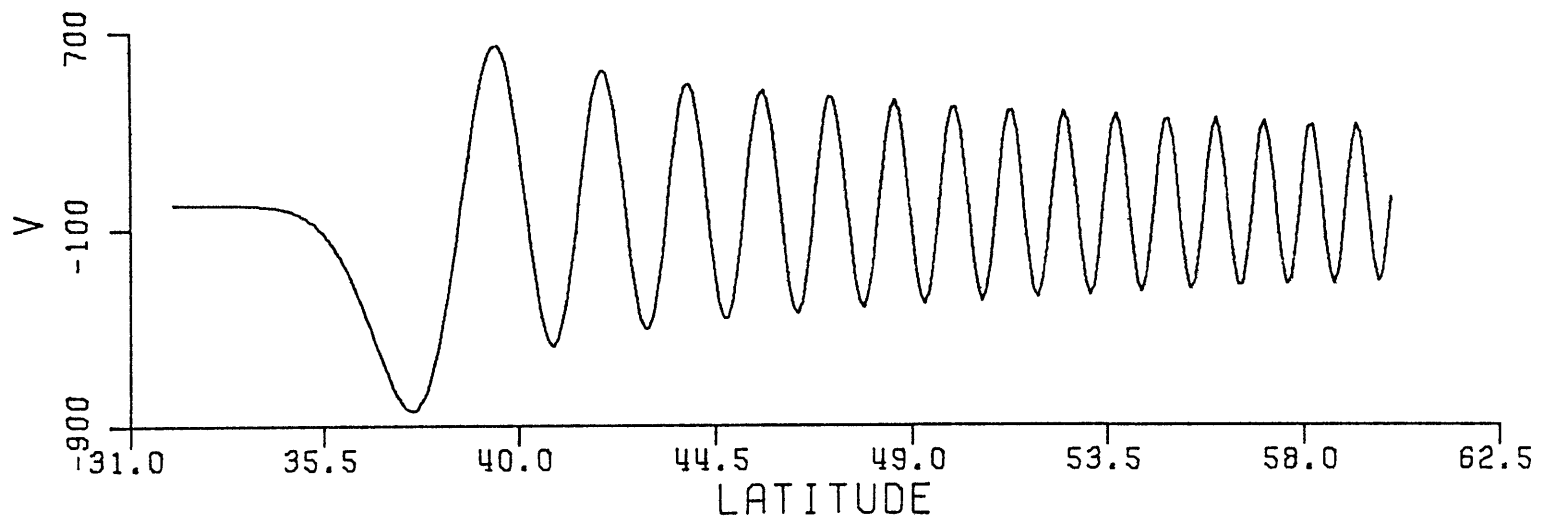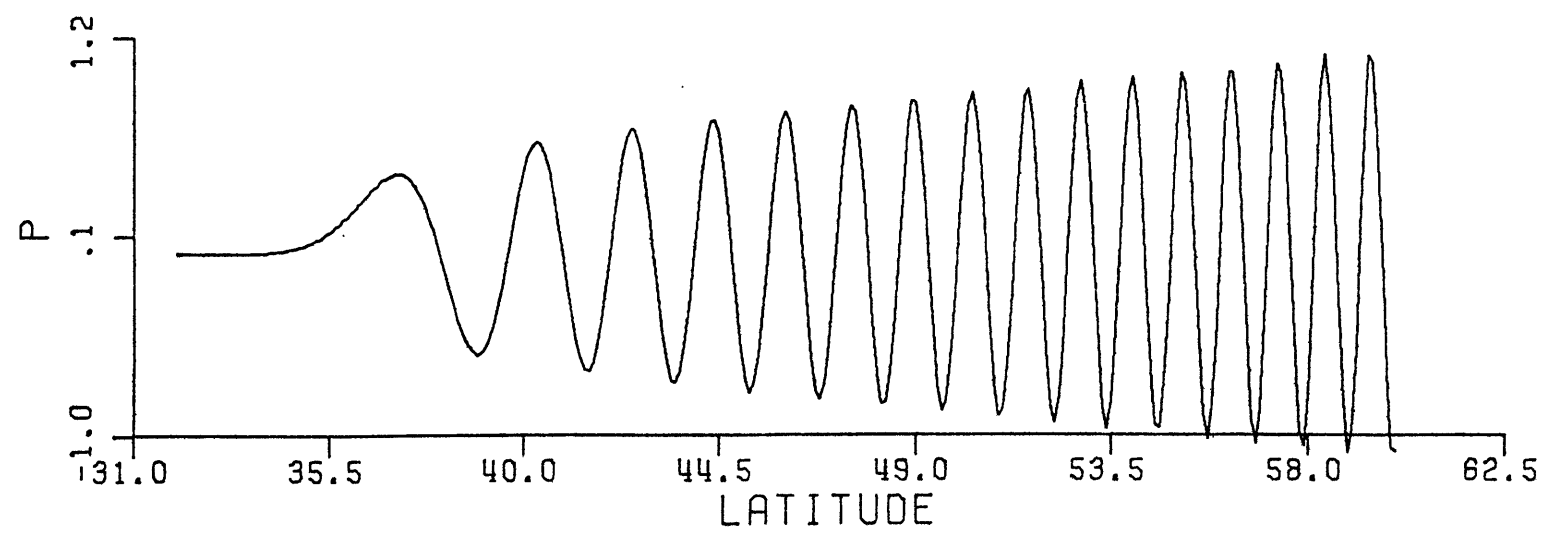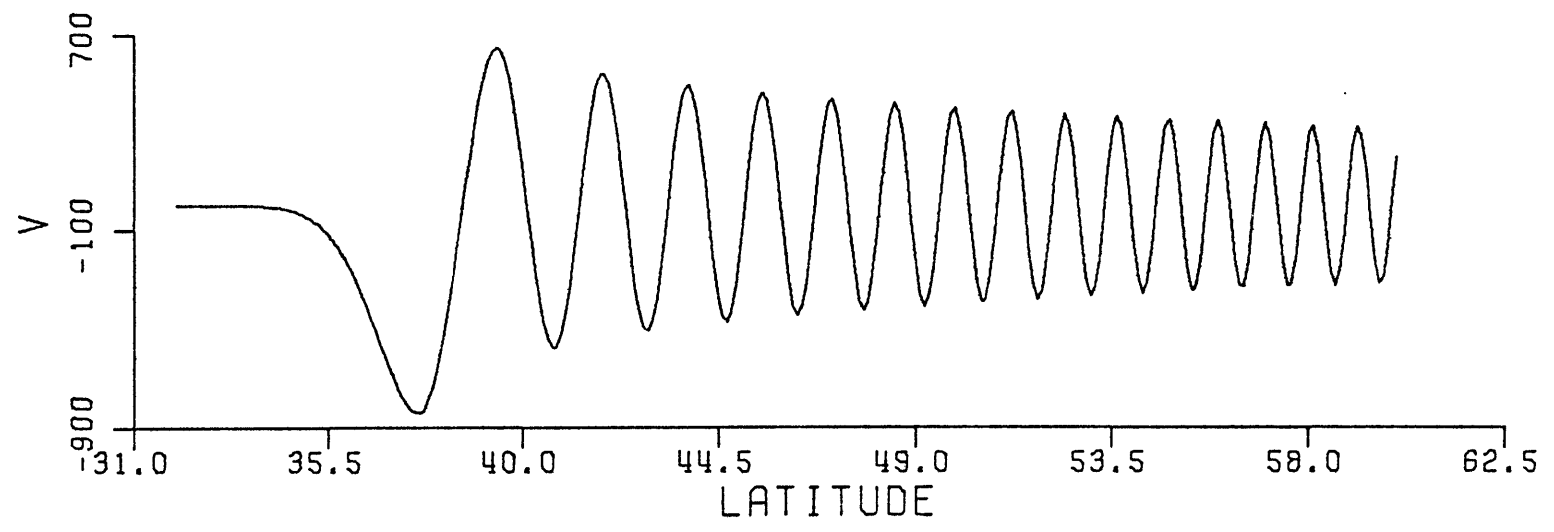Figure 5.2a   As in Fig. 5.1a except that n = 31 and $(- \epsilon_n)^{1/2}$ = 573.1.

Figure 5.2b As in Fig. 5.1a except that n = 31, $(-\epsilon_h)^{1/2}$ = 573.1, and k = -50.

$$\sum_{n=n_1}^{n_2} |a_{n,\sigma}|^2 N_{n,\sigma} + \sum_{m=n_3}^{n_4} |a_{m,\sigma}|^2 N_{m,\sigma} \geq 0.9 \int_{-\phi_b}^{\phi_b} |\hat{w}_b|^2 d\phi \quad , \qquad (5.62)$$

$$\underbrace{\qquad\qquad}_{\epsilon_{n,\sigma} < 0} \qquad \underbrace{\qquad\qquad}_{\epsilon_{m,\sigma} > 0}$$

where
$$N_{n,\sigma} = \int_{-\phi_b}^{\phi_b} P_{n,\sigma}^2 (\phi) \, d\phi$$

Values of n_1, n_2, n_3, and n_4 for nine selected frequencies

in $[\sigma_1, \sigma_2]$ are listed in Table 5.2 for three different forcing

scales: L = 300 km, 150 km, and 75 km. For frequencies sufficiently

greater than $\sin\phi_0$, we need only positive modes to describe $\hat{W}_b(\phi)$

because negative modes are trapped far to the north of the forced

region. For frequencies close to $\sin\phi_0$, we need both kinds of mode and

the expansion is not particularly efficient; it needs several hundred

modes. It is conceivable that for frequencies much less than $\sin\phi_0$

(not shown), only negative modes will contribute because positive modes

are trapped far to the south of ϕ_0. It is also expected from Fourier

theory that smaller scale forcing requires more modes to describe. Note

that although some mode numbers in Table 5.2 are small, their

corresponding eigenvalues are at least O(2000) -- still large enough for

the validity of the asymptotic expansion. For the case with L = 300 km,

the forcing function $\hat{W}_b(\phi)$ and its expansion in terms of $P_{n,\sigma}$ are

displayed in Figs. 5.3a and 5.3b for $\sigma = \sin\phi_0$ and $\sigma = 1.12 \sin\phi_0$

respectively. Slightly wavy behavior is observed when $\sigma = \sin\phi_0$;

however, the localized shape is well reproduced. The results for other

forcing scales are similar.

Table 5.2

Values of n_1, n_2, n_3, n_4

L = 300 km

$\dfrac{\sigma}{sin\phi_o}$	n_1	n_2	n_3	n_4
.94	2	65	4	110
1.	4	66	2	140
1.01	11	46	2	111
1.02			3	86
1.035			3	66
1.06			6	46
1.12			6	44
1.19			6	41
1.26			5	41

L = 150 km

$\dfrac{\sigma}{sin\phi_o}$	n_1	n_2	n_3	n_4
.94	6	80	34	81
1.	17	181	16	386
1.01	17	61	16	226
1.02			16	141
1.035			16	106
1.06			15	76
1.12			13	72
1.19			12	70
1.26			12	68

Table 5.2 (contd.)

L = 75 km

$\dfrac{\sigma}{\sin\phi_o}$	n_1	n_2	n_3	n_4
.94	11	102		
1.	53	450	54	1010
1.01	60	102	54	440
1.02			52	261
1.035			48	170
1.06			44	158
1.12			19	140
1.19			16	130
1.26			25	125

Figure 5.3   The forcing function $\hat{w}_b(\phi)$ (solid curve) and its expansion in terms of $P_{n,\sigma}$ (symbols) for (a) $\sigma = \sin \phi_o$ and (b) $\sigma = 1.12 \sin \phi_o$, where $\phi_o = 36^o$ and the forcing scale $L = 300$ km.
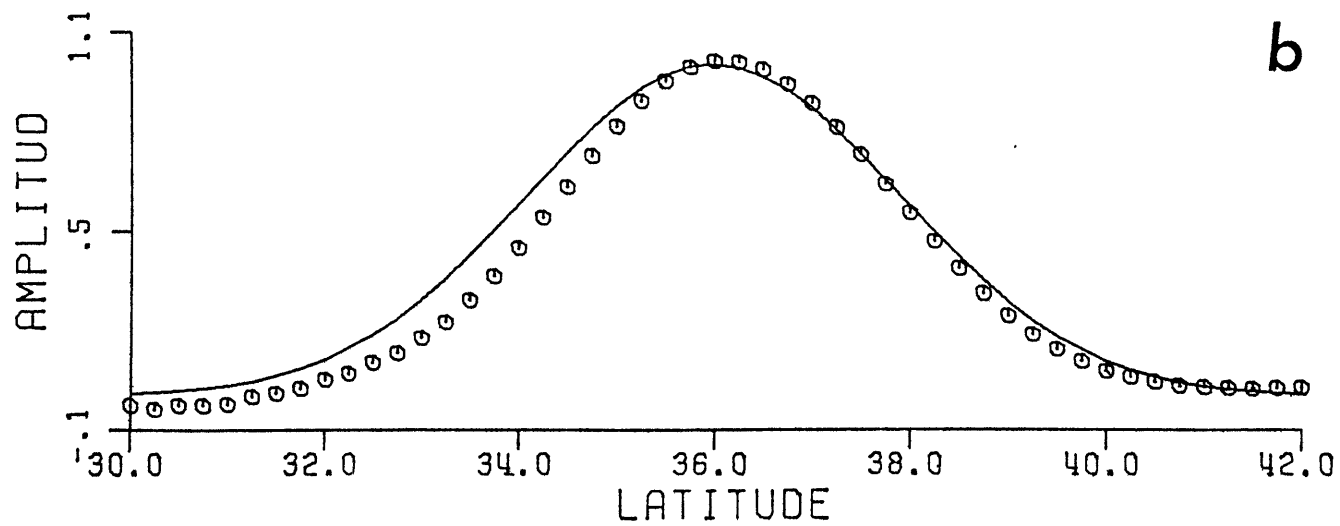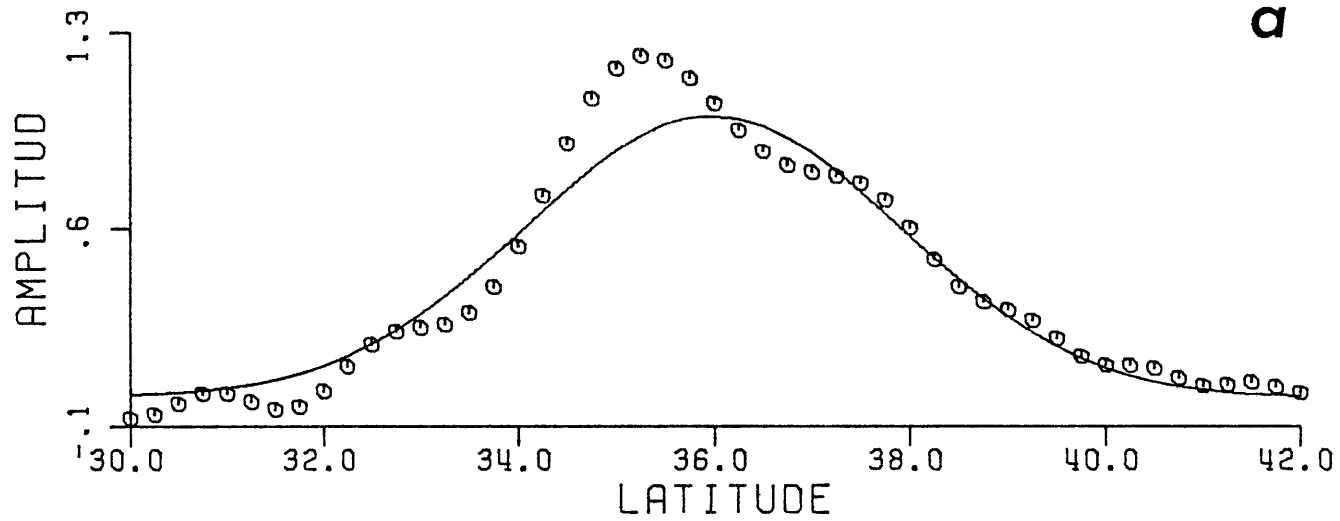
5.4a Surface forcing

We first discuss the response spectrum for the case of surface forcing. With the arbitrary assumption that $|\hat{W_b}|^2_{f_o} = 1$ cm^2/sec^2/cycle per 2Ω , the spectra at different depths are shown in Figs. 5.4(a, b), 5.5(a, b), and 5.6(a, b) for L = 300 km, 150 km, and 75 km respectively. At sub-inertial frequencies, the response is trapped near the surface as expected. At super-inertial frequencies, the response is propagating downward with $|\hat{V}|^2$ decreasing and $|\hat{W}|^2$ increasing with depth. At frequencies sufficiently higher than f, the vertical variation scales in the WKBJ sense. In the velocity spectrum there is a peak slightly above f whose characteristics vary with depth and L : in general, its frequency increases and its strength (peak height) decreases with depth; its bandwidth decreases with L. For instance, at 200 m where the peak is strongest, the bandwidth and peak height (the latter is defined as the difference between the maximum power and the minimum power with $\omega > f$) are listed in Table 5.3 for different values of L. The peak height is not particular dependent on L although the bandwidth is.

Table 5.3

Characteristics of the horizontal velocity spectra for different values of L

L (km)	peak height (db)	bandwidth
300	8.5	0.14
150	9.	0.09
75	9.	0.04

Figure 5.4   Response spectra of (a) w-velocity and (b) v-velocity
at four different depths (numbers are in meters). The unit of the
vertical axis is $cm^2/sec^2/cph$. The forcing is imposed at the
surface (z_b = 0) with L = 300 km and ϕ_o = 360. A straight line
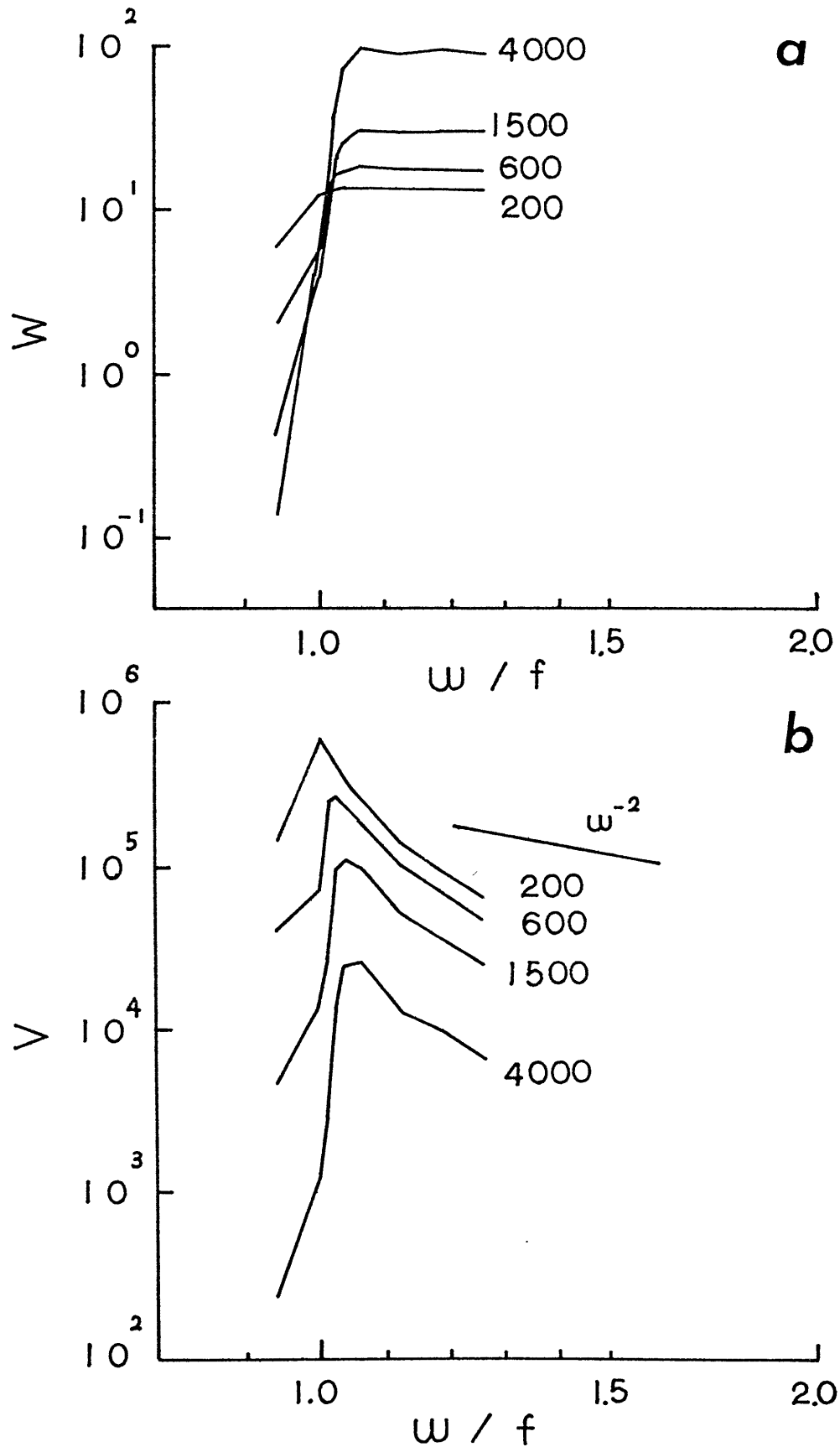representing the ω^{-2} spectrum is drawn for reference.
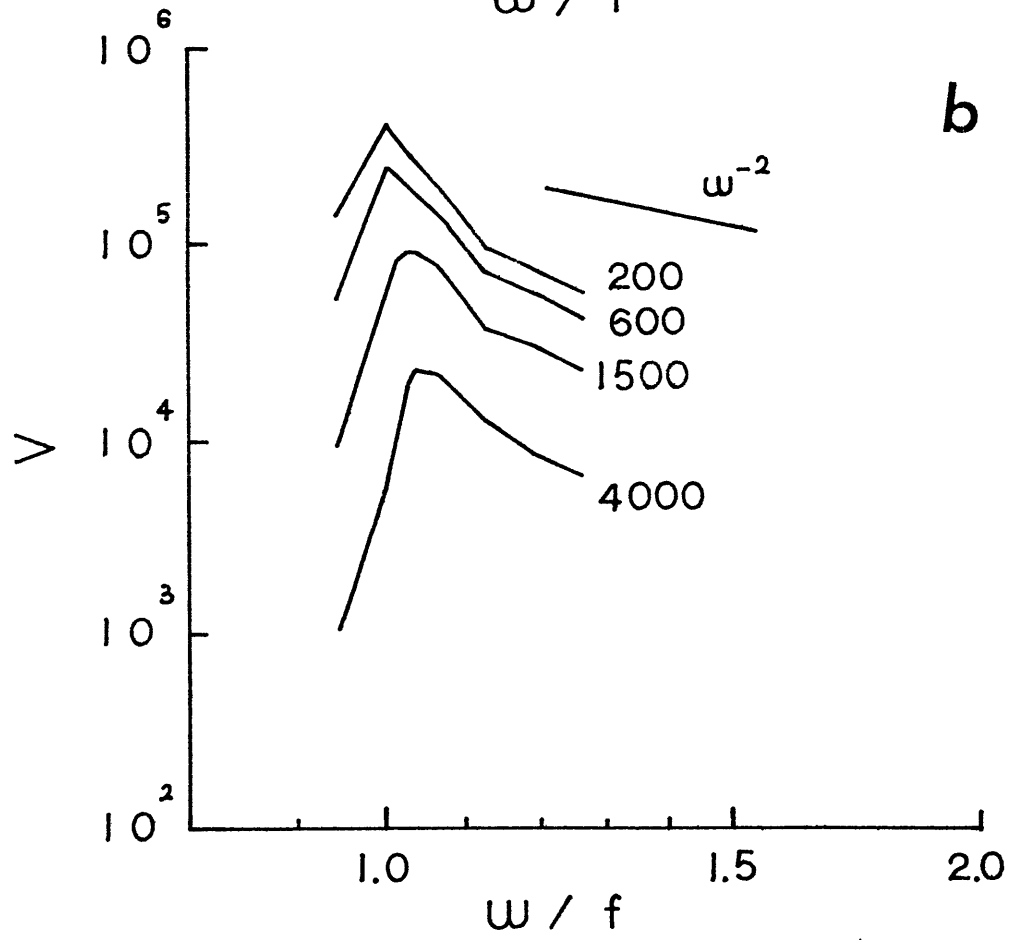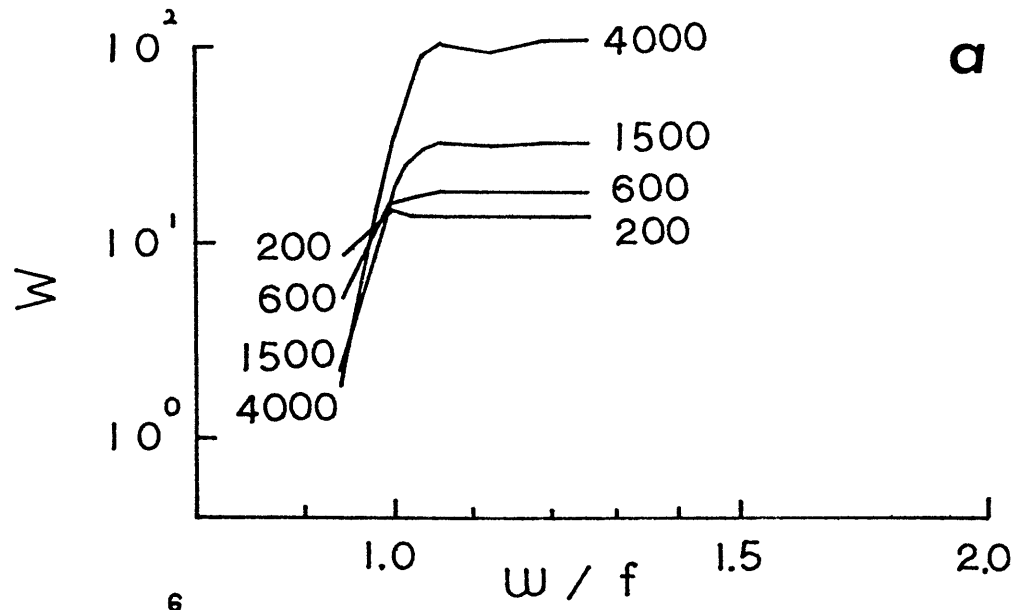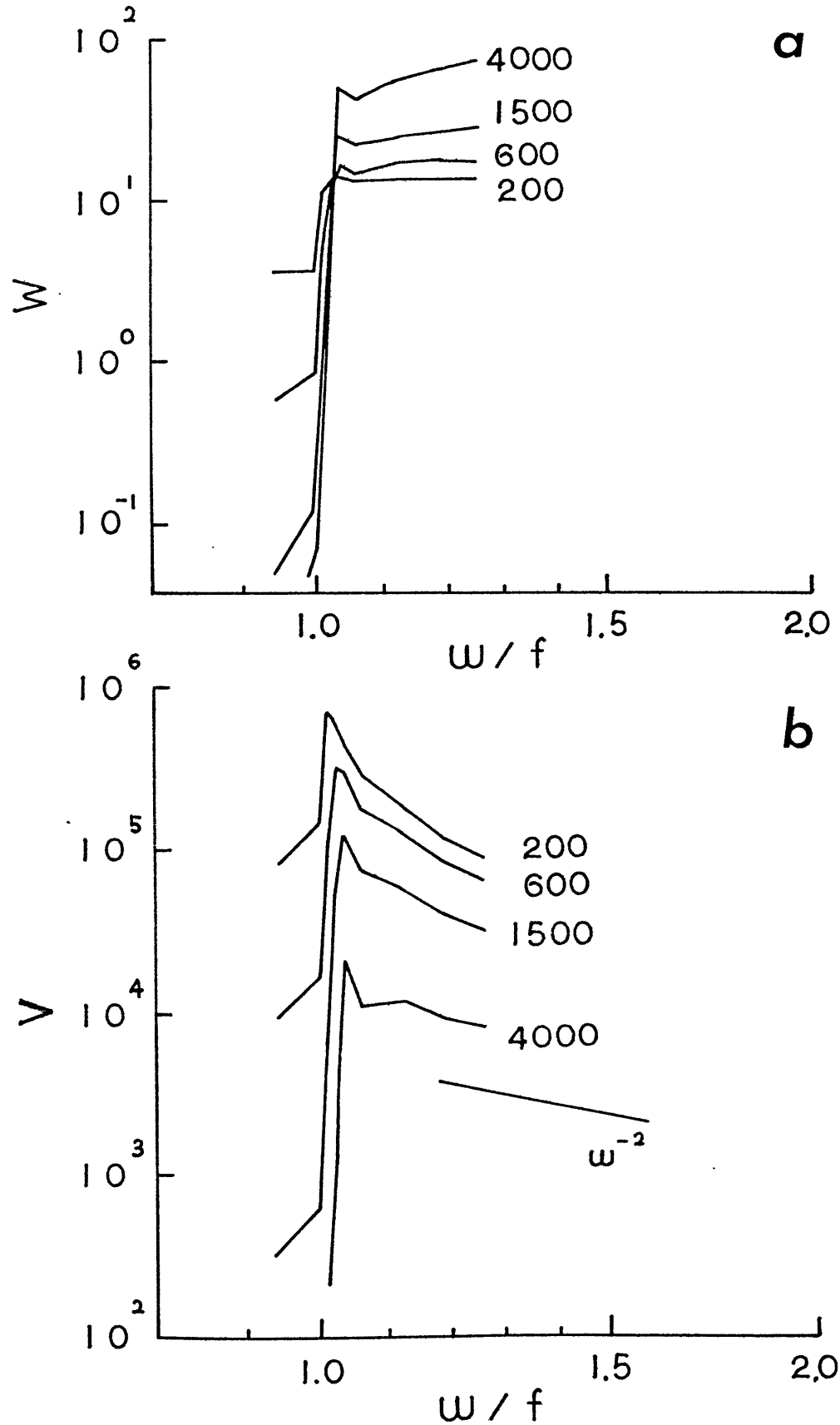
Figure 5.5   As in Fig. 5.4 except that L = 150 km.

Figure 5.6   As in Fig. 5.4 except that L = 75 km.

Now we can qualitatively explain why the observed spectra have stronger peaks and smaller blue shifts in the upper ocean (class 2a) than in the deep ocean over smooth topography (class 3). In the upper ocean, inertial waves are primarily locally forced as described by the model; hence the resulting peak frequency is indistinguishable from f, and the forced response is confined to the upper ocean. Together with the global wave spectrum whose shape is the same at all depths, the inertial peak is then stronger in the upper ocean. This interpretation can be illustrated by a schematic diagram, as shown in Fig. 5.7, of the ray paths of both the global and local wave field. Because of the nearly horizontal propagation of inertial waves, locally surface-generated waves will propagate away from their forced region before reaching the bottom; hence they can be measured only by instruments at shallow depths. On the other hand, globally generated waves can be measured at all depths. Therefore what the upper instrument measures is a combination of the local and global wave field, while the lower instrument only measures the global wave field. In the absence of the local wave field in the deep ocean, the significant blue shift there is accounted for by the global model (Chapter 4). Because the upper ocean observations suggest that the bandwidth is less than 0.1 f, we expect from Table 5.3 that small scale forcing is more important in producing the observed features.

Can we interpret the dependence of the response spectrum on depth and L in terms of the properties of the excited waves ? We have seen from Table 5.2 that considerably more high order negative modes are excited at near-inertial frequencies than super-inertial frequencies.
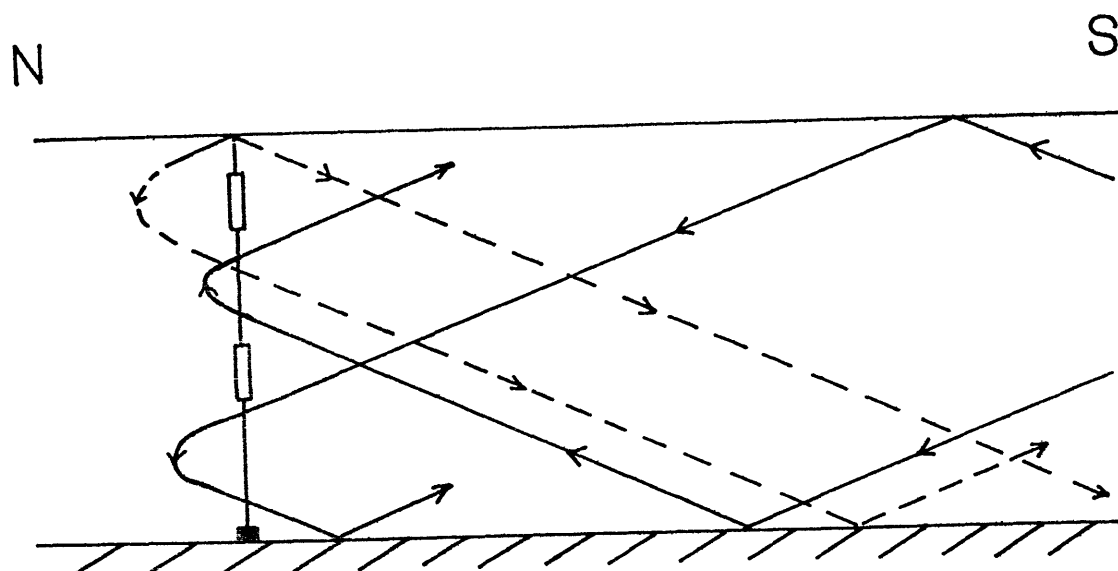
Figure 5.7   Schematic diagram showing the ray paths of the local wave field (dashed lines) and the global wave field (solid lines). A mooring with two current meters measuring the wave field is also shown.

For negative modes, the vertical structure is exponential (c.f. Eqs. (5.24), (5.25)) with trapping scale decreasing with increasing $|\epsilon_n|$. Therefore a substantial amount of the near-inertial wave energy is confined to small depths, but most of the super-inertial wave energy can penetrate to great depths. This is why the blue shift increases with depth. Moreover, because super-inertial waves are far from their turning latitudes, the wave amplitudes are only weakly dependent on frequency and the result of superposition has no prominent peaks. Hence with a white noise local forcing at the surface, there will be no prominent inertial peaks at great depths unless there is a global wave field.

The fact that the inertial peaks are stronger for smaller forcing scales can be explained as follows. As noted before, smaller scale forcing excites more high order modes; because high modes tend to interfere with each other more severely than low modes outside the inertial frequency band (see Chapter 4), the resulting peak will be stronger if there are more high modes involved.

Because the bandwidth of the inertial peak is controlled by the Airy frequency scale L_σ (c.f.Eq. (4.19)) which decreases with latitude, the latitudinal dependence of the response spectrum should be similar to that of the global wave spectrum as shown in Fig. 4.2. With L = 150 km, the response spectrum was calculated at $15°$ and $50°$ to explore the latitudinal dependence. The results for the v component of velocity are shown in Figs. 5.8a and 5.8b; the results for the vertical velocity are not sensitive to latitude and are not shown here. As expected, the inertial peak is generally weaker at lower latitudes. At $15°$ the substantial response at sub-inertial frequencies results in the absence
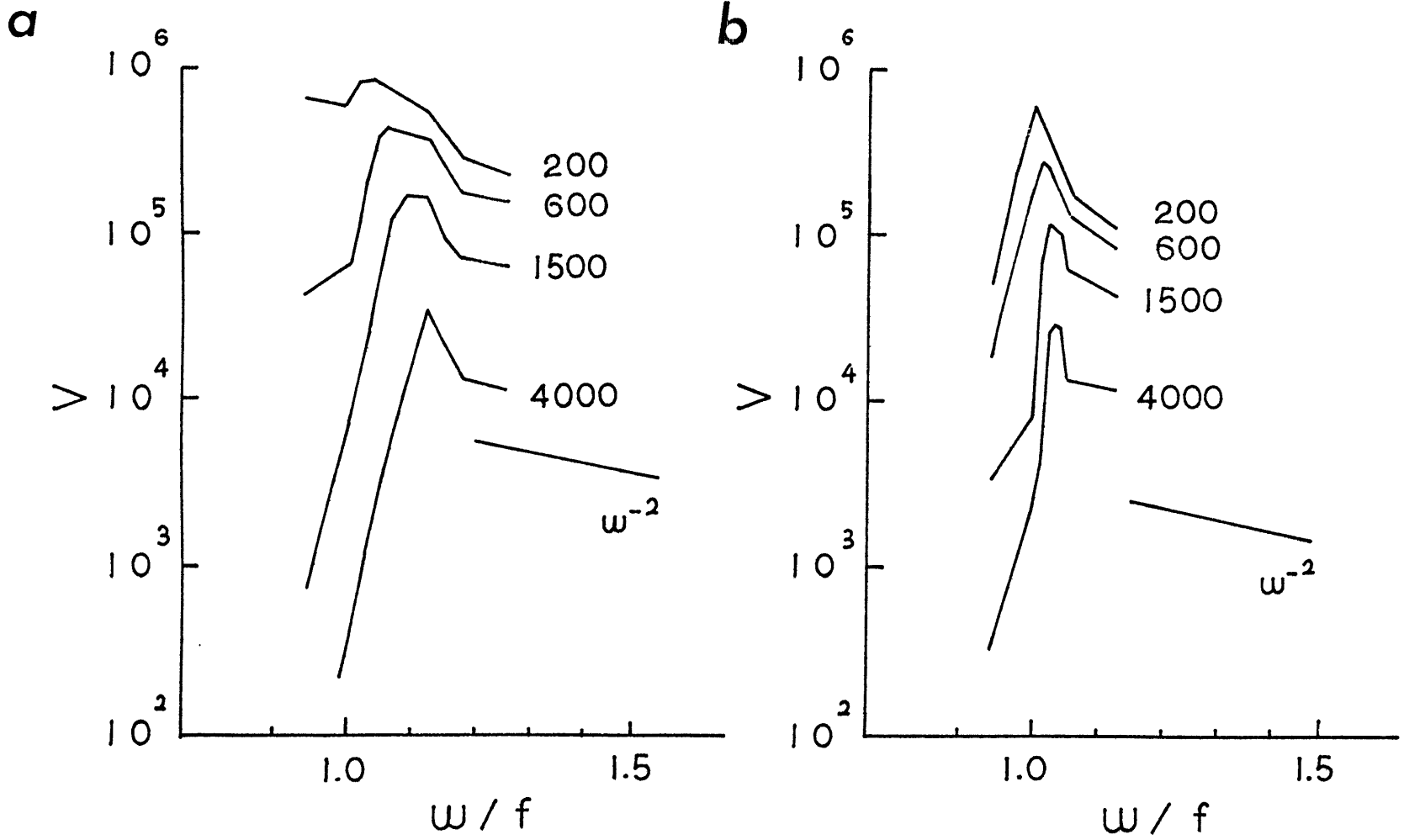
Figure 5.8   Response spectra of v-velocity at (a) 15o and
(b) 50o, with L = 150 km.

of an inertial peak at 200 m. The large magnitudes of the blue shift

reflect the character of equatorially trapped modes; recall the results

of Eriksen (1979). At 50° the bandwidth is reduced to 0.05f, and the

sub-inertial energy is also greatly reduced. However, the peak energy

level does not change much with latitude.

One way to estimate the possible forcing amplitude, $|\hat{W}_b|^2_{\phi_o}$, is to

find the value of $|\hat{W}_b|^2_{\phi_o}$ such that the energy level of $|\hat{V}|^2$ near f is

consistent with the upper ocean observations. For instance, by comparing

the spectra at 200 m in Figs. 5.4b, 5.5b, and 5.6b with the observed

spectra at 200m of the PMIII, we have $|\hat{W}_b|^2_{\phi_o}$ = 2 x 10⁻³

cm²/sec²/c.p.2Ω , which yields a root mean square amplitude of w

in $[\sigma_1,\sigma_2]$ equal to 2 x 10⁻² cm/sec. For a mixed layer 40 meters deep,

this vertical velocity field could be produced by the convergence and

divergence of surface inertial currents of amplitudes 50 cm/sec and

wavelength 100 km. Another interesting quantity is the corresponding

downward energy flux G which can be calculated as follows,

$$ G = \int_{\sigma_1}^{\sigma_2} \frac{1}{2} \, Real \, (\hat{p}\, \hat{w}^*) \Big|_{z=0} \, d\sigma \qquad (5.63) $$

With $\hat{p}$ obtained from Eq. (5.9) we have

G = 9.3 erg/cm²sec   for L = 300 km,

G = 3.2 erg/cm²sec   for L = 150 km.

G = 1.3 erg/cm²sec   for L = 75 km

The reason for the increase of G with L is that, larger scale forcing

excites more low modes which have larger vertical group velocity. These

numbers suggest that this forcing mechanism, if realistic, is an

important one for the internal wave field, which, with total energy 4 x

10^6 erg/cm^2 (Garrett and Munk, 1972), can be set up in couple of

weeks by this mechanism.

5.4b Bottom forcing

The response spectra at 36° for bottom forcing with L = 150 km

are shown in Figs. 5.9(a, b). Now the sub-inertial response is trapped

to the bottom, while the super-inertial response behaves the same way as

in the case of surface forcing. The inertial peak is strongest at deep

levels and the blue shift increases with height from the bottom (at

z^*= -4500 m). This explains why the observed inertial peak at deep

levels over rough topography (class 2b) is as strong as that at upper

levels (class 2a). In fact, what one would observe over rough topography

is predominantly a local wave field with both surface and bottom

sources, and the observed spectra is a superposition of the results

shown in Figs. 5.9 and 5.5 with proper forcing amplitudes. By requiring

that the modelled inertial wave energy levels be equal to the observed

values, such a superposition is shown in Fig. 5.10. The spectral shape

is basically the same at all depths, consistent with the observations

over rough topography (see Fig. 2.3b). The dependence of the results on

L and latitude is essentially the same as that for the case of surface

forcing.

The forcing amplitude required at the bottom to produce the spectra

shown in Fig. 5.10 is such that $\left|\hat{w}_b\right|^2 = 8 \times 10^{-3}$ cm^2/sec^2/c.p.2Ω ,

corresponding to a root mean square vertical velocity of 8 x 10^{-2}

cm/sec. The resulting vertical energy flux from the bottom to the

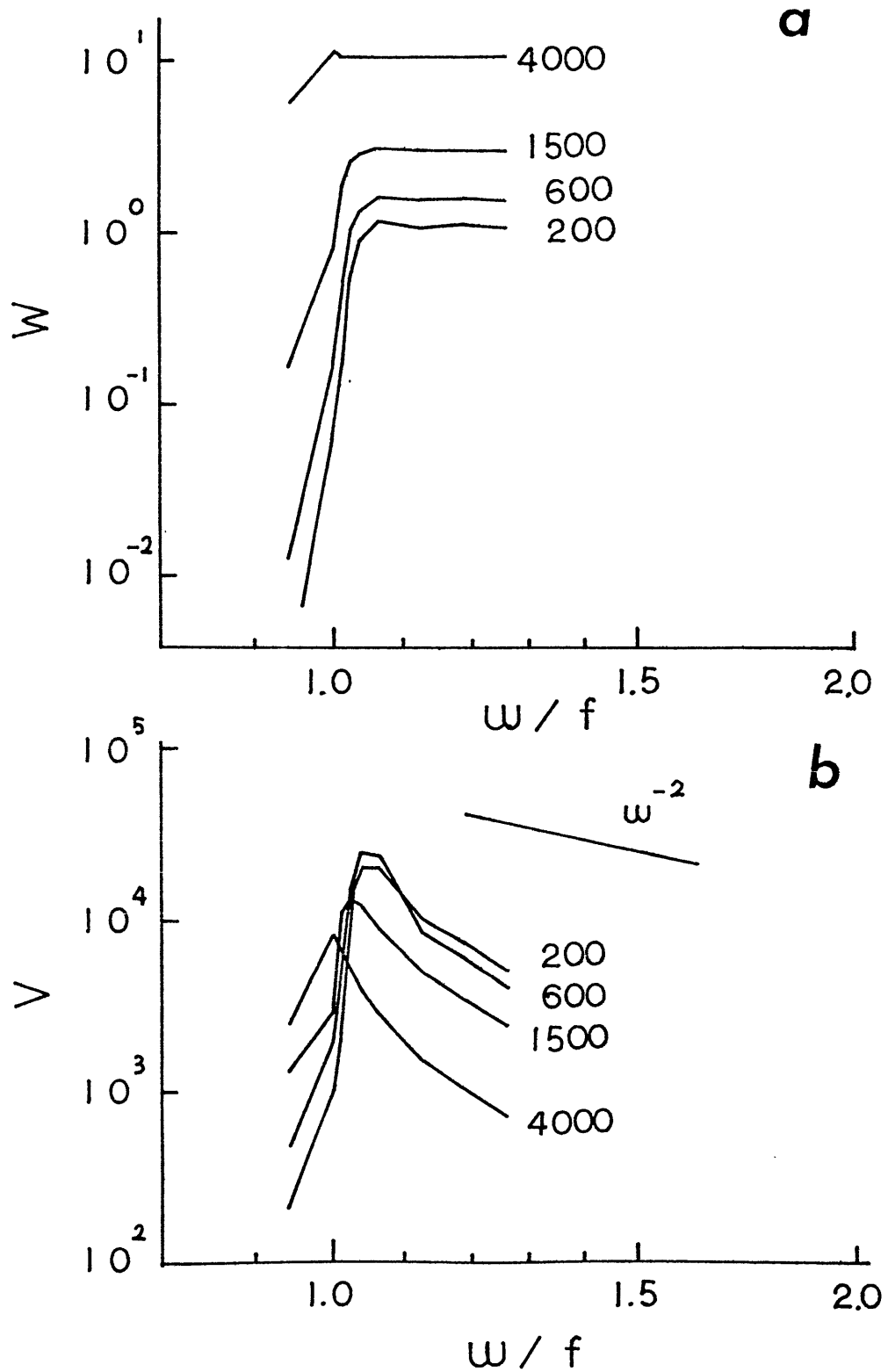interior is about 1.6 erg/cm^2 sec. Assuming that the energy source is

Figure 5.9   As in Fig. 5.4 except for bottom forcing ($z_b = -1$)
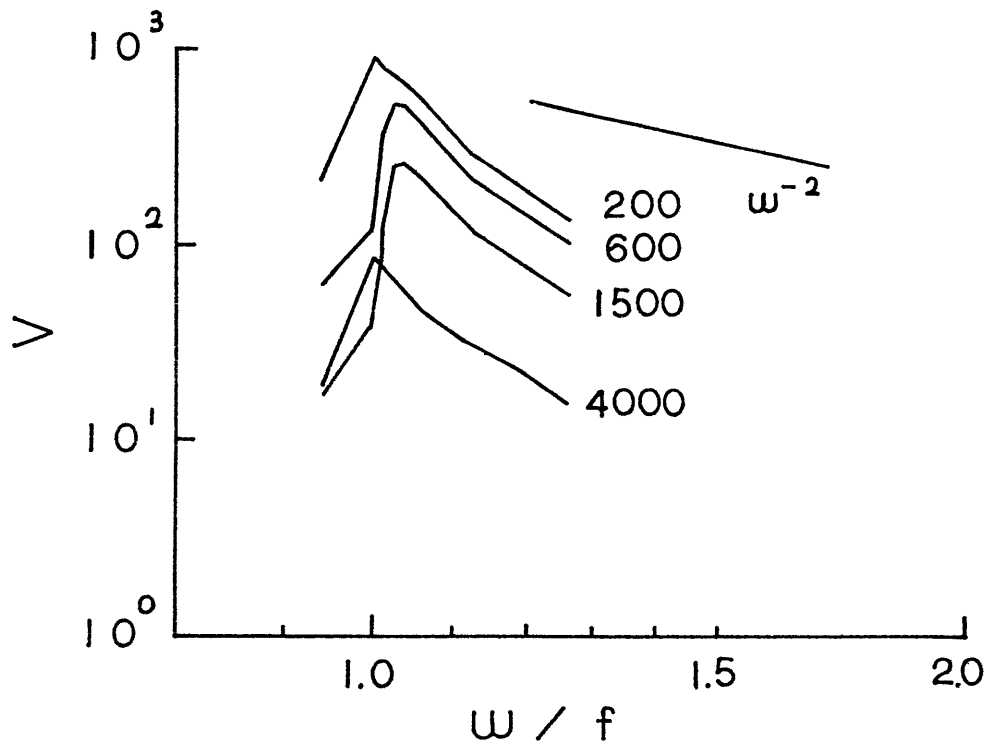and L = 150 km.

Figure 5.10 Response spectra of v-velocity with both surface
forcing ($|\hat{w}_b|^2$ $= 2 \times 10^{-3}$ $cm^2/sec^2/c.p.2$) and bottom
forcing ($|\hat{w}_b|^2$ $= 8 \times 10^{-3}$ $cm^2/sec^2/c.p.2$).

from the interaction between rough topography and a barotropic eddy with horizontal velocity amplitude of 5 cm/sec, it will take about 40 days to convert the eddy energy into internal wave energy. This result suggests that rough topography could be a potential sink (source) for eddy (internal wave) energy and explains why the observed eddy energy at great depths over rough topography is an order of magnitude less than that over smooth topography (Schmitz, 1978; Fu and Wunsch, 1979).

5.5 Summary and discussion

A forced model based on latitudinal modal decomposition is developed to study locally forced inertial waves. Asymptotic solutions of the LTE which are suitable for inertial waves are obtained and applied to the problem. The modal decomposition is cumbersome as expected of a localized function; however, it provides an accurate description of the transition of oceanic response from sub-inertial frequencies to super-inertial frequencies, a singular problem in the conventional f-plane model.

The forcing is through a specified vertical velocity field in a narrow band centered on f at the top and/or bottom boundaries. For surface forcing, the differences in the observed inertial wave spectra between upper ocean (class 2a) and the deep ocean over smooth topography (class 3) can be qualitatively described by the model. For bottom forcing, the strong inertial peaks observed in the deep ocean over rough topography (class 2b) also can be accounted for by the model.

The model results are dependent on forcing scale and latitude; the inertial peak is stronger for smaller forcing scale and/or higher latitude. In order to produce the observed energy level in the upper ocean, a downward energy flux with magnitude from 1.5 to 12 erg/cm^2sec is required for forcing scale from 75 km to 300 km. Over rough topography with scale of 150 km, an upward energy flux of 1.6 erg/cm^2 sec is estimated.

Chapter 6   The Reflection of Inertial Waves from the Benthic

Boundary Layers

6.1 Introduction

The foregoing interpretation of the observed inertial wave energy

over smooth topography as the combination of a vertically symmetric

global wave field and a downward propagating local wave field is based

on the crucial assumption that dissipation is negligible for the

energy-containing low wavenumber components. If dissipation is

substantial, then the waves are not able to propagate for great

distance, and the energy balance is between local forcing at the surface

and dissipation at the bottom. This is the interpretation proposed by

Leaman (1976) for the observed dominance of downward energy propagation

in profiler measurements. Displayed in Fig. 6.1 is a schematic diagram

showing the difference between Leaman's interpretation and ours. Another

assumption underlying Leaman's interpretation is that all the reflected

wave energy can be measured by a local profiler. This would be the case

if the wave field is horizontally homogeneous, which requires that the

wave frequency be at least greater than 1.15 f. However, as noted in

Chapter 5, because ray paths are nearly horizontal for inertial waves

(c.f. Eq. (5.2)), their reflections from the bottom occur at a great

distance from their source region (see Fig. 5.7), and cannot be measured

by a local instrument. Even for perfect reflections, the propagation of

local inertial waves as observed by a profiler tends to be predominantly

downward. Hence the reflection coefficient estimated by Leaman as the

ratio of upward energy to downward energy observed in profiler measure-

ments is likely an underestimate, and the observed appreciable amount of

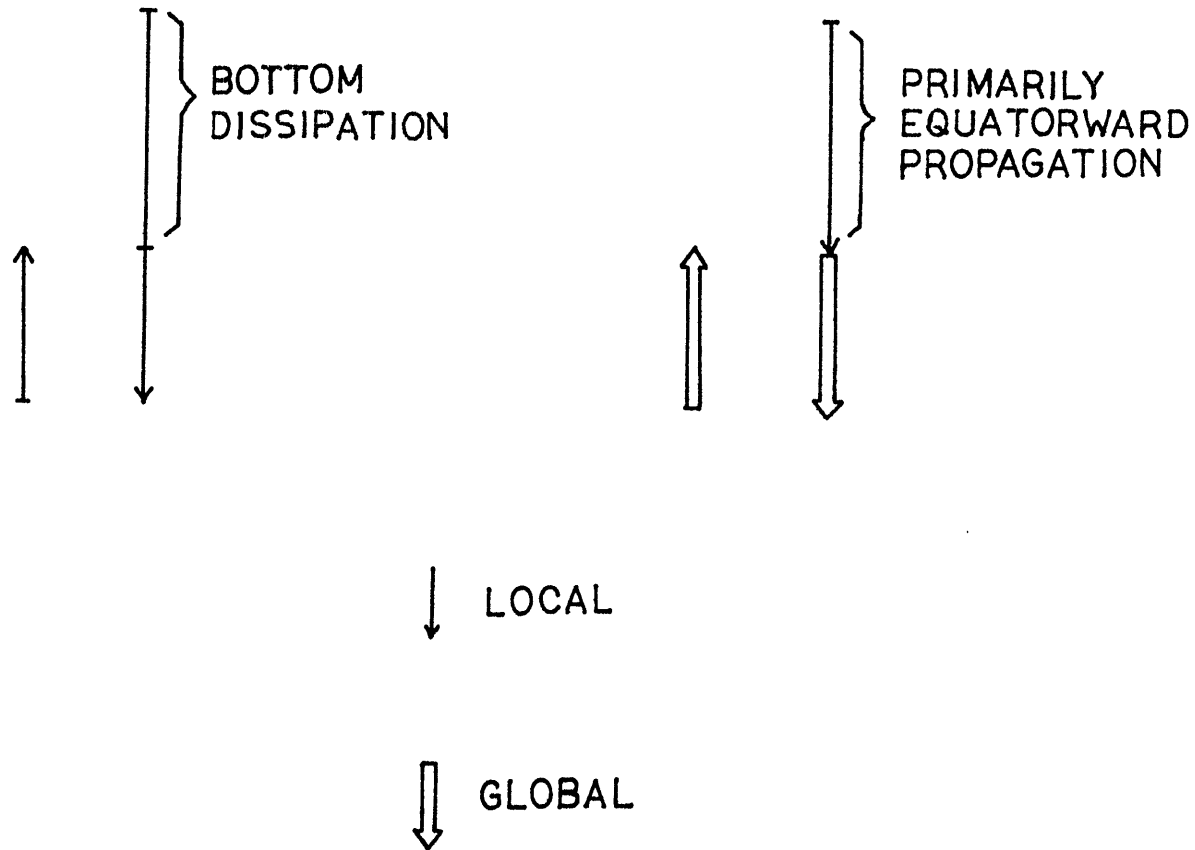upward energy should be interpreted as part of the global wave field.

Figure 6.1   Schematic diagram showing two different interpretations of the observed dominance of downward energy propagation of inertial waves. The left figure is Leaman's (1976), and the right figure is ours. The arrow represents the direction of propagation and its length is proportional to the corresponding amount of energy.

Existing models for the reflection of inertial waves from rigid boundaries (e.g. Phillips, 1963; Leaman, 1975) usually assume a constant viscosity coefficient and solve for the Ekman boundary layer. For near-inertial frequencies, the resulting boundary layer depth is of the order of the ocean depth and the reflection coefficient is zero. However, this singular solution is not applicable to the real ocean for the following reasons: firstly, such an order-one viscous layer is not observed (e.g. large amplitudes at great depths are inconsistent with a viscous decay); secondly, the benthic mixed layer in which most dissipation occurs has been neglected. Recent observations (e.g. Armi and D'Asaro, 1979) suggest that near the bottom, a well-mixed boundary layer with depth a few tens of meters is quite common. For a review of theoretical models and earlier observations of this boundary layer see Wimbush and Munk (1970). The inclusion of this layer in the dynamics is important especially when dissipation is concerned. It is the purpose of this chapter to present a simple model for the reflection of inertial waves from the bottom in the presence of a benthic mixed layer. The major question is whether we can obtain a reflection coefficient comparable to that estimated by Leaman (1976).

6.2 The model

The benthic ocean is modelled as a uniformly stratified layer of infinite depth on top of a homogeneous layer of depth D. The existence of this mixed layer is assumed a priori; presumably it is maintained by turbulence produced in the shear zone near the bottom. Fig. 6.2 shows the model configuration. Wave packets come from infinity and reflect
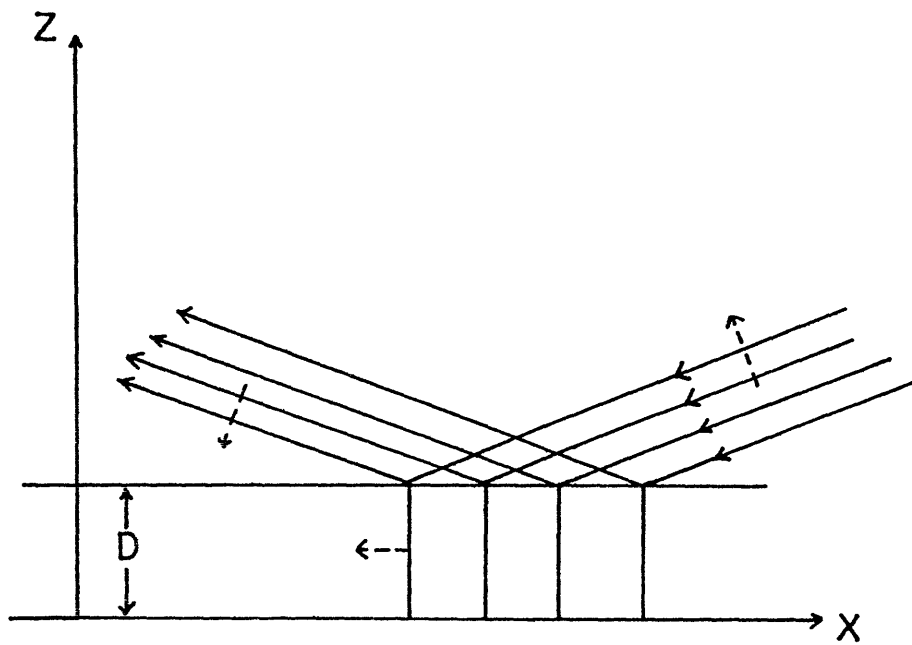
Figure 6.2   Schematic diagram of the model configuration. Solid arrows represent the ray paths and their directions of propagation; dashed arrows represent the directions of phase propagation.

back from the boundary layer. Because our major interests are the energy containing waves with low vertical wavenumbers, the viscous effects can be neglected in the interior. For instance, the wave Ekman number, $\nu m^2/f$, is $O(10^{-4})$, where ν is the eddy viscosity (~ 1 cm^2/sec), m is the vertical wavenumber ($\sim 10^{-4}$cm^{-1}), and $f=7.27 \times 10^{-5}$sec^{-1}. In the mixed layer, all the dynamic variables are nearly uniform in the vertical as the result of turbulent mixing (Armi and D'Asaro, 1979). Hence the slab model used in the upper oceanic mixed layer (Pollard and Millard, 1970) and in the atmospheric boundary layer (Geisler and Kraus, 1969) can be applied here. The frictional drag produced at the bottom can be written as

$$\vec{\tau} = c_D \left| \vec{u} \right| \vec{u} , \qquad (6.1)$$

where c_D is a drag coefficient which is hardly dependent on velocity at high Renolds number; $\vec{u}$ is the velocity vector, and $\left| \vec{u} \right|$ is its magnitude. Then the effects of $\vec{\tau}$ in the mixed layer is simply modelled as a uniform body force $\vec{\tau}/D$. Mean flow effects (including low frequency eddies) are not considered in this model; this is a serious restriction because the nonlinear drag law has been used to model frictional effects. However, for places in the mid-ocean where low frequency flow is weak, this model should be a zero order approximation.

The Boussinesq equations on an f-plane can be written

$$u_t - fv = -P_x \qquad \qquad \qquad (6.2)$$

$$V_t + f u = -P_y \tag{6.3}$$

$$U_x + V_y + W_z = 0 \qquad \text{for } z > D, \tag{6.4}$$

$$0 = -P_z - \frac{\rho}{\rho_o} g \tag{6.5}$$

$$\rho_t - \frac{\rho_o}{g} N_b^2 W = 0 \tag{6.6}$$

and

$$u'_t - f v' = -P'_x - B u' \tag{6.7}$$

$$V'_t + f u' = -P'_y - B v' \tag{6.8}$$

$$U'_x + V'_y + W'_z = 0 \qquad \text{for } D > z > 0 . \tag{6.9}$$

$$0 = -P'_z \tag{6.10}$$

where

$$B = (u'^2 + v'^2)^{1/2} C_D / D , \tag{6.11}$$

u, v, and w are the east, north, and vertical velocity components, ρ_o = mean density, ρ = perturbation density, p= pressure/ρ_o , N_b = buoyancy frequency, g= gravity; the primed variables are the corresponding ones in the mixed layer. The hydrostatic approximation is assumed in (6.5) and (6.10). At z = D, the matching conditions are

$$p = p' \tag{6.12a}$$

$$w = w' \tag{6.12b}$$

At z = 0, the boundary condition is

$$w' = 0 \tag{6.13}$$

Eqs. (6.2)-(6.13) are nonlinear because of the nonlinear dependence of B on u' and v'. However, for typical values $C_D = 2 \times 10^{-3}$ (Wimbush and Munk, 1970), u'= 3cm/sec and D = 20 m (Armi and D'Asaro, 1979), we have $B = 3 \times 10^{-6} \text{sec}^{-1}$, which is only 0.04 f at 30° latitude. Hence the linear wave solution should be a good zero order solution. Moreover, at near-inertial frequencies the horizontal particle speed, $(u'^2+v'^2)1/2$, of the zero order solution is independent of both time and space (properties of inertial waves). So we can simplify the equations by treating B as a constant, and seek wave solutions of the following form:

$$(u, v,...) = \text{Real } (\hat{u}, \hat{v}, ...) \exp(i(kx \pm mz - \omega t)) \tag{6.14}$$

$$(u', v',...) = \text{Real}(\hat{u}', \hat{v}',...) \exp(i(kx - \omega t)) \tag{6.15}$$

where the hatted variables are complex amplitudes; k and m are the horizontal and vertical wavenumbers; ω is the frequency. Assuming $m > 0$, then the upper sign in (6.14) corresponds to the incident (downward energy) waves and the lower sign to the reflected waves. Substituting (6.14) and (6.15) into Eqs. (6.2)-(6.10), we obtain

$$i\omega \hat{u} + f \hat{v} = ik \hat{p} \tag{6.16}$$

$$-i\omega \hat{v} + f \hat{u} = 0 \tag{6.17}$$

$$ik\,\hat{u} \;\pm\; im\,\hat{w} \;=\; 0 \qquad\qquad \Big\} \quad z > D \qquad (6.18)$$

$$0 \;=\; \mp im\,\hat{p} \;-\; \frac{\hat{\rho}}{\rho_0}\,g \qquad\qquad\qquad\qquad (6.19)$$

$$i\omega\,\hat{\rho} \;+\; w\,N_b^2\,\frac{\rho_0}{g} \;=\; 0 \qquad\qquad\qquad\qquad (6.20)$$

and

$$(B - i\omega)\,\hat{u}' \;-\; f\,\hat{v}' \;=\; -ik\,\hat{p}' \qquad\qquad \Big\} \qquad\qquad (6.21)$$

$$f\,\hat{u}' \;+\; (B - i\omega)\,\hat{v}' \;=\; 0 \qquad\qquad \Big\} \quad D > z > 0 \qquad (6.22)$$

$$ik\,\hat{u}' \;+\; \hat{w}'_z \;=\; 0 \qquad\qquad\qquad (6.23)$$

Differentiating (6.23) with respect to z, we have

$$\hat{w}'_{zz} = 0 \;,$$

of which the solution satisfying (6.13) is

$$\hat{w}' \;=\; -ik\hat{u}'z \qquad\qquad\qquad (6.24)$$

From (6.21) and (6.22) we obtain

$$\hat{u}' \;=\; \frac{-ik\,\hat{p}'\,(B - i\omega)}{(B - i\omega)^2 + f^2} \quad , \quad \hat{v}' \;=\; \frac{ik\,\hat{p}'\,f}{(B - i\omega)^2 + f^2} \qquad\qquad (6.25)$$

The matching conditions (6.12a) and (6.12b) become

$$\hat{p}' \;=\; \hat{p}_i\,e^{imD} \;+\; \hat{p}_r\,e^{-imD} \qquad\qquad , \qquad\qquad (6.26a)$$

$$\hat{w}' \;=\; -ik\,\hat{u}'D \;=\; \hat{w}_i\,e^{imD} \;+\; \hat{w}_r\,e^{-imD} \qquad , \qquad (6.26b)$$

where "i" and "r" represent the incident and reflected waves respectively. From (6.19) and (6.20) we have

$$\hat{P}_i = -\frac{N_b^2}{\omega m}\hat{W}_i \quad , \quad \text{and} \quad \hat{P}_r = \frac{N_b^2}{\omega m}\hat{W}_r \qquad (6.27)$$

Then from (6.26a), (6.26b), (6.25), and (6.27), the following expression is obtained:

$$Z \equiv \frac{\hat{W}_r}{\hat{W}_i}e^{-2imD} = \frac{m(\omega^2-f^2)D(\beta-i\omega)-\omega\left[(\beta-i\omega)^2+f^2\right]}{m(\omega^2-f^2)D(\beta-i\omega)+\omega\left[(\beta-i\omega)^2+f^2\right]} \qquad (6.28)$$

where the dispersion relation

$$k^2 N_b^2 = m^2(\omega^2 - f^2)$$

has been used. The reflection coefficient r is defined as the ratio of the reflected energy flux to the incident energy flux, which is proportional to $|\hat{W}_r|^2/|\hat{W}_i|^2$, so we have

$$r = |Z|^2$$

Because β is still unknown, another equation is needed to solve for Z in terms of the parameters of incident waves. From Eqs. (6.25)-(6.27) we obtain

$$\hat{u}' = \frac{-ik\hat{P}_i e^{imD}(\beta-i\omega)(1-Z)}{(\beta-i\omega)^2 + f^2} \qquad ; \qquad (6.29)$$

with the use of Eqs. (6.16) and (6.17) which yields

$$\hat{P}_i = \frac{\omega^2-f^2}{\omega k}\hat{u}_i \qquad ,$$

the following relation between $\hat{u}'$ and $\hat{u}_i$ is obtained:

$$\hat{u}' = \frac{-i(w^2 - f^2)(B - iw)e^{imD}(1 - Z_i)}{w[(B - iw)^2 + f^2]}\hat{u}_i \qquad (6.30)$$

In order to be consistent with the requirement that B be a constant, we must have

$$\frac{\hat{u}'}{\hat{v}'} = -i \qquad . \qquad (6.31)$$

As a consistency check of the solutions, we should test the validity of (6.31). From (6.25) we have

$$\frac{\hat{u}'}{\hat{v}'} = \frac{-B}{f} + i\frac{w}{f} \qquad (6.32)$$

For $B \ll f$ and $w \approx -f$, our solutions are self consistent. Therefore a consistent approximation for B can be written

$$B = \frac{C_D}{D}|\hat{u}'| \qquad (6.33)$$

For given $\hat{u}_i$, Eqs. (6.28) and (6.30) then form a closed set of nonlinear algebraic equations with unknowns Z and $\hat{u}'$, which can be solved numerically using an iteration method.

6.3 Results

The model results are presented by showing r and d ($\equiv |\hat{u}'|/|\hat{u}_i|$), the reflection coefficient and the ratio of the horizontal velocity in

the mixed layer to that of the incident wave, as functions of frequency

with the other five model parameters -- m, D, C_D, N_b, and $|\hat{u}_i|$ --

varying in their typical ranges. Instead of the vertical wavenumber m,

we use its equivalent mode number j defined as

$$m = j \, \pi \, \hat{M} \, N_b/N_o \qquad\qquad (6.34)$$

where N_o = 3 cph, $\hat{M}$ = 0.122 x 10^{-3} cycle/meter. Eq. (6.34) expresses

the relation between j and m above the mixed layer where we have assumed

constant buoyancy frequency N_b, according to the N(z) used by Garrett

and Munk (1972).

There are five cases to be discussed; in each case we vary only one

parameter with the others fixed at the following reference parameters: j

= 3, D = 20 m, C_D = 0.002, N_b = 0.2 cph, $|\hat{u}_i|$ = 3 cm/sec. The

value for j is the mode number scale, i.e., j_*, proposed by Cairns and

Williams (1976) for the vertical wavenumber spectrum, corresponding to a

870 m wavelength in the thermocline. The values for N_b and $|\hat{u}_i|$ are

typical of the benthic ocean (D'Asaro, 1979; personal communication).

Fig 6.3 shows r and d as functions of ω with different j. For ω ,

1.2 f is probably the upper bound for the validity of the solutions.

First of all, r is greater than 0.9 for j $\lesssim$ 20, where lies most of the

energy of the vertical structure of inertial waves. Thus the estimate of

Leaman (Fig. 13, 1976) -- r $\approx$ 0.6 for 75 % of the energy -- cannot be

accounted for by the model. When ω = f, the vertical velocity of the

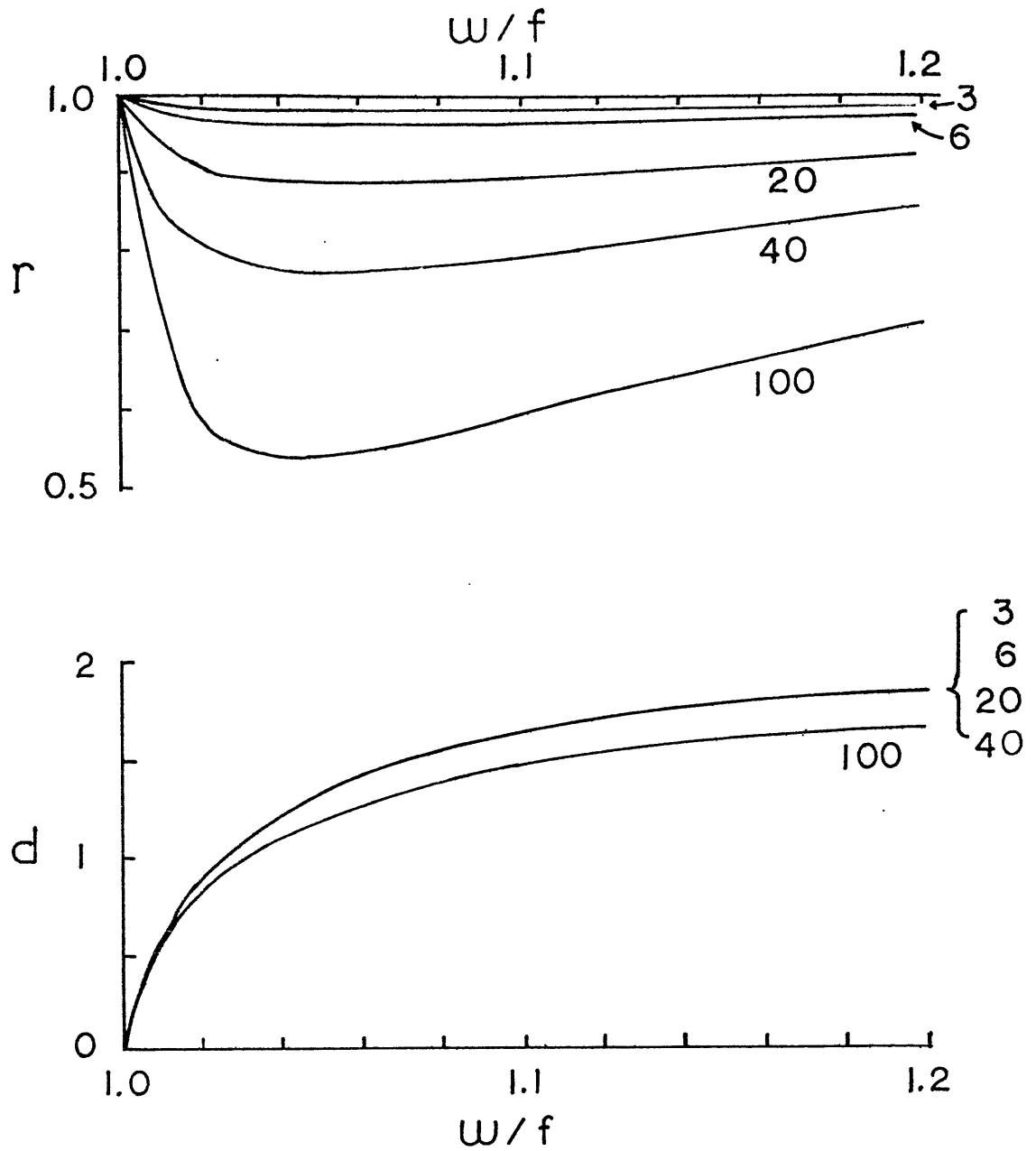incident waves vanishes in an f-plane model, so the mixed layer is

Figure 6.3   r and d as functions of frequency for different values of vertical wavelength (labelling numbers are equivalent mode numbers).

decoupled from the interior, yielding $|\hat{u}'| = 0$ and $r = 1$. When $(\omega - f)$

increases, B becomes increasingly negligible in the denominator in

(6.30); hence $|\hat{u}'|$ increases toward its inviscid limit $2 |\hat{u}_i|$ for

$mD \ll 1$. For $\omega \gtrsim 1.04$ f, both d $(\equiv |\hat{u}'| / |\hat{u}_i|)$ and the dissipation

rate, $C_D |\hat{u}'|^3$, increase very slowly; the slight increase of r

with ω can then be explained by the rapid increase with ω of the

vertical group velocity, yielding a rapid increase of the dissipation

rate for fixed r, therefore r has to increase with ω at a rate which

makes the dissipation rate change slowly as shown in Fig. 6.3. Similarly

the decrease of r with increasing m also can be explained by the

decrease of the vertical group velocity with increasing m and the

insensitivity of d (hence the dissipation) to m. Recall that the

vertical group velocity can be written

$$\frac{\partial \omega}{\partial m} = \frac{-(\omega^2 - f^2)}{\omega m} = \pm \frac{(\omega^2 - f^2)^{3/2}}{\omega k N} \qquad (6.35)$$

Is the result of nearly perfect reflection at small j sensitive to

the particular model parameters used ? Fig 6.4 shows the sensitivity of

the model results to the mixed layer depth D. Note that the scale for

the r-axis has been changed — from 0.5-1. in Fig. 6.3 to 0.9-1. For

typical range of D observed in the ocean — from 5 m to 60 m (Armi and

D'Asaro, 1979), r varies only in a narrow range from 0.94 to 1. Because

B (frictional effects) decreases with increasing D, d is closer to the

inviscid limit for larger D, resulting in smaller r.

Fig 6.5 shows the sensitivity to N_b, the buoyancy frequency above

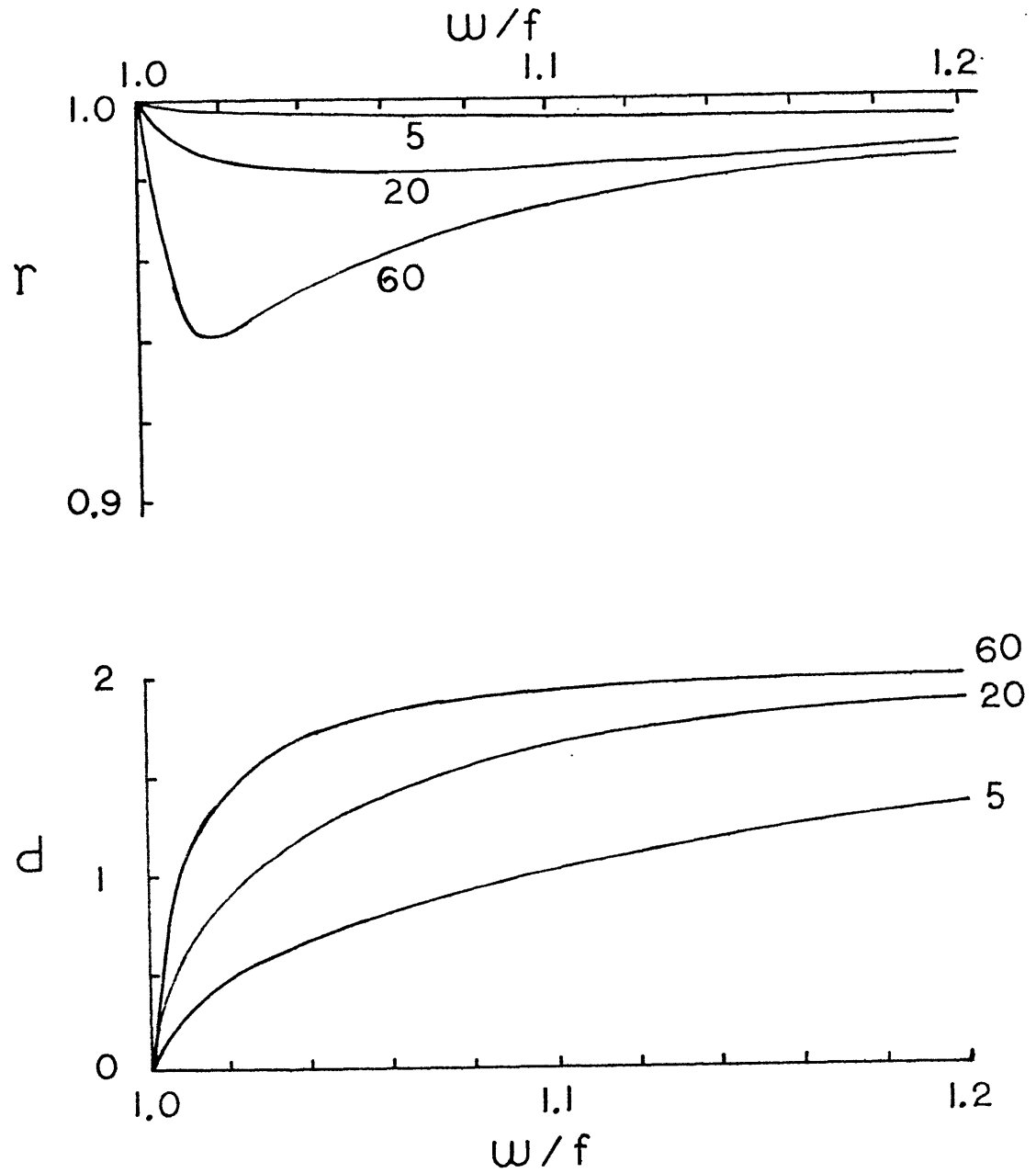the mixed layer. For a rather unlikely large value, $N_b = 0.8$ cph, the

Figure 6.4   As in Fig. 6.3 except for different values of the
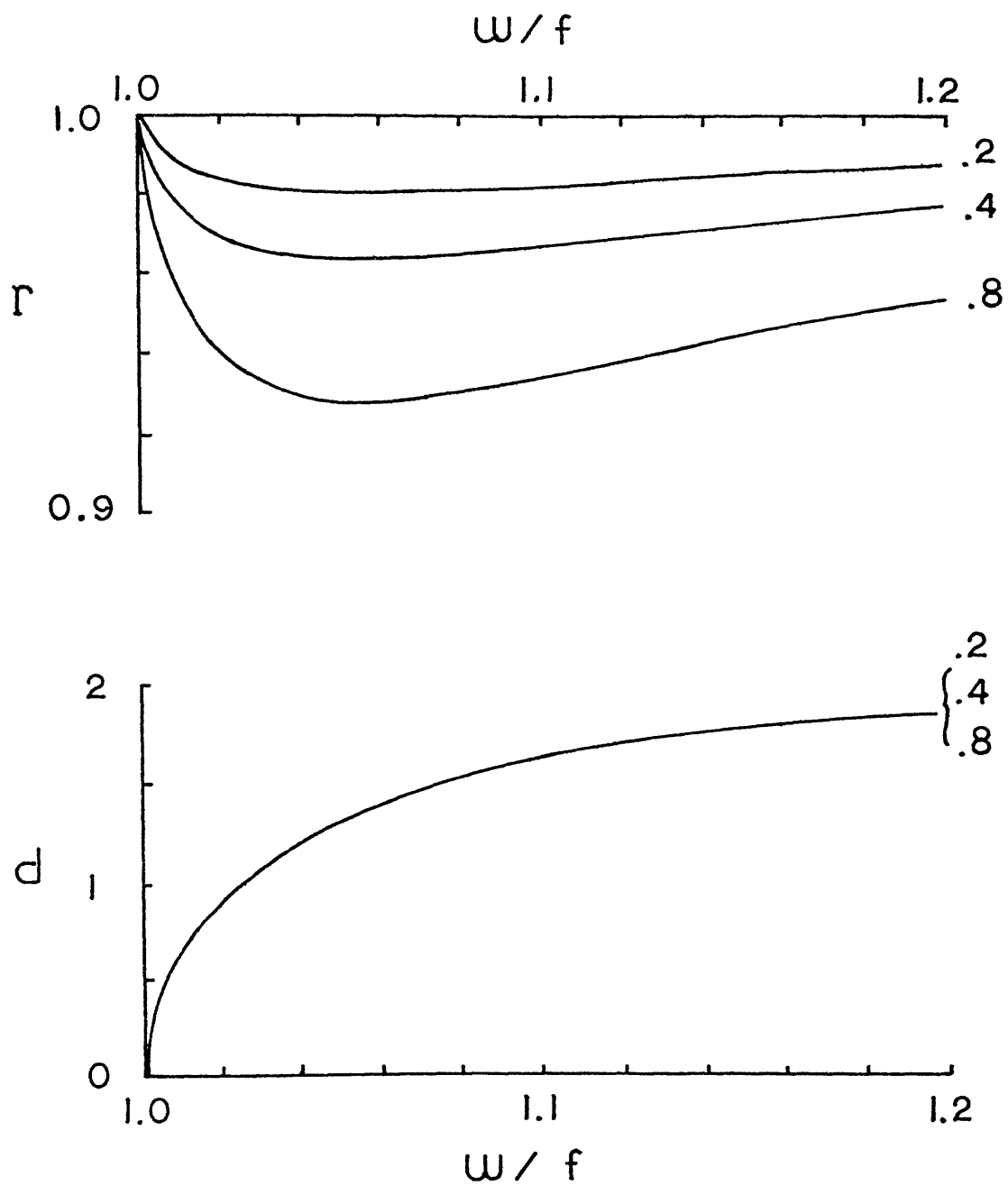mixed layer depth D (numbers are in meters).

Figure 6.5   As in Fig. 6.3 except for different values of the buoyancy frequency N_b (in cph) on top of the mixed layer.

lowest value of r is about 0.93. The behavior of d does not change with N_b at all -- the same as in Fig. 6.4 with D = 20 m. The decrease of r with increasing N_b is cause by the increase of vertical group velocity with N_b (c.f. Eq. (6.35)).

Fig. 6.6 shows that $r \gtrsim 0.99$ is essentially insensitive to the drag coefficient C_D in the range 0.002- 0.01; the typical range of C_D in the benthic ocean is from 0.002 (smooth bottom) to 0.005 (rough bottom) (Wimbush and Munk, 1970). As expected, d decreases with increasing C_D. The crossings of the r curves at intermediate frequencies can be explained by the following relation:

$$(1 - r) \propto C_D \, d^3 \, |\hat{u}_i|$$

(6.36)

For different values of C_D, the behavior of the corresponding r could be different from that of d.

The behavior of r for different values of the incident wave velocity $|\hat{u}_i|$ (Fig. 6.7) is pretty much the same as that shown in Fig. 6.6, because $|\hat{u}_i|$ plays the same role as C_D in Eq. (6.36). Smaller $|\hat{u}_i|$ induces smaller $|\hat{u}'|$ and hence smaller frictional effects, so d is larger for smaller $|\hat{u}_i|$ as shown.

6.4 Summary and discussion

A simple model has been developed to calculate the reflection coefficient of inertial waves in the presence of a well mixed bottom boundary layer. The interior dynamics is assumed to be inviscid. The mixed layer is modelled as a slab and the frictional drag at the bottom
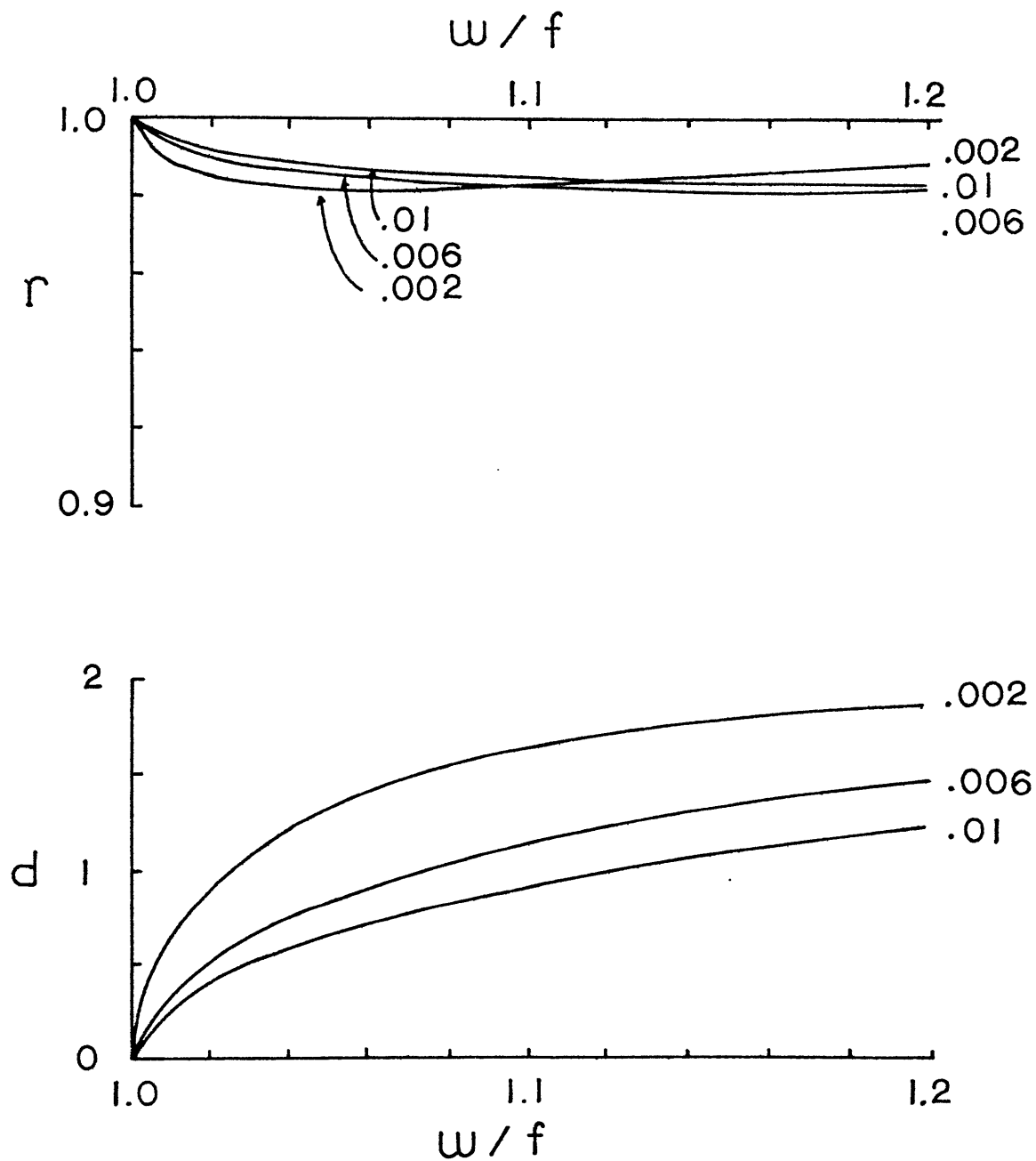
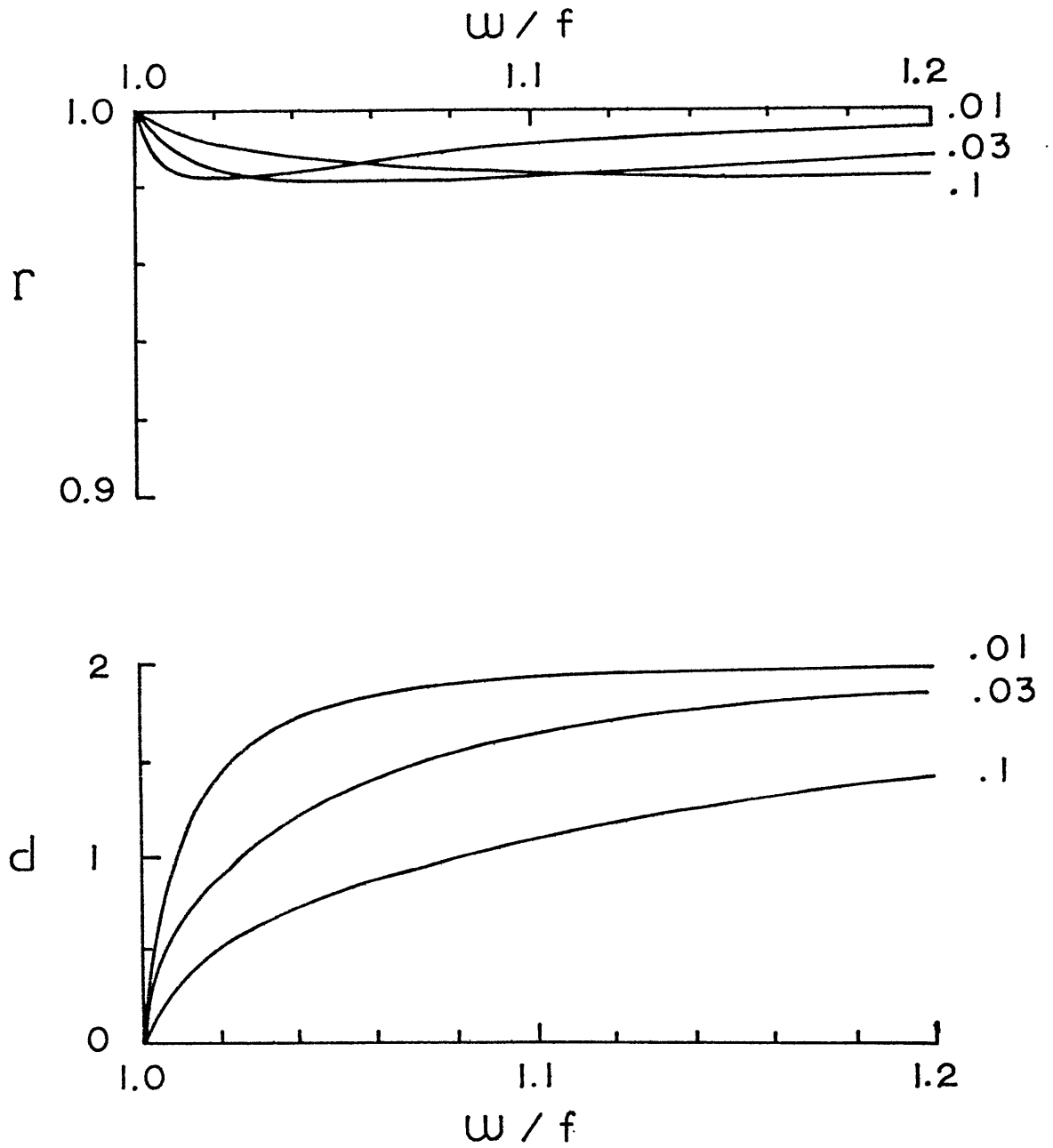Figure 6.6   As in Fig. 6.3 except for different values of the drag coefficient C_D.

Figure 6.7   As in Fig. 6.3 except for different values of the
incident wave amplitude $|\hat{u}_i|$ (in m/sec).

is quadratic in the horizontal wave speed. An approximate wave solution

has been obtained with error of order max.$\left(\dfrac{C_D}{D} \dfrac{|\hat{u}'|}{f}, \dfrac{(\omega - f)}{f} \right)$, where

C_D= drag coefficient, D = boundary layer depth, $|\hat{u}'|$ = wave amplitude

in the boundary layer. For typical conditions in the benthic ocean, the

resulting reflection coefficient is generally greater than 0.9 for waves

with equivalent mode number less than 20, and the results are not

sensitive to model parameters. The relatively low values estimated by

Leaman (1976) cannot be accounted for by the model.

Because of the nonlinearity introduced by the friction law, we

cannot superpose wave solutions. However, the observed vertical

wavenumber spectrum is dominated by low wavenumber components; our

results for low wavenumber waves should be fairly representative. The

existence of inertial waves in the benthic boundary layer and its high

coherence with those above (Armi and D'Asaro, 1979) suggest that the

effects of low frequency flow on inertial waves through nonlinear

frictional effects are probably not important. The model results are

then a valid zero order description; however, a numerical model

including a mean flow would be necessary to verify this speculation.

That the reflection coefficient is near unity is consistent with the

existence of a global inertial wave field as described in Chapter 4.

Chapter 7   Conclusions

Our work can be summarized as a spectral description of inertial

waves observed in the Western North Atlantic from subtropical to

temperate latitudes, and an attempt to interpret it in terms of the

proposed models of the global and local wave field.

The observations presented in Chapter 2 suggest that a universal

frequency spectrum does not exist near the inertial frequency f, where

the spectral shape is very sensitive to the local environment. In most

of the data, there is a prominent inertial peak slightly above f in the

horizontal velocity spectrum as previously described; however, the peak

height above the background continuum varies with instrument depth and

geographical environment. According to the peak height, three classes of

environment and their corresponding spectra emerge: class 1 is the 1500 m

level near the Mid-Atlantic Ridge, with the greatest peak height of 18

db; class 2 includes (a) the upper ocean (depth less than 2000 m), (b)

the deep ocean (depth greater than 2000 m) over rough topography, and

(c) the deep ocean underneath the Gulf Stream, with intermediate peak

height of 11.5 db; class 3 is the deep ocean over smooth topography,

with the lowest peak height of 7.5 db. In the inertial frequency band,

the estimated horizontal coherence scale is 0(60 km) at depths from 200 m

to 600 m, and probably less than this value at great depths. The order

of magnitude is consistent with the theory of Munk and Phillips (1968).

The estimated vertical coherence scale is 0(200 m) just below the main

thermocline, resulting in a wavenumber band in close agreement with the

result of Cairns and Williams (1976).

A model spectrum for the global wave field is developed in Chapter 4

based on the wave functions obtained by Munk and Phillips (1968) and the assumption that the frequency-wavenumber spectrum is given by the GM model at lower latitudes. The most significant result of our work perhaps is the success of the global wave model in describing the observations of class 3. Both the energy level and the height of the observed inertial peak are well-described by the model. The amount of the blue shift of the inertial peak predicted by the model is dependent on the zonal wavenumber band. To be consistent with the observed blue shifts, zonal wavelengths are required to be less than $O(90$ km$)$. The observed frequency bandwidths of the inertial peak are slightly larger than the model results due to the kinematic effects of low frequency motions; however, their latitudinal dependence is consistent with the model. The latitudinal limits of the validity of the model is roughly from 10° to 68°.

For the observed spectra of class 1 and class 2, the excess inertial wave energy above what the global model predicts is interpreted as the result of local forcing. In the upper ocean, the most likely local forcing is from the mixed layer and the forced waves transfer energy downward. With this assumption , we have estimated a budget for downward and upward travelling energy which is in close agreement (10 % difference) with a recent estimate of Sanford. To make the idea of local forcing more concrete, a forced model is develped in Chapter 5 based on the latitudinal modal decomposition of a localized forcing function using the asymptotic eigensolutions of the Laplace's tidal equation. The forcing is through a vertical velocity field specified at the top and/or bottom boundaries. For surface forcing, major characteristics of the

class 2a spectra can be qualitatively described by the model. For bottom

forcing, the resulting spectra show prominent inertial peaks at deep

levels, consistent with observations over rough topography (class 2b).

The estimated vertical energy flux from local sources to the interior

suggests that both the surface and bottom sources are fairly efficient

to generate inertial waves; the total internal wave energy could be set

up in couple of weeks. If the bottom source is from typical mid-ocean

eddies, the resulting "spin- down" time scale for the eddies is about a

month.

In order that energetic low mode waves can propagate over great

distance to form the global wave field, dissipation rates must be very

small for these waves. A model is proposed in Chapter 6 to study the

reflection of inertial waves from the benthic boundary layer, which is

turbulent and homogeneous and hence can be modelled as a slab.

Frictional effects are confined to this boundary layer and modelled by a

quadratic drag law. For given incident waves, reflection coefficients

are calculated. For waves with equivalent mode number less than 20,

which contain most of the energy, the reflection coefficient is greater

than 0.9 and increases with decreasing mode number. This is inconsistent

with Leaman's estimate ($\approx$ 0.6; 1976) from the difference between

downward and upward travelling energy as measured by velocity profilers.

From the geometry of the ray paths of locally surface-forced waves, it

can be shown that most of the reflected waves cannot be measured by a

local profiler. Hence the interpretation that the excess downward

travelling energy measured by profilers is primarily dissipated in the

bottom boundary layer is misleading.

In summary, among the different classes of observations, we have successfully interpreted class 3, class 2a, and class 2b. In order to explain the observations of class 1, interactions between the Mid-Atlantic Ridge and low frequency motions which is the only apparent energy source available at intermediate and deep levels, must be adequately modelled. Time dependent models like Bell's (1975) are possible approaches. In addition to the huge inertial peaks, other features of the class 1 spectrum are also interesting: huge M_2 tidal peak, prominent super-M_2 tidal peaks, small spectral slope and excess high frequency energy. Are these caused by the topographic effects of the Mid Atlantic Ridge ? When the moorings of the PMIII were deployed, a discontinuity in water mass was found in the cluster B area (Joyce, 1977). Is this frontal feature dynamically important ? Some theoretical work is needed here.

Concerning the strong inertial peaks found underneath the Gulf Stream (class 2c), observations at upper levels are important to determin the nature of the forcing. But the maintenance of moorings within the core of the Gulf Stream is still beyond the current capability of mooring technology. Theoretical work on the interactions between ineritial waves and strong time dependent current would be illuminating.

Appendix A   <u>Temperature Spectra in the Inertial Frequency Band</u>

The occurrence of apparent inertial peaks in observed temperature

spectra as shown in Fig. 4.11 is not universal in the data examined. For

instance, Fig. A.1 shows the temperature spectra at Stations 1 (3500 m)

and 7 (600 m) of the PMII, where no prominent peaks show up near f;

however, prominent inertial peaks were observed at the 4000 m depth of

Station 7 and at the same depth of Station 3 (see Fig. 4.11) which was

only 30 km north of Station 1. We have not found any correlation between

the occurrence of the temperature inertial peaks and their physical

environment except that, there is always a strong temperature inertial

peak at all depths of those stations roughly along 28°N. Because the

diurnal tidal frequencies are so close to the local inertial frequency

there, the observed temperature peaks are probably due to tidal motions.

Elsewhere, the occurrence of temperature peaks is essentially

unpredictable. We hereby investigate two possible mechanisms to account

for their occasional occurrence.

As shown in Fig. 4.11, the observed inertial peaks in the

temperature spectra are not consistent with the global wave model which,

on the other hand, is consistent with the corresponding observed

velocity spectra. For frequencies near f, the motion of free linear

waves is nearly horizontal, and there should be no appreciable

temperature fluctuations if the temperature gradient is essentially

vertical. However, in the presence of meso-scale eddies, appreciable

horizontal temperature gradient could exist in the mid-ocean

occasionally; when advected by large horizontal inertial currents, it
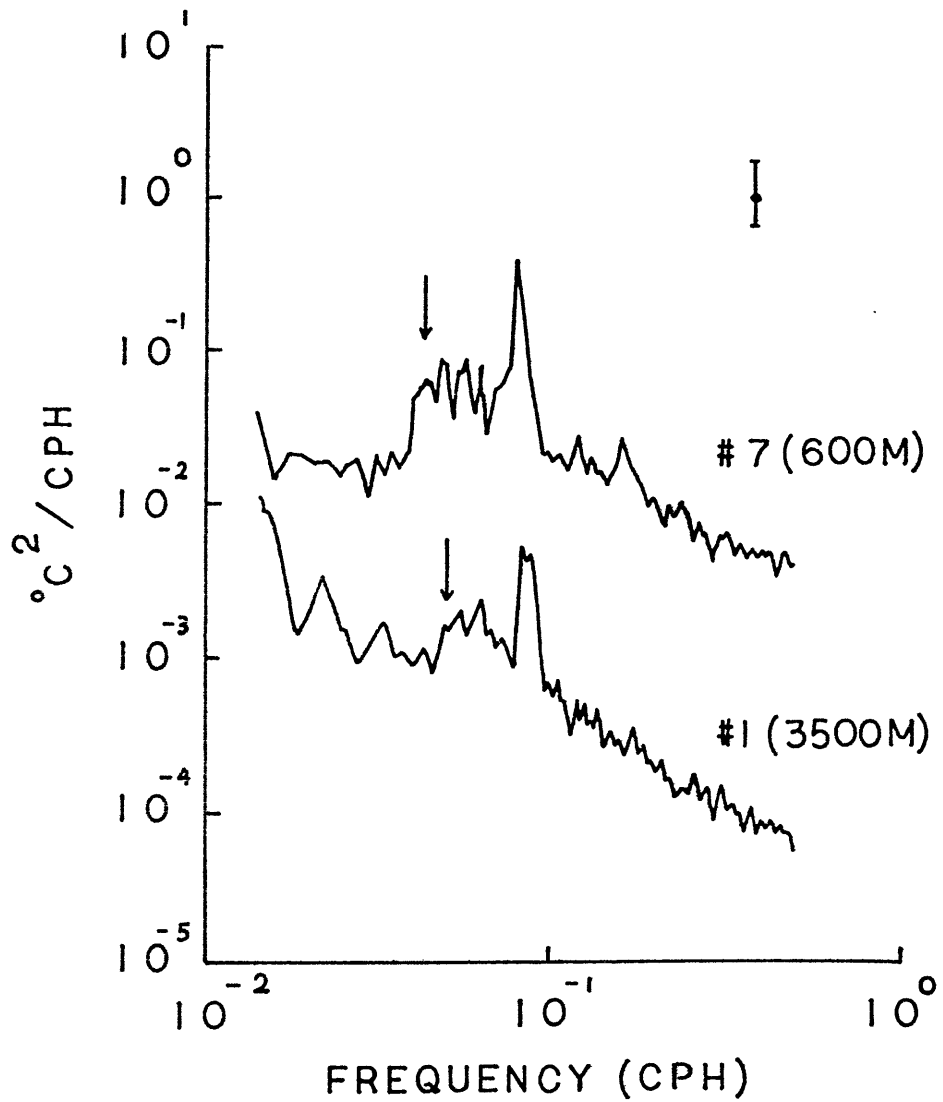
\

Figure A.1   Temperature spectra at 600 m at Station 1 (36°N, 55°W), and at 3500 m at Station 7 (31.6°N, 55°W) of the PMII. Arrows showing the location of the local f; error bar showing the 95 % confidence interval.

could produce appreciable temperature signals with near inertial frequencies. The possibility that this mechanism accounts for the observed temperature peaks is discussed in Section A.1.

It is well-known that moored temperature measurements are subject to contamination caused by vertical mooring motion. Pressure spectra measured by TP recorders (Wunsch and Dahlen, 1974) show fairly strong inertial peaks, indicating strong vertical mooring motion in the inertial frequency band. A typical pressure spectrum is shown in Fig. A.2. Possible effects of this mechanism on observed temperature spectra are discussed in Section A.2.

A.1 Advection of horizontal temperature gradient by inertial waves

The propagation of internal waves in the presence of a baroclinic mean flow was investigated by Mooers (1975). For low frequency waves, he showed that the combined effect of mean shear and its resulting horizontal density gradient was to extend the free wave frequency band to an anomalous low frequency limit. It can be shown that this low frequency limit is at most a few percent lower than the local f for typical mid-ocean conditions, and that the characteristics of velocity solutions are only slightly modified by the mean flow. However, the density (or temperature) solutions are seriously affected by the presence of a horizontal density gradient. Assuming that all the field variables are independent of y, the temperature equation can be written

$$T_t + u \frac{\partial \bar{T}}{\partial x} + w \frac{\partial \bar{T}}{\partial z} = 0, \qquad (A.1)$$

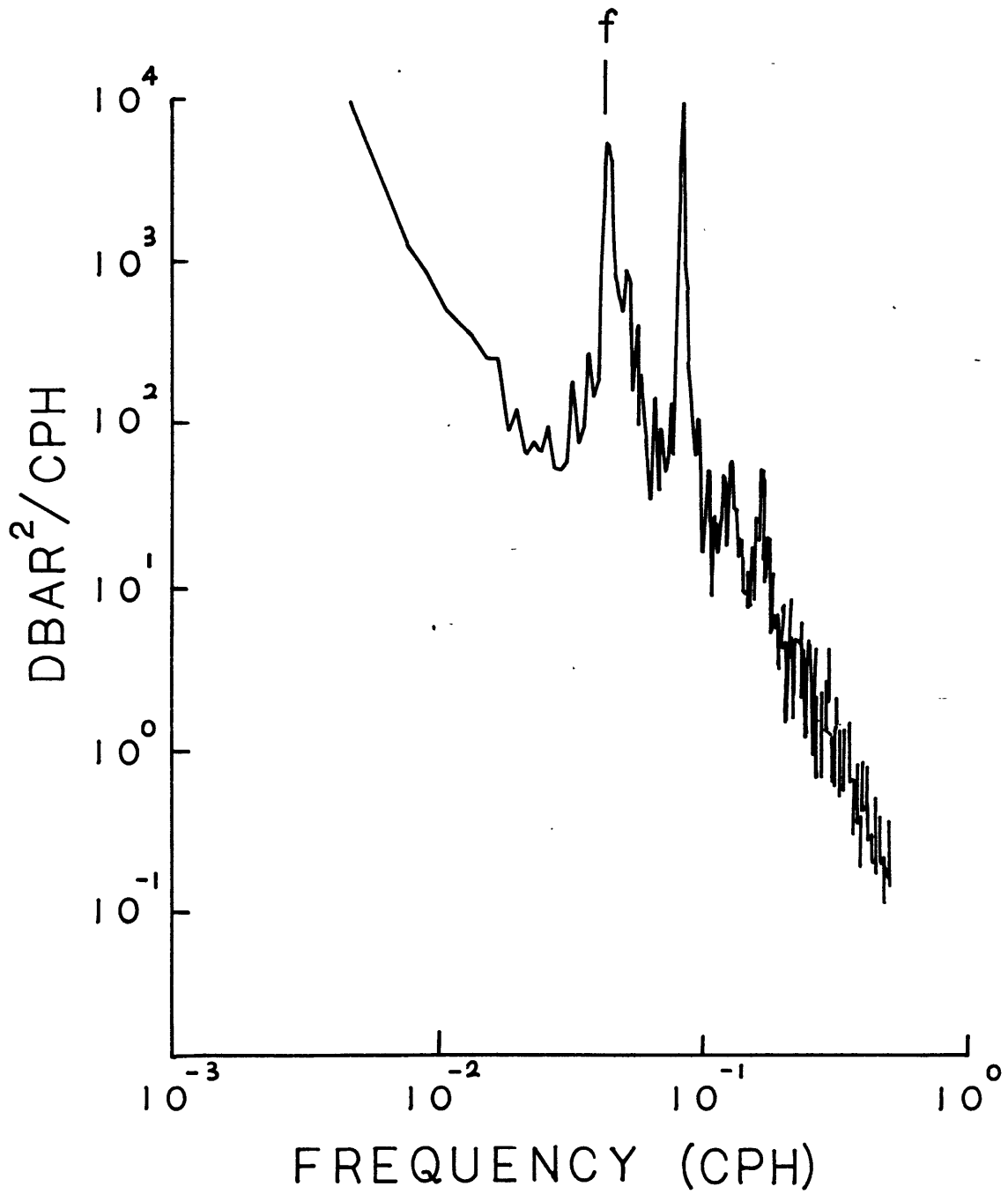where $\bar{T}$ is the mean temperature field. For wave motion with frequencies

Figure A.2   Pressure spectrum of Record 5482 (31°N, 60°W) at 800 m.

near f, it can easily be shown that the horizontal advection dominates the vertical advection. Then the temperature spectral shape is the same as that of the horizontal velocity, having an inertial peak. The amplitude of the temperature fluctuation, $\overline{T'^2}^{1/2}$, can be estimated as the product of $\left| \frac{\partial \overline{T}}{\partial x} \right|$ and the radius of inertial circle, u_o/f (u_o is a typical horizontal speed of inertial waves). For a typical mid-ocean eddy, $\left| \frac{\partial \overline{T}}{\partial x} \right|$ in the main thermocline is about 3×10^{-2} deg.C/km (see MODE-1 Atlas Group, 1977). With $u_o = 10$ cm/sec and $f=7.27 \times 10^{-5}$ sec^{-1}, we have $\overline{T'^2}^{1/2} \sim 0.04$ deg.C, which is within order of magnitude of the observed values in the main thermocline (c.f. Table A.1, which shows the values for some strong temperature peaks). Therefore this mechanism could, to some extent, explain the observed inertial peaks in temperature spectra.

A.2 Mooring motion in the inertial frequency band

If the observed temperature signals are solely caused by the vertical mooring motion, we should have

$$ T_t + P_t \frac{\partial T}{\partial P} = 0 \qquad\qquad (A.2) $$

For a linear vertical temperature gradient, which is approximately the case for small vertical excursions, we should have significant coherence between T and P with 180° phase difference. The T-P coherence was calculated for a great number of stations, and significant coherence with 180° phase difference in the inertial band was found only at those stations where the mooring motion was relatively strong. At these

stations, the temperature spectra indeed have strong inertial peaks. It seems that strong mooring motion is a sufficient (but not necessary) condition for the occurrence of temperature inertial peaks. To test whether the observed temperature peaks are indeed caused by mooring motion, we have calculated for four selected stations the root mean square amplitudes of both temperature and pressure fluctuations in the inertial frequency band, denoted by $\overline{T'^2}^{1/2}$ and $\overline{P'^2}^{1/2}$ respectivcely, and also calculated the corresponding local temperature gradient dT/dp from CTD casts. By comparing $\overline{T'^2}^{1/2}$ with dT/dP x $\overline{P'^2}^{1/2}$, we can tell the significance of the contribution of mooring motion to the temperature peaks. These values are listed in Table A.1. For the three records (5482, 5792, and 5492) where mooring motion is strong and the T-P coherence is high, the temperature fluctuations are mainly caused by mooring motion; with weak mooring motion and low T-P coherence, the temperature fluctuations at 5422 cannot be attributed to mooring motion.

<div style="text-align:center">

Table A.1

</div>

Tabulation of $\overline{T'^2}^{1/2}$ (deg), $\overline{P'^2}^{1/2}$ (dbar), dT/dP (deg/dbar), and $\overline{P'^2}^{1/2}$ x dT/dP (deg) in the main thermocline for selected records.

Record	$\overline{T'^2}^{1/2}$	$\overline{P'^2}^{1/2}$	dT/dP	$\overline{P'^2}^{1/2}$ x dT/dP
5482	.252	9.6	.0203	.195
5792	.152	5.34	.0206	.11
5492	.1	2.91	.0202	.06
5422	.16	.586	.0187	.011

A.3 Summary

For records from moorings with high T-P coherence with 180° phase difference in the inertial frequency band, a prominent inertial peak is usually observed in the temperature spectrum and is mainly caused by mooring motion. For records from moorings with low T-P coherence in the inertial frequency band, the occasional occurrence of temperature peaks is probably due to the advection of horizontal temperature gradient by the strong horizontal motion of inertial waves.

\

Appendix B   Evaluation of Elliptic Integrals with Parameters

Greater than One

In the calculation of the wave functions $V(\phi)$ and $P(\phi)$ using

Eqs. (3.27) and (3.19), we need to evaluate the following three

quantities ξ , $\dfrac{d\xi}{d\phi}$, and $\dfrac{d^2\xi}{d\phi^2}$. From Eq. (3.26),

$$\frac{2}{3}\,\xi^{3/2} = \int_\phi^{\phi_s} (\sin^2\phi_s - \sin\phi')\,d\phi' \quad , \tag{B.1}$$

we have

$$\frac{d\xi}{d\phi} = -\xi^{-1/2}\left(\sin^2\phi_s - \sin^2\phi\right)^{1/2} \quad , \tag{B.2}$$

and

$$\frac{d^2\xi}{d\phi^2} = -\frac{1}{2}\,\xi^{-1}\left(\frac{d\xi}{d\phi}\right)^2 - \frac{1}{2}\,\xi^{-1}\sin 2\phi\left(\frac{d\xi}{d\phi}\right)^{-1} . \tag{B.3}$$

Once ξ is known, $\dfrac{d\xi}{d\phi}$ and $\dfrac{d^2\xi}{d\phi^2}$ can be easily calculated using Eqs. (B.2)

and (B.3). The integral on the right-hand side of (B.1) is an elliptic

integral of the second kind. Using the notation of Abramowitz and Stegun

(1964), (B.1) can be written

$$\frac{2}{3}\,\xi^{3/2} = m^{-1/2}\left[E(\phi_s, m) - E(\phi, m)\right] \quad , \tag{B.4}$$

where $m = \dfrac{1}{\sin^2\phi_s}$ (hence $m > 1$); m is the parameter and ϕ is the

amplitude of the elliptic integrals. Because most of the formulae and

numerical methods for the evaluation of elliptic integrals are

formulated under the assumption that $|m| < 1$, we have to transform the

elliptic integrals in (B.4) into their corresponding forms with

parameters less than one.

\

In terms of u defined as

$$u = \int_0^{\phi} (1 - m\sin^2\lambda)^{-1/2} \, d\lambda \; , \tag{B.5}$$

we have (see Abramowitz and Stegun, 1964; p.593)

$$E(u|m) = m^{1/2} E(um^{1/2} \,|\, m^{-1}) - (m-1)u \; ; \; (m > 1) \tag{B.6}$$

The relation between u and ϕ is usually written as

$$\text{sn}(\, u \,|\, m \,) = \sin\phi \; , \tag{B.7}$$

where sn is a Jacobian elliptic function. The integral in (B.5) is the elliptic integral of the first kind, i.e.,

$$\begin{aligned} u &= F(\phi \,|\, m) \\ &= m^{-1/2} F(\theta \,|\, m^{-1}) \quad (m > 1) \end{aligned} \tag{B.8}$$

where

$$\theta = \sin^{-1}(m^{1/2} \sin\phi) \tag{B.9}$$

$F(\theta \,|\, m^{-1})$ can be calculated by using a rapidly convergent series (Dwight, 1968) :

$$F(\theta|m^{-1}) = \frac{2\phi}{\pi} K - \sin\theta\cos\theta \left(\frac{1}{2} \frac{A_1}{m} + \frac{1\cdot3}{2\cdot4} \frac{A_2}{m^2} + \frac{1\cdot3\cdot5}{2\cdot4\cdot6} \frac{A_3}{m^3} + \cdots \right) \tag{B.10}$$

where

$$K = \int_0^{\frac{\pi}{2}} \left(1 - m^{-1}\sin^2\theta\right)^{-\frac{1}{2}} \text{ (complete elliptic integrals of the 1st kind)}$$

$$= \frac{\pi}{2}(1+P)\left[1 + \frac{1}{2^2}P^2 + \frac{1\cdot 3^2}{2^2\cdot 4^2}P^4 + \frac{1\cdot 3^2\cdot 5^2}{2^2\cdot 4^2\cdot 6^2}P^6 + \cdots\right],$$

$$P = \frac{\left[1 - (1 - m^{-1})^{\frac{1}{2}}\right]}{\left[1 + (1 - m^{-1})^{\frac{1}{2}}\right]} \quad ;$$

$$A_1 = \frac{1}{2}, \qquad A_2 = \frac{3}{2\cdot 4} + \frac{1}{4}\sin^2\theta,$$

$$A_3 = \frac{3\cdot 5}{2\cdot 4\cdot 6} + \frac{5}{4\cdot 6}\sin^2\theta + \frac{1}{6}\sin^4\theta.$$

with u known the remaining calculation in (B.6) is $E(um^{1/2}\,|\,m^{-1})$,

which has a similar series representation :

$$E\left(um^{\frac{1}{2}}\,\middle|\,m^{-1}\right) = \frac{2\phi}{\pi}E + \sin\alpha\cos\alpha\left(\frac{1}{2}\frac{A_1}{m} + \frac{1\cdot 3}{2\cdot 4}\frac{A_2}{m^2} + \frac{1\cdot 3\cdot 5}{2\cdot 4\cdot 6}\frac{A_3}{m^3} + \cdots\right) \quad (B.11)$$

where $\quad \sin\alpha = sn\left(um^{\frac{1}{2}}\,\middle|\,m^{-1}\right) ;$

$$E = \int_0^{\frac{\pi}{2}}\left(1 - m^{-1}\sin^2\lambda\right)^{\frac{1}{2}}d\lambda \text{ (complete elliptic integral of the 2nd kind)}$$

$$= \frac{\pi}{2(1+P)}\left[1 + \frac{1}{2^2}P^2 + \frac{1}{2^2\cdot 4^2}P^4 + \frac{1\cdot 3^2}{2^2\cdot 4^2\cdot 6^2}P^6 + \cdots\right] ;$$

A_1, A_2, A_3 .... are the same as before except that $\sin\theta$ is

replaced by $\sin\alpha$.

The value of $sn(um^{1/2} \mid m^{-1})$ can be calculated by using the

ascending (increase m^{-1}) or descending (decrease m^{-1})

transformations (Abramowitz and Stegun, 1964), depending on whether

$m^{-1} > 0.5$ or $m^{-1} < 0.5$. Then $sn(x \mid r)$ can be approximated by

$$sn(x \mid r) \approx \sin x - \frac{r}{4}(x - \sin x \cos x)\cos x \qquad (r \ll 1)$$

or

$$sn(x \mid r) \approx \tanh x + \frac{1-r}{4}(\sinh x \cosh x - x)\operatorname{sech}^2 x \qquad (r \approx 1).$$

References

Abramowitz, M., and I.A. Stegun (1964). Handbook of Mathematical Functions. Appl. Math. Ser. 55, National Bureau of Standards, Washinton, D.C., 1046pp.

Armi, L, and E. D'Asaro (1979). Flow structures of the benthic ocean. J. Geophys. Res. (in press).

Bell, T.H. (1975). Lee waves in stratified flows with simple harmonic time depencence. J. Fluid Mech., vol. 67, 705-722.

Bretherton, F.P., and C. Garrett (1969). Wavetrains in inhomogeneous moving media. Proc. Roy. Soc. London, Ser. A, vol. 302, 529-554.

Briscoe, M. (1975). Preliminary results from the trimoored internal wave experiment (IWEX). J. Geophys. Res., vol. 80, 3872-3884.

Cairns, J.L., and G.O. Williams (1976). Internal wave observations from a midwater float, 2. J. Geophys. Res., vol. 81, 1943-1950.

Charney, J.G. (1971). Geostrophic turbulence. J. Atmos. Sci., vol. 28, 1087-1095.

Desaubies, Y.J.F. (1975). A linear theory of internal wave spectra and coherences near the Vaisala frequency. J. Geophys. Res., vol. 80, 895-899.

Desaubies, Y.J.F. (1976). Analytical representation of internal wave spectra. J. Phys. Oceanogr., vol. 6, 976-981.

Dwight, H.B. (1968). Tables of Integrals and Other Mathematical Data. Macmillan, New York, 4th ed., 336pp.

Eckart, C. (1960) Hydrodynamics of Oceans and Atmospheres. Pergamon Press, New York, 290pp.

Ekman, V.W. (1905). On the influence of the earth's rotation on ocean currents. Ark. Mat. Astr. Fys., vol. 2, 1-52.

Eriksen, C.C. (1978). Measurements and models of fine structure, internal gravity waves, and wave breaking in the deep ocean. J. Geophys. Res., vol. 83, 2989-3009.

Eriksen, C.C. (1979). Evidence for a continuos spectrum of equatorial waves in the Indian Ocean. Submitted to J. Geophys. Res.

Flattery, T.W. (1967). Hough Functions. Tech. Rep. 21, Dep. of Geophys. Sci., Univ. of Chicago, Chicago, Ill.

Fofonoff, N.P. (1969). Spectral characteristics of internal waves in the ocean. Deep-Sea Res., supplement to vol. 16, 59-71.

Fomin, L.M. (1973). Inertial oscillations in a horizontally inhomogeneous current velocity field. IZV, vol. 9, 75-83.

Fomin, L.M., and M.T. Savin (1973). Vertical coherence of inertial motions in the ocean. IZV, vol. 9, 331-334.

Fomin, L.M., and A.D. Yampol'skiy (1975). Vertical structure of inertial motions in the sea. Oceanology, vol. 15, 21-26.

Fu, L.L., and C. Wunsch (1979). Recovery of POLYMODE Array III Clusters A and B. POLYMODE News, No. 60 (unpublished manuscript), Woods Hole Oceanogr. Inst., Woods Hole, Mass.

Garrett, C., and W. Munk (1972 a). Space-time scales of internal waves. Goephys. Fluid Dyn., vol. 2, 225-264.

Garrett, C., and W. Munk (1972 b). Oceanic mixing by breaking internal waves. Deep-Sea Res., vol. 19, 823-832.

Garrett, C., and W. Munk (1975). Space-time scales of internal waves : a progress report. J. Geophys. Res., vol. 80, 291-297.

Garrett, C., and W. Munk (1979). Internal waves in the ocean. Annual Review of Fluid Mechanics, vol. 11, 339-369.

Geisler, J.E., and E.B. Kraus (1969). The well-mixed Ekman boundary layer. Deep-Sea Res., supplememt to vol. 16, 73-84.

Gonella, J. (1972). A rotary-component method for analysising meteorological and oceanographic vector time series. Deep-Sea Res., vol. 19, 833-846.

Hendershott, M.C. (1973). Inertial oscillations of tidal period. Progress in Oceanograophy, vol. 6, 1-27, Pergamon Press, New York.

Hendry, R.M. (1975). The generation, energetics and propagation of internal tides in the Western North Atlantic Ocean. Ph.D. thesis, Massachusetts Inst. of Tech./Woods Hole Oceanogr. Inst.

Johnson, W.R., J.C. Van Leer, and C.N.K. Mooers (1976). A cyclesonde view of coastal upwelling. J. Phys. Oceanogr., vol. 6, 556-574.

Joyce, T. (1977). CTD observations during KNORR 66 Leg II. POLYMODE News, No.33 (unpublished manuscript) Woods Hole Oceanogr. Inst., Woods Hole, Mass.

Kamenkovich, V.M., and T.B. Tsybaneva (1975 a). Analysis of Laplace's tidal equations in a short-wave approximation (finite longitudinal wave numbers). Oceanology, vol. 15, 151-156.

Kamenkovich, V.M., and T.B. Tsybaneva (1975 b). Analysis of Laplace's
    tidal equations in a short-wave approximation (large longitudinal
    wave numbers). Oceanology, vol. 15, 271-275.

Kamenkovich, V.M., and A.V. Kulakov (1977). Influence of rotation on
    waves in a stratified ocean. Oceanology, vol. 17, 260-266.

Kamenkovich, V.M., V.I. Ul'yanova, and T.B. Tsybaneva (1977).
    Dispersion relation for gravity and Rossby waves in the ocean.
    Oceanology, vol. 17, 256-259.

Käse, R.H., and C.L. Tang (1976). Spectra and coherence of
    wind-generated internal waves. J. Fish. Res. Board Can., vol. 33,
    2323-2328.

Kroll, J. (1975). The propagation of wind-generated inertial
    oscillations from the surface into the deep ocean. J. Mar. Res.,
    vol. 33, 15-51.

Kundu, P.K. (1976). An analysis of inertial oscillations observed near
    Oregon Coast. J. Phys. Oceanogr., vol. 6, 879-893.

Lamb, H. (1932). Hydrodynamics. Cambridge Univ. Press.

Leaman, K. (1975). The vertical propagation of inertial waves in the
    ocean. Ph.D. thesis. Massachusetts Inst. of Tech./Woods Hole
    Oceanogr. Inst.

Leaman, K. (1976). Observations on the vertical polarization and
    energy flux of near-inertial waves. J. Phys. Oceanogr., vol. 6,
    894-908.

Leaman K., and T. Sanford (1975). Vertical energy propagation of
    inertial waves. J. Geophys. Res., vol. 80, 1975-1978.

Lindzen, R. (1967). Planetary waves on beta-planes. Mon. Weather Rev.,
    vol. 95, 441-451.

Longuet-Higgins, M.S. (1965). Planetary waves on a rotating sphere II.
    Proc. Roy. Soc. London, Ser. A, vol. 289, 40-54.

Longuet-Higgins, M.S. (1968). The eigenfunctions of Laplace's tidal
    equations over a sphere. Phil. Trans. Roy. Soc. London, Ser. A,
    vol. 262, 511-607.

Mathews, J, and R.L. Walker (1970). Mathematical Methods of Physics.
    W.A. Benjamin, 501pp.

Matsuno, T. (1966). Quasi-geostrophic motions in equatorial areas. J.
    Meteorol. Soc. Jap., 2(44), 25-43.

McComas, C.H. (1977). Equilibrium mechanisms within the oceanic internal wave fild. J. Phys Oceanogr., vol. 7, 836-845.

McComas, C.H., and F.P. Bretherton (1977). Resonant interaction of oceanic internal waves. J. Geophys. Res., vol. 82, 1397-1412.

Miles, J.W. (1974). On Laplace's tidal equations. J. Fluid Mech., vol. 66, 241-260.

Miles, J.W. (1977). Asymptotic eigensolutions of Laplace's tidal equation. Proc. Roy. Soc. London, Ser. A, vol. 353, 377-400.

MODE-1 Atlas Group (1977). Atlas of the Mid-Ocean Dynamics Experiment (MODE-1). V. LEE and C. Wunsch, editors, Massachusetts Inst. of Tech., Cambridge, Mass.

Mooers, C.N.K. (1973). A technique for the cross-spectrum analysis of pairs of complex-valued time series, with emphasis on properties of polarized components and rotational invariants. Deep-Sea Res., vol. 20, 1129-1141.

Mooers, C.N.K. (1975). Several effects of a baroclinic currents on the cross-stream propagation of inertial-internal waves. Geophys. Fluid Dyn., vol. 6, 245-275.

Moses, H.E. (1971). Vertical shear modes in inertial waves on a rotating earth. J. Geophys. Res., vol. 76, 2156-2163.

Müller, P., and D.J. Olbers (1975). On the dynamics of internal waves in the deep ocean. J. Geophys. Res., vol. 80, 3848-3860.

Müller, P., D.J. Olbers, and J. Willebrand (1968). The IWEX spectrum. J. Geophys. Res., vol. 83, 479-500.

Munk, W. (1979). Internal wave spectra at the buoyant and inertial frequencies. (unpublished manuscript).

Munk, W., and N. Phillips (1968). Coherence and band structure of inertial motion in the sea. Rev. Geophys., vol. 6, 447-472.

Nayfeh, A. (1973). Perturbation Methods. Wiley, New York, 425pp.

Needler, G.T., and P.H. LeBlond (1973). On the influence of the horizontal component of the earth's rotation on long period waves. Geophys. Fluid Dyn., vol. 5, 23-46.

Odulo, A.B. (1972) A qualitative analysis of the Laplace's tidal equations. IZV., Atmospheric and Oceanic Phys., vol. 8, 752-754.

Olbers, D.J. (1976). Non-linear energy transfer and the energy balance of the internal wave field in the deep ocean. J. Fluid Mech., vol. 74, 375-399.

Perkins, H. (1970). Inertial oscillations in the Mediterranean. Ph.D. thesis, Massachusetts Inst. of Tech./Woods Hole Oceanogr. Inst.

Perkins, H. (1976). Observed effect of an eddy on inertial oscillations. Deep-Sea Res., vol. 23, 1037-1042.

Philander, S.G.H. (1978). Forced oceanic waves. Rev. Geophys. Space. Phys., vol. 16, 15-46.

Phillips, N.A. (1966). The equations of motion for a shallow rotating atmosphere and the "traditional approximation". J. Atmos. Sci., vol. 23, 626-628.

Phillips, N.A. (1968). Reply to Veronis' comments. J. Atmos. Res., vol. 25, 1155-1157.

Phillips, O.M. (1963). Energy transfer in rotating fluids by reflection of inertial waves. Phys. Fluids, vol. 6, 513-520.

Phillips, O.M. (1977). The Dynamics of the Upper Ocean. 2nd ed., Cambridge Univ. Press, 336pp.

Pollard, R.T. (1970). On the generation by winds of inertial waves in the ocean. Deep-Sea Res., vol. 17, 795-812.

Pollard, R.T., and Millard, R.C. Jr. (1970). Comparison between observed and simulated wind-generated inertial oscillations. Deep-Sea Res., vol. 17, 813-821.

Rosenberg, N.W. (1968). Statistical analysis of ionospheric winds II. J. Atmos. Terres. Phys., vol. 30, 907-917.

Rossby, C.G. (1938). On the mutual adjustment of pressure and velocity distributions in certain simple current systems, Part II. J. Mar. Res., vol. 1, 239-263.

Sanford, T.B. (1975). Observations of the vertical structure of internal waves. J. Geophys. Res., vol. 80, 3861-3871.

Schmitz, W.J. Jr. (1978). Observations of the vertical distribution of low frequency kinetic energy in the Western North Atlantic. J. Mar. Res., vol. 36, 295-310

Schott, F. (1971). Spacial structure of inertial-period motions in a two layered sea, based on observations. J. Mar. Res., vol. 29, 85-102.

Spiegel, E.A., and G. Veronis (1960). On the Boussinesq approximation for a compressible fluid. Astrophys. J., vol. 131, 442-447.

Stern, M.E. (1977). Interaction of inertia-gravity waves with the wind. J. Mar. Res., vol. 35, 479-498.

Stewartson, K., and J.A. Rickard (1969). Pathological oscillations of a rotating fluid. J. Fluid Mech., vol. 35, 759-773.

Stewartson, K., and I.C. Walton (1976). On waves in a thin shell of stratified rotating fluid. Proc. Roy. Soc. London, Ser. A, vol. 349, 141-156.

Thompson, R.O.R.Y. (1978). Observation of inertial waves in the stratosphere. Q. J. R. Met. Soc., vol. 104, 691-698.

Uchupi, E. (1971). Bathymetric Atlas of the Atlantic, Carribean and Gulf of Mexico. Rept. 71-72, Woods Hole Oceanographic Inst., 10 Charts.

US Polymode Organizing Committee (1976). US POLYMODE Program and Plan. Cambridge, Mass.

Veronis, G. (1956). Partition of energy between geostrophic and non-geostrophic oceanic motions. Deep-Sea Res., vol. 3, 157-177.

Veronis, G. (1968). Comments on Phillips' proposed simplification of the equations of motion for a shallow rotating atmosphere. J. Atmos. Sci., vol. 25, 1154-1155.

Webster,F. (1968). Observations of inertial-period motions in the deep sea. Rev. Geophys., vol. 6, 473-490.

White, W.B. (1972). Doppler shift in the frequency of inertial waves observed in moored spectra. Deep-Sea Res., vol. 19, 595-600.

Wimbush, M., and W. Munk (1970). The benthic boundary layer. The Sea, vol. 4, part 1, New York, Wiley, 731-758.

Wunsch, C. (1976). Geographical variability of the internal wave field: A search for sinks and sources. J. Phys. Oceanogr., vol. 6, 471-485.

Wunsch, C. (1977). Response of an equatorial ocean to a periodic monsoon. J. Phys. Oceanogr., vol. 7, 497-511.

Wunsch, C., and J. Dahlen (1974). A moored temperature and pressure recorder. Deep-Sea Res., vol. 21, 145-154.

Wunsch, C., and A.E. Gill (1976). Observations of equatorially trapped waves in Pacific sea level variations. Deep-Sea Res., vol. 23, 371-390.

Wunsch, C., and R. Hendry (1972). Array measurements of the bottom boundary layer and the internal wave field on the continental slope. Geophys. Fluid Dyn., vol. 4, 101-145.

Wunsch, C., and S. Webb (1979). The climatology of deep ocean internal waves. J. Phys. Oceanogr., vol. 9, 235-243.

Biographical Note

The author was born on October 10, 1950 in Taipei, Taiwan. He attended Lung-An Elementary School, Ta-An Junior High School, and Chien-Kuo High School. He earned his B.S. degree in Physics from National Taiwan University in June, 1972. As a R.O.T.C. officer, he served in the Chinese Marine Corps for two years. He came to the United States in 1974. After finishing the first year of graduate study in Physical Oceanography at the University of Miami, he was admitted to the Joint Program in Oceanography of M.I.T./W.H.O.I.. He was married to Cecilia C. Liu on March 26, 1977.